LIMITED-JERK SINUSOIDAL TRAJECTORY DESIGN FOR FIELD ORIENTED CONTROL OF PERMANENT MAGNET SYNCHRONOUS MOTORS WITH H-INFINITY OPTIMAL CONTROLLER

A THESIS SUBMITTED TO
THE GRADUATE SCHOOL OF NATURAL AND APPLIED SCIENCES
OF
MIDDLE EAST TECHNICAL UNIVERSITY

BY

MEHMET KAAN MUTLU

IN PARTIAL FULFILLMENT OF THE REQUIREMENTS
FOR
THE DEGREE OF MASTER OF SCIENCE
IN
ELECTRICAL AND ELECTRONICS ENGINEERING

SEPTEMBER 2019

Approval of the thesis:

LIMITED-JERK SINUSOIDAL TRAJECTORY DESIGN FOR FIELD ORIENTED CONTROL OF PERMANENT MAGNET SYNCHRONOUS MOTORS WITH H-INFINITY OPTIMAL CONTROLLER

submitted by **MEHMET KAAN MUTLU** in partial fulfillment of the requirements for the degree of **Master of Science in Electrical and Electronics Engineering Department, Middle East Technical University** by,

Prof. Dr. Halil Kalıpçılar _____
Dean, Graduate School of **Natural and Applied Sciences**

Prof. Dr. İlkay Ulusoy _____
Head of Department, **Electrical and Electronics Engineering**

Assist. Prof. Dr. Ozan Keysan _____
Supervisor, **Electrical and Electronics Engineering Dept.**

Dr. Barış Ulutaş _____
Co-supervisor, **REHIS - MMTM, ASELSAN**

Examining Committee Members:

Assoc. Prof. Dr. Afşar Saranlı
Electrical and Electronics Engineering Dept., METU _____

Assist. Prof. Dr. Ozan Keysan
Electrical and Electronics Engineering Dept., METU _____

Assist. Prof. Dr. Emine Bostancı
Electrical and Electronics Engineering Dept., METU _____

Assist. Prof. Dr. Emre Özkan
Electrical and Electronics Engineering Dept., METU _____

Prof. Dr. Işık Çadırcı
Electrical and Electronics Engineering Dept., Hacettepe University _____

Date: _____

I hereby declare that all information in this document has been obtained and presented in accordance with academic rules and ethical conduct. I also declare that, as required by these rules and conduct, I have fully cited and referenced all material and results that are not original to this work.

Name, Last Name: Mehmet Kaan Mutlu

Signature :

ABSTRACT

LIMITED-JERK SINUSOIDAL TRAJECTORY DESIGN FOR FIELD ORIENTED CONTROL OF PERMANENT MAGNET SYNCHRONOUS MOTORS WITH H-INFINITY OPTIMAL CONTROLLER

Mutlu, Mehmet Kaan
M.S., Department of Electrical and Electronics Engineering
Supervisor : Assist. Prof. Dr. Ozan Keysan
Co-Supervisor : Dr. Barış Ulutaş

September 2019, 109 pages

Trajectory planning has a significant role in meeting the strict requirements of the systems in motion. Focus of the trajectory design can be minimum response time, minimum error or extended service life depending on the application. Limited time and error minimization requirements can be achieved in the systems with small inertia without any visible problems. However, torque ripples and vibration create fatigue in the mechanical parts. In this study, limited-jerk sinusoidal trajectory (also known as cycloidal follower motion) is proposed in the field oriented control (FOC) of permanent magnet synchronous motors (PMSM) to achieve precise motion control, reduced torque ripple and extend service life. In order to show the effectiveness of the proposed method in this study, simulation results of the closed-loop systems are compared with reference trajectories calculated using various methods. The velocity and the position of the load are controlled with an H-infinity optimal controller that is designed after the open-loop system identification.

Keywords: Sinusoidal limited-jerk, trajectory design, precise motion control, field oriented control, permanent magnet synchronous motors, torque ripple reduction

ÖZ

H-SONSUZ OPTİMUM KONTROLCÜ KULLANILAN SABİT MIKNATISLI SENKRON MOTORLARIN VEKTÖR KONTROLÜNE SARSIM LİMİTLİ SÜNÜSOİDAL YÖRÜNGE TASARIMI

Mutlu, Mehmet Kaan
Yüksek Lisans, Elektrik ve Elektronik Mühendisliği Bölümü
Tez Yöneticisi : Yrd. Doç. Dr. Ozan Keysan
Ortak Tez Yöneticisi : Dr. Barış Ulutaş

Eylül 2019 , 109 sayfa

Yörünge tasarımının, hareketli sistemlerin sıkı gereksinimlerinin karşılanmasında kritik bir rolü bulunmaktadır. Uygulamaya bağlı olarak bu yörüngenin odağı güç tüketimi, minimum tepki süresi, minimum hata, genişletilmiş servis ömrü olabilmektedir. Sınırlı zaman ve hata azaltma gereksimimleri, düşük ataletli sistemlerde gözle görülür problemler oluşturmadan sağlanabilir. Ancak, tork dalgalanmaları ve titreşim sistemdeki mekanik aksamda yorulma yaratmaktadır. Bu çalışmayla, (yuvarlanma eğrisi takibi olarak da anılan) sarsım limitli sinüsoidal yörünge kullanılarak, sabit mıknatıslı senkron motorun vektör kontrolüne ait hassas hareket kontrolü, azaltılmış tork dalgalanması, daha düşük güç tüketimi ve genişletilmiş servis ömrü sağlanabilmesi hedeflenmiştir. Bu çalışmada sunulan yöntemin etkinliğini gösterebilmek için, farklı methodlar için hesaplanan referans yörüngelerinin kapalı çevrim benzetim sonuçları karşılaştırılmıştır. Yükün hız ve pozisyonu, açık-çevrim sistem karakteristiğinin belirlenmesinden sonra tasarlanan H-sonsuz kontrolcü kullanılarak sağlanmıştır.

Anahtar Kelimeler: Sinüsoidal limitli sarsım, yörünge tasarımı, hassas hareket kontrolü, vektör kontrol, sabit mıknatıslı senkron motorlar, tork salınımının azaltılması

To my wife...

ACKNOWLEDGMENTS

Firstly, I would like to express my sincere gratitude to Assist. Prof. Dr. Ozan Keysan for his continuance motivation and endless encouragement. As his lectures were always beyond the walls of the class, his guidance was also far beyond my thesis.

I would like to thank examinig committee members Prof. Dr. Işık Çadırcı, Assoc. Prof. Dr. Afşar Saranlı, Assist. Prof. Dr. Emine Bostancı and Assist. Prof. Dr. Emre Özkan as the second readers of this thesis.

Starting my graduate studies would not be possible without my background in Yıldız Technical University. Therefore, I would also like to thank Assoc. Prof. Dr. Umut Engin Ayten for his support that enlarged my knowledge in engineering.

I would like to thank ASELSAN Inc. for its valuable support throughout my graduate studies. Outstanding experimental test setup has benefited my work greatly. I also would like to thank my co-supervisor and old colleague Dr. Barış Ulutaş for his endless support to complete my study and to extend my vision.

There is no words of thanks or gratitude that can represent my indebtedness to my mother. I am very thankful for her unending support during my whole life.

And lastly, I would like to express my heartfelt thanks to my wife Meryem Mutlu. I feel deeply grateful to her for her endless patience, support and motivation not only for this study but also at every aspect of my life.

TABLE OF CONTENTS

LIST OF TABLES

TABLES

LIST OF FIGURES

FIGURES

LIST OF ABBREVIATIONS

ABBREVIATIONS

AC	Alternating Current
CNC	Computer Numerical Control
DC	Direct Current
EMC	Electromagnetic Compatibility
FOC	Field Oriented Control
GCDs	Greatest Common Divisors
LPTN	Lumped Parameter Thermal Network
MCU	Micro Controller Unit
MMF	Magnetomotive Force
MTBF	Mean Time Between Failures
MTPA	Maximum Torque per Ampere
N4SID	Numerical Algorithm for Subspace SS System Identification
PI	Proportional-Integral
PID	Proportional-Integral-Derivative
PMSM	Permanent Magnet Synchronous Motor
PWM	Pulse Width Modulation
RF	Radio Frequency
RMS	Root Mean Square
RPM	Revolution per Minute
SS	State Space
SVD	Singular-Value Decomposition

LIST OF SYMBOLS

SYMBOLS

a	Acceleration
A	State Matrix of State Space Representation
α	Angular Acceleration
B	Input Matrix of State Space Representation
$\mathcal{O}_i$	Extended Observability Matrix
C	Output Matrix of State Space Representation
D	Direct Transition Matrix of State Space Representation
E_f	Noise Innovation Future Matrix
E_p	Noise Innovation Past Matrix
F	Force
G_d	Desired Closed-loop Shaping of the Plant
G_p	Position Open-loop Transfer Function
G_s	Obtained Closed-loop Shaping of the Plant
G_v	Velocity Open-loop Transfer Function
Γ_i	Oblique Projection Matrix
H_∞	H-infinity
i	Index of the Sample
i_d	Direct-axis Current
I_{dq}	Direct and Quadrature Axes Currents
I^*_{dq}	Direct and Quadrature Axes Reference Currents
i_q	Quadrature-axis Current
J	Inertia

$\widehat{J}$	Jerk Coefficient
K	Kalman Filter Gain
K_c	Current Controller
K_p	Position Controller
K_v	Velocity Controller
L	Lower Triangular Matrix
L_d	Direct-axis Inductance
L_q	Quadrature-axis Inductance
λ_f	Flux Linkage
m	Mass
N_p	Number of Pole Pairs
ω	Angular Velocity
ω^*	Reference Angular Velocity
ω_e	Electrical Angular Velocity
$\{\omega_{min}, \omega_{max}\}$	Desired Frequency Range for H_∞ Loop Shaping
Q	Orthogonal Matrix
R_s	Stator Resistance
T	Controllability Matrix
T_e	Electromagnetic Torque
T_m	Mechanical Torque
θ^*	Reference Electrical Rotor Angle
θ_r	Electrical Rotor Angle
U	Left Singular Vector
u_d	Excitation Voltage
u_{d-off}	Direct-axis Voltage Offset for Current Decoupling
U_f	Future Input Matrix
U_p	Past Input Matrix

$\tilde{U}_i$	Estimate of Input Matrix
u_q	Torque Voltage
u_{q-off}	Quadrature-axis Voltage Offset for Current Decoupling
V	Right Singular Matrix
V^*_{abc}	A,B,C Axes Reference Voltages
V^*_d	Direct Axis Reference Voltage
V^*_{dq}	Direct and Quadrature Axes Reference Voltages
V^*_q	Quadrature Axis Reference Voltage
W_p	Past Data Matrix
X_i	i^{th} State Sequence Matrix
X_f	State Sequence Future Matrix
X_p	State Sequence Past Matrix
$\tilde{X}_i$	Estimate of i^{th} State Matrix
$\tilde{X}_{i+1}$	Estimate of $(i+1)^{th}$ State Matrix
Y_f	Future Output Matrix
$\tilde{Y}_i$	Estimate of Output Matrix

CHAPTER 1

INTRODUCTION

Permanent magnet synchronous motors (PMSM) have been widely used in areas where precise motion control is required. Thanks to their high efficiency, high torque density, wide velocity and torque ranges they are also preferred in traction, robotics and aerospace applications [1]. Field oriented control (FOC) technique is one of the most popular methods used in control of synchronous motors [2]. FOC is based on the idea of decoupling the magnetizing and torque components of the current in the excitation.

Permanent magnets are used in the rotors of synchronous motors, eliminate the need of an excitation current (unless in special cases such as in [3]) and this current must be minimized for an optimal system efficiency. PMSM control systems are commonly used with three control loops: position, velocity and current loops. The position loop is the outer loop with the slowest bandwidth. The velocity and the current loops are sequentially placed inside the position loop [1]. For reference tracking with minimum error, all of these loops are needed to be tuned according to the operation conditions and the load's specifications. Conventional tuning methods like PI and PID controllers [4] are still commonly used. However, when it comes to the stability and robust performance requirements, various control methods such as H_∞ optimal control and the structured singular value technique have received considerable attention [5]. As control theory is improved and new methods are introduced, input-output relations of the open-loop systems to be controlled have become more valuable. Therefore, system identification has started to play an important role in the control of electrical machines [6]. In this study, the velocity and the position open-loop system characteristics are obtained to achieve better closed-loop controllers.

H_∞ control techniques aim to design a controller that will bound the closed-loop system H_∞ gain less than a desired value [7]. Using the open-loop system characteristics of the velocity and position loops, a controller designed with this idea, improves desired performances by having a wider bandwidth. However, it is important to keep in mind that designed controller is only optimal with the predefined closed-loop bandwidth and its robustness is valid under the elimination of non-linear constraints.

Trajectory selection for the torque, velocity and position control is as important as the controller's itself since it has great influence on the system's performance. Planning the reference path with the bandwidth information is a good approach but not enough for the perfect motion control. Jerk, which is the derivative of acceleration, is also an important parameter and should be taken into account in the motion profile selection in order to minimize torque ripples and the fatigue in mechanical components [8].

Trapezoidal speed control is one of the most popular motion profiles [9]. However, large vibrations are induced with these kind of motions due to the discontinuity of the acceleration and infinite jerk value. Therefore, acceleration and jerk should be limited as presented in [8–11]. A constant acceleration is suggested as a simple approach for the minimum peak value of acceleration, but it is not adequate for precision applications. Trapezoidal and sinusoidal accelerations, trapezoidal and parabolic jerk changes all reduce the vibration levels and improve the performances of the system. However, perfect motions are not achieved due to the discontinuity of the jerk or lack of controller's bandwidth. Sinusoidally limited-jerk trajectory is proposed for the optimal solution for both time optimality and jerk continuity.

1.1 Field Oriented Control of Permanent Magnet Synchronous Motors

The vector control of currents and voltages results in control of the spatial orientation of the electromagnetic fields in the machine and has led to the term field orientation [12]. For PMSM, this term is reserved for controllers which maintain a 90° spatial orientation between the direct and the quadrature axes. The current on the direct axis corresponds to the excitation whereas the quadrature axis current is for the torque generation. These axes and electrical rotor angle θ_r are shown in the Fig. 1.1 [13].

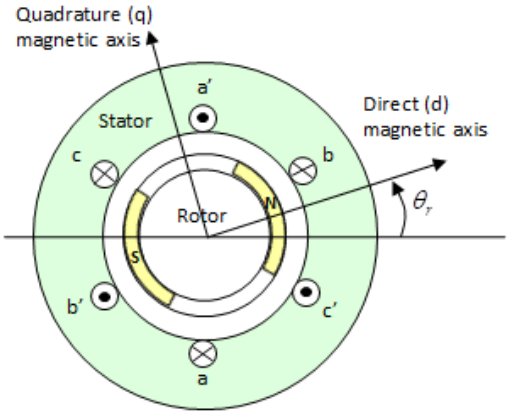

Figure 1.1: Illustration of direct and quadrature axes [13]

The mathematical model of a PMSM in two-phase rotating coordinate system is as follows:

$$u_d = R_s i_d + L_d \frac{d(i_d)}{dt} - \omega_e L_q i_q \tag{1.1}$$

$$u_q = R_s i_q + L_q \frac{d(i_q)}{dt} + \omega_e L_d i_d + \omega_e \lambda_f \tag{1.2}$$

where u_d and u_q are d-q voltage components; i_d, i_q are current components; L_d, L_q are stator inductances in the d-q coordinate system; R_s is the stator resistance, ω_e is the electrical angular velocity, λ_f is the flux linkage.

For cylindrical-rotor machines magnetic energy does not change since L_d and L_q inductances are equal. Therefore, considering Eq. (1.3), it is directly possible to say that direct axis current is ineffective in creating electromagnetic torque for these machines. Even with inequality of the d-q inductances, direct axis current's effect to the electromagnetic torque is less than that of a quadrature axis current:

$$T_e = N_p \lambda_f i_q + N_p (L_d - L_q) i_d i_q \tag{1.3}$$

where T_e is the electromagnetic torque and N_p is the number of pole pairs. The torque and the current controls are performed in the d-q domain, but applied voltages and the measured currents are still in three phase a-b-c real-time domain. Required transformation between these domains are performed in the current control loop.

1.1.1 Voltage Control Loop in the Field Oriented Control

Voltage control loop is the inner and basic mechanism of the FOC. Basically it realizes the idea given in the Eq. (1.1) and Eq. (1.2) by converting electrical voltage to the torque in true direction. If the voltage level is enough to create an electromechanical torque that is greater than the friction, to PMSM starts rotating. As far as there is difference between the electrical torque and the mechanical torque, this difference accelerates the motor until there is a balance between them. During this control loop, feedback from the system is not needed except for the electrical angle between the rotor and the magnetic axis of phase-A. Since there is no controller in the loop this control method is considered as open-loop and its structure is given in the Fig. 1.2.

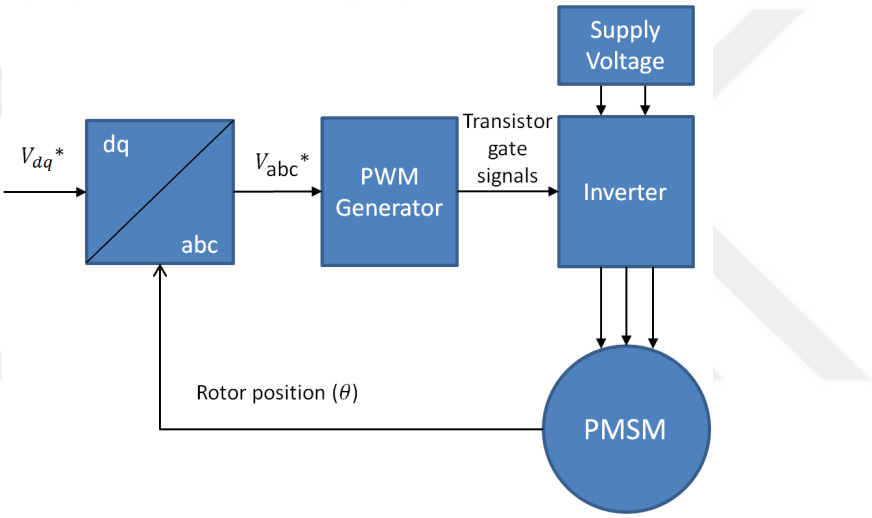

Figure 1.2: The open-loop voltage control of a PMSM with field oriented control

1.1.2 Current Control Loop in the Field Oriented Control

Current control loop is the inner closed loop that corresponds to the torque control. In the field oriented control method, the i_q current creates the significant part of the electromechanical torque which is directly related with the mechanical output power. Since the efficiency is the ratio between this output power and the input power, minimizing the i_d current, which is not helping to create electromechanical torque, reduces the copper loss effectively and improves the efficiency of the drive [14]. However, controlling the direct and quadrature currents, in a way that they are equal, yields

to the maximum torque per ampere (MTPA) case. For different applications that requires both high efficiency and high torque per ampere, a combined approach can be implemented to the field oriented control of PMSM as defined in [15].

The first step of the current control is the open-loop voltage control which its block diagram is given in Fig. 1.2. In this loop, reference d-q voltages are converted first to the α-β domain then to the synchronously rotating a-b-c domain by using Inverse Park and Clarke's transformations. The only required input for the transformation is electrical rotor angle. Voltages in the a-b-c domain are used in the PWM generator to create the gate signals of the inverter. Bus voltage of the inverter can be supported by a DC voltage source or can be rectified from an AC voltage source.

Voltage control loop can be converted into the closed loop current control by sensing the 3-phase motor currents and adding a current controller to minimize the difference between the references and the real values. Measured currents are needed to be transformed into the stationary d-q domain by using Clarke and Park's transformations. Selection of the current controller and its parameter's tuning should be done considering the system requirements and the motor's specifications. Block diagram of the closed-loop current controller is given in Fig. 1.3.

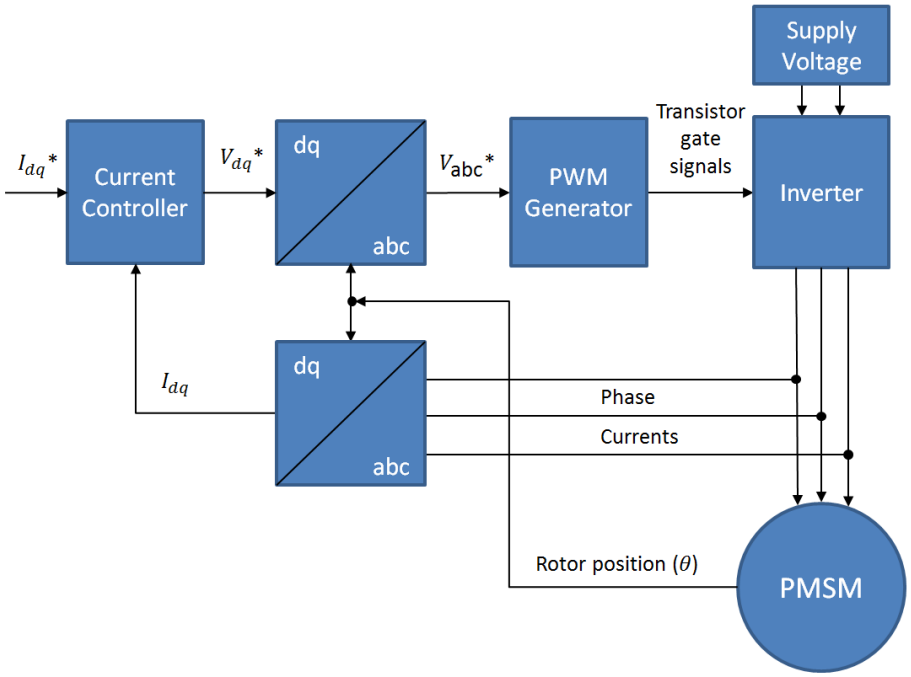

Figure 1.3: The closed-loop current control of a PMSM with FOC

Eq. (1.1 and 1.2) show that d-q domain currents exist also in cross voltages' formulations. This phenomena is known as cross-coupling and it is the magnetic interaction between a phase current and a magnetic axis other than its own axis. Therefore, even if the i_d current reference is zero, its real value becomes different from the expectation due to nonzero i_q current. The influence of FOC can be improved by feed forward compensation to achieve d-q domain current decoupling.

$$u_{q-off} = \omega_e L_d i_d + \omega_e \lambda_f \tag{1.4}$$

Using Eq. (1.4) at the output of the current controller, as given in the Fig. 1.4, provides current decoupling where i_d is current component, L_d is stator inductance in the d-q coordinate system; ω_e is the electrical angular velocity and λ_f is the flux linkage.

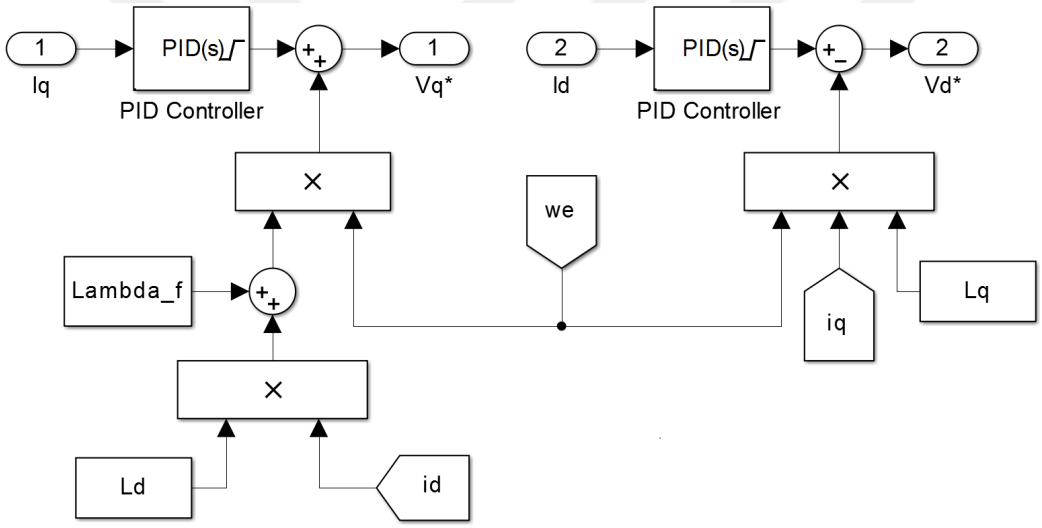

Figure 1.4: Current decoupling application at the output of i_d Controller

Decoupling only the i_q current is not enough for a full decoupling. Therefore, Eq. (1.5) is also needed to be used at the output of i_d controller as also given in Fig. 1.4.

$$u_{d-off} = -\omega_e L_q i_q \tag{1.5}$$

If the d-q domain currents are changing with a transient state, effects of the decoupling becomes more dominant. In that case, a more detailed current decoupling method that also considers the parameters of the inverter can be used [16].

1.1.3 Velocity Control Loop in the Field Oriented Control

Control of the output velocity is important for most of the industrial applications such as traction and aerospace [1]. As long as mechanical coupling between the motor and the load is well known, it is easy to obtain velocity of the load and the motor by using the data of the electrical load angle that is sensed by using encoder, resolver, hall effect sensors or determined by using sensorless control techniques. Electrical rotor angle is used for the field oriented control transformations and already defined in the control loop. Derivation of this angle gives the velocity and by adding an extra controller to the current control loop, structure of the velocity control can be completed as shown in Fig. 1.5.

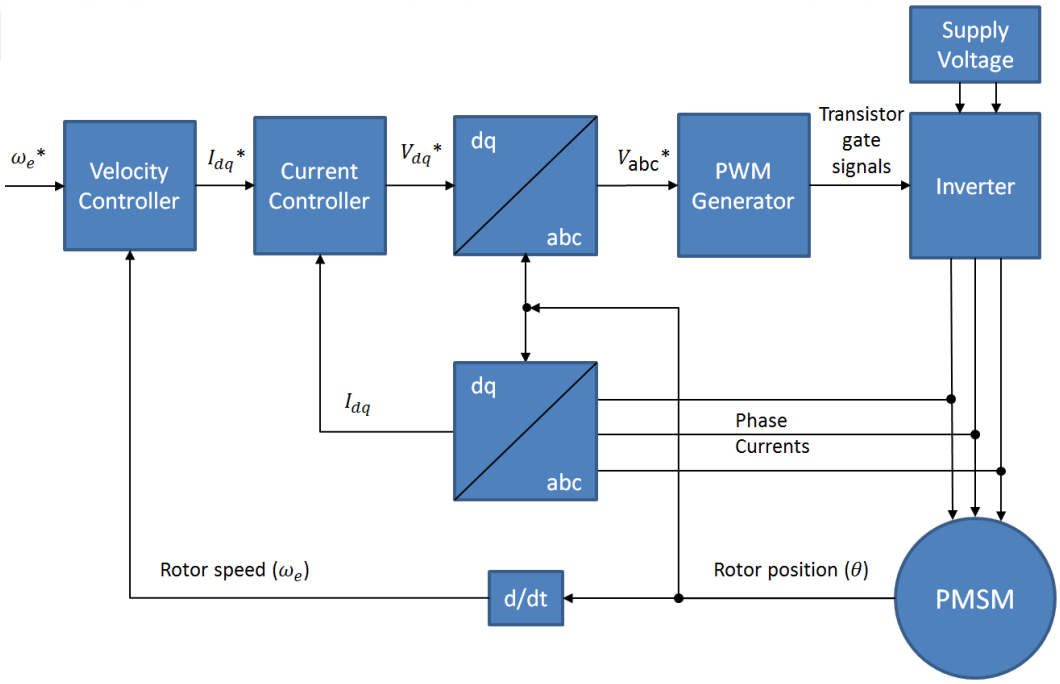

Figure 1.5: The closed-loop velocity control of a PMSM with FOC

1.1.4 Position Control Loop in the Field Oriented Control

Precise position control is widely required in various industrial applications and robotics. Upgrading a velocity controller to the closed-loop position control loop requires an additional controller and the relation between the electrical rotor angle and the position of the mechanical load. All the ratios that come from pole pairs of the motor,

gearbox and pinion are needed to be taken into consideration to define the connection between the electrical and the mechanical positions. Moreover this transformation, offset between the electrical and the mechanical positions should be determined by a proper homing process. Block diagram of the closed loop position control of a permanent magnet synchronous motor is given in Fig. 1.6.

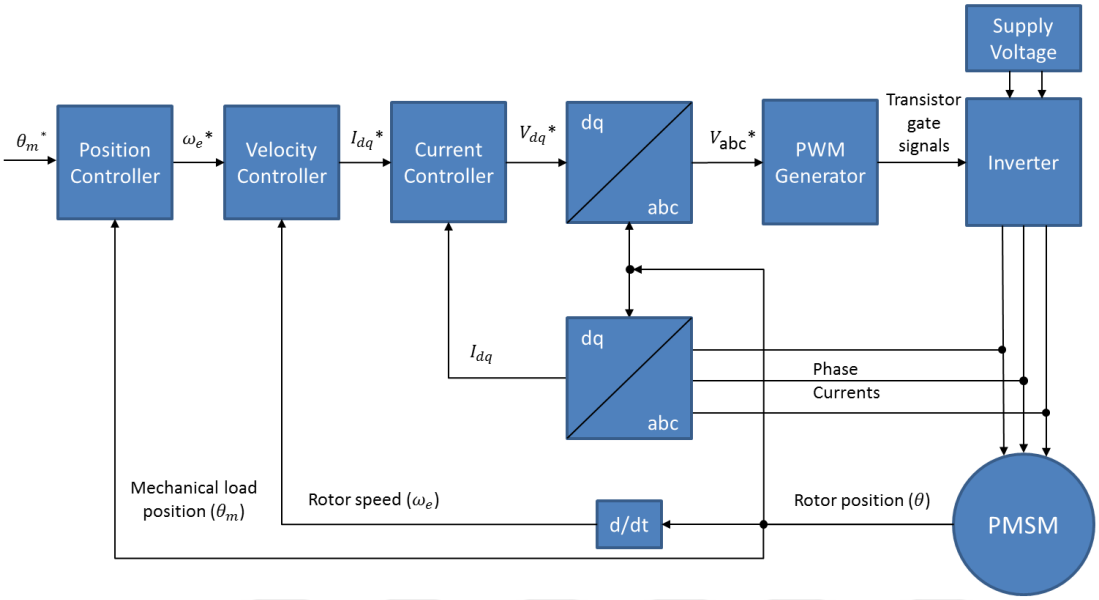

Figure 1.6: The closed-loop position control of a PMSM with FOC

1.2 Jerk Limitation in the Literature

Limiting the jerk for a better motion or time optimality has been studied in different researches and this concept is started to be used in the various electromechanical applications. Mostly, the motivation behind these researches is to reduce the torque ripples in the system and create a smoother motion. According to the surveys reported for the failed components in the field, more than half of the failures are fatigue and vibration related [8]. Since the jerk limitation works in harmony with vibration reduction, it is not only a way of improving the quality of the motion, but also a compulsory action to improve the reliability of the system [9].

Jerk limitation in the motion trajectory design is also studied for improving the time optimality of the motion [10, 11, 17]. In these studies, jerk of the system is bounded

with different shapes and performances of the systems are compared. Mathematical calculations and shared results show that jerk limitation is important for the time optimality of the motion.

Even if the trajectories are being used during only the position or the velocity changing intervals, their impact to the quality of the motion is incontrovertible. In the study of [18], limiting the jerk is considered as corner smoothing of the kinematic trajectory and transient parts of the motion is modified for cycle time reduction and energy optimization of the movement. Results show that corner smoothing gives a better working condition for both time and energy efficiency. Another study, which is described in the [19], shows that limiting jerk results as reduction of the harmonics of the motion and this also corresponds to decrease in the vibration.

Except for jerk limitation's effects on vibration reduction in electromechanical systems, time optimality and reliability; it is also studied to see the biomechanical effects on humans. Researches show that humans can detect acceleration easily, but once it is not constant, non-zero jerk is created and actually humans can experience it as a discomfort feeling [20]. Experiments show that these biomechanical effects can even harm to the health of the person. Therefore, it is possible to say that limiting the jerk is not only beneficial to the electromechanical systems but also for humans. Other studies focused on imitating the human movements show that muscular movements are naturally in a form with limited-jerk [21]. Therefore, the idea of jerk limitation is being used for a long time in the robotic applications that imitates human behaviors [22].

Due to all of the advantages and the similarities of natural movements, the jerk-limitation is also used in the industrial applications, as it is done in this study, CNC systems [23] and quadrotors [24].

1.3 Thesis Outline

Motivation behind this study was to develop an electromechanical system control solution with accurate and fast response for position control and high reliability for antenna rotation systems developed in Aselsan, which can be accelerated up to 100

RPM with 0.01° resolution and input power was limited with 750 W. For this purpose different principles, such as field oriented control, system identification and H_∞ control design, are gathered together as a whole solution and trajectory of the motion is reshaped with a limited-jerk approach. This method is compared with conventional techniques and both simulation and experimental results are shared within the study.

This thesis is divided into six chapters and organized as follows:

Chapter 1 introduces the necessity and the motivation of the jerk-limitation. Auxiliary methods used in this study such as system identification and H_∞ control are also introduced and detailed information about the field oriented control is provided in this chapter.

Limited-jerk sinusoidal trajectory design is mathematically introduced and motion intervals of acceleration, constant speed and deceleration are defined in Chapter 2. Other trajectories that are used in the simulations and experiments, such as the motion with constant speed and the motion with constant acceleration, are also introduced in this chapter.

In Chapter 3, a subspace identification algorithm namely the numerical algorithms for subspace state space system identification (N4SID) is explained technically. In this study, controllers for the identified loops are designed using H_∞ optimal control method which is also introduced technically in this chapter. Since the identification of the system provides input to the controller designing process, these two steps are taken into account together.

All previously given information are used in Chapter 4 to establish the basic control loops for the position control of PMSM and simulation results for different motion profiles are given together with their compared differences.

In Chapter 5, experimental test setup is explained and all required basic control loops are constructed. Afterwards experimental results for different motion profiles are given and compared to indicate their advantages over each other.

Finally, Chapter 6 is the conclusion chapter and some possible future works are outlined.

CHAPTER 2

LIMITED-JERK SINUSOIDAL TRAJECTORY DESIGN

Permanent magnet synchronous motors are mainly used in applications where high-performance position control is required such as machinery tools, industrial robots and aerospace [9]. In most of these systems, the load accelerates and decelerates frequently. Furthermore, fast and accurate motion control is expected from the servo control systems.

Limited time and error minimization requirements can be achieved in the systems with small inertia without any noticeable problems. However, torque ripples and vibrations create fatigue in the mechanical parts of the systems in motion. A study that is done with induction motors shows that 51% of the failures are caused by the bearings in the system and vibration is the main cause of these failures [8]. Independent from type of the motor, elimination of these failures can not be possible without reducing the vibration of the mechanism. In systems with low inertia the torque ripple levels can be negligibly small but created vibration might still affect the lifetime of the system. However, motion profile selection becomes important for the systems with large inertias.

The velocity and the acceleration are well known as the first and the second derivatives of the position. But the higher derivatives of motion are rarely discussed in the teaching of classical mechanics of rigid bodies. But in fact, these terms are important for a good motion by means of lifetime of the mechanical parts and even the ergonomics since humans can also experience the effect of jerk and snap (jounce) [20]. In this chapter, different motion profiles are discussed under the following sections.

2.1 Motion with a Constant Velocity

For all traveling objects that have mass, Newton's second law of motion works for acceleration and they require a force as defined in Eq. (2.1), where m is mass and a is acceleration which is the derivative of velocity v.

$$F = m\frac{d(v)}{d(t)} = ma \tag{2.1}$$

For a rotating system, Eq. (2.1) can be rewritten in the following form:

$$T_m = J\frac{d(\omega)}{d(t)} = J\alpha \tag{2.2}$$

where T_m is torque, J is inertia and α is the change of angular velocity (ω) with respect to the time.

Accelerating a load of inertia to a certain velocity requires both enough torque and enough time. But if a motion with a constant velocity is expected, it means that the inertia and the damping effects are ignored and the mechanical time constant is considered as zero. Even if these values are very small, still a certain amount of time is required to supply the phase currents to the motor due to the electrical time constant. Therefore, it is not possible to achieve these kind of motions without performance drops.

In an ideal motion with constant velocity, the position of the load changes linearly during the movement. So it is expected to have an infinite amount of acceleration at the beginning of the motion and negative infinite acceleration at the end as shown in Fig. 2.1. The jerk which is the derivative of the acceleration is not shown in this figure since it is also discontinuous and impulsive.

Even if achieving this motion can be mathematically possible; physical limits, electrical and mechanical time constants avoid to perform such kind of a motion without errors in the tracking of reference. Therefore undesired vibrations are created in the mechanical system with this trajectory.

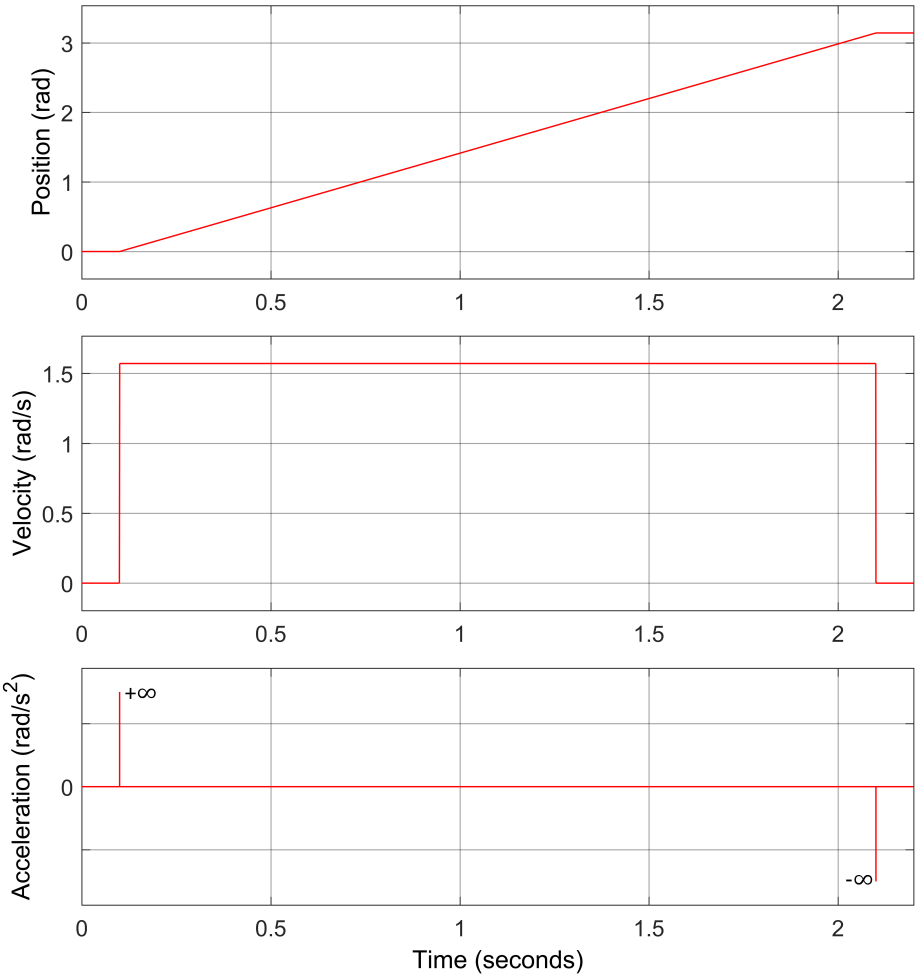

Figure 2.1: Constant velocity kinematic profiles

Fourier's analysis of the position waveform, that is given in Fig. 2.1, shows the situation about waveform's frequency distribution over the spectrum. These calculations are completed for the waveform that changes the load's position from $0°$ to $180°$ in 2 seconds and results are shared in Fig. 2.2. Numerical values in this profile are selected as example and independent from the system used in this study.

The relation between the spectrum of the position reference and the quality of the motion can be established over the bandwidth of the position controller. If some of the components in the frequency spectrum are not in the bandwidth of the controller, the tracking of the reference can not be fully achieved.

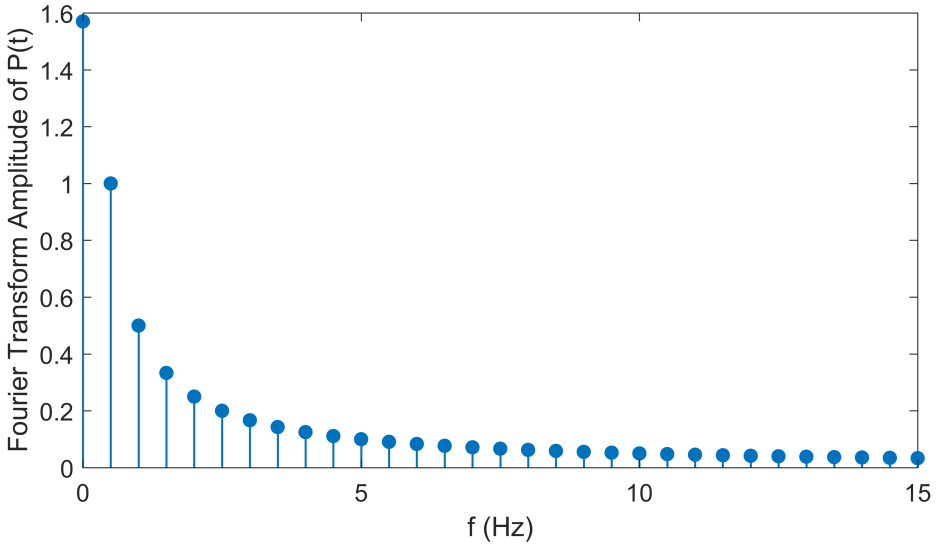

Figure 2.2: Single-sided amplitude spectrum of the constant velocity reference

2.2 Motion with a Constant Acceleration Trajectory

Limitation of the acceleration is an important aspect to achieve a smoother motion. By this way, the required torque can be finite and the motion can be achievable not only mathematically but also physically. Since it is the most popular one in the field [9], trapezoidal velocity trajectory with constant acceleration is evaluated in this section.

As the acceleration is limited by a constant value, the velocity of the motor changes linearly. Therefore the change of the load's position is parabolic as shown in Fig. 2.3. This trajectory can be considered as a basic example of S-curve but smoothness is not passed on the derivations of the position.

Compared to the motion with the constant velocity, this motion is much better for the condition of the mechanical parts of the system. But discontinuity of the jerk stands creating vibrations for the motion. Therefore, even if the position change is smooth and in a shape of S-curve, sharp edges of the acceleration waveform shown in Fig. 2.3 requires transient currents from the inverter of the motor drive and it is a challenge for the current controller of the electrical system. Even though the bandwidth of the controller is high enough to follow a step reference, the derivative of the acceleration,

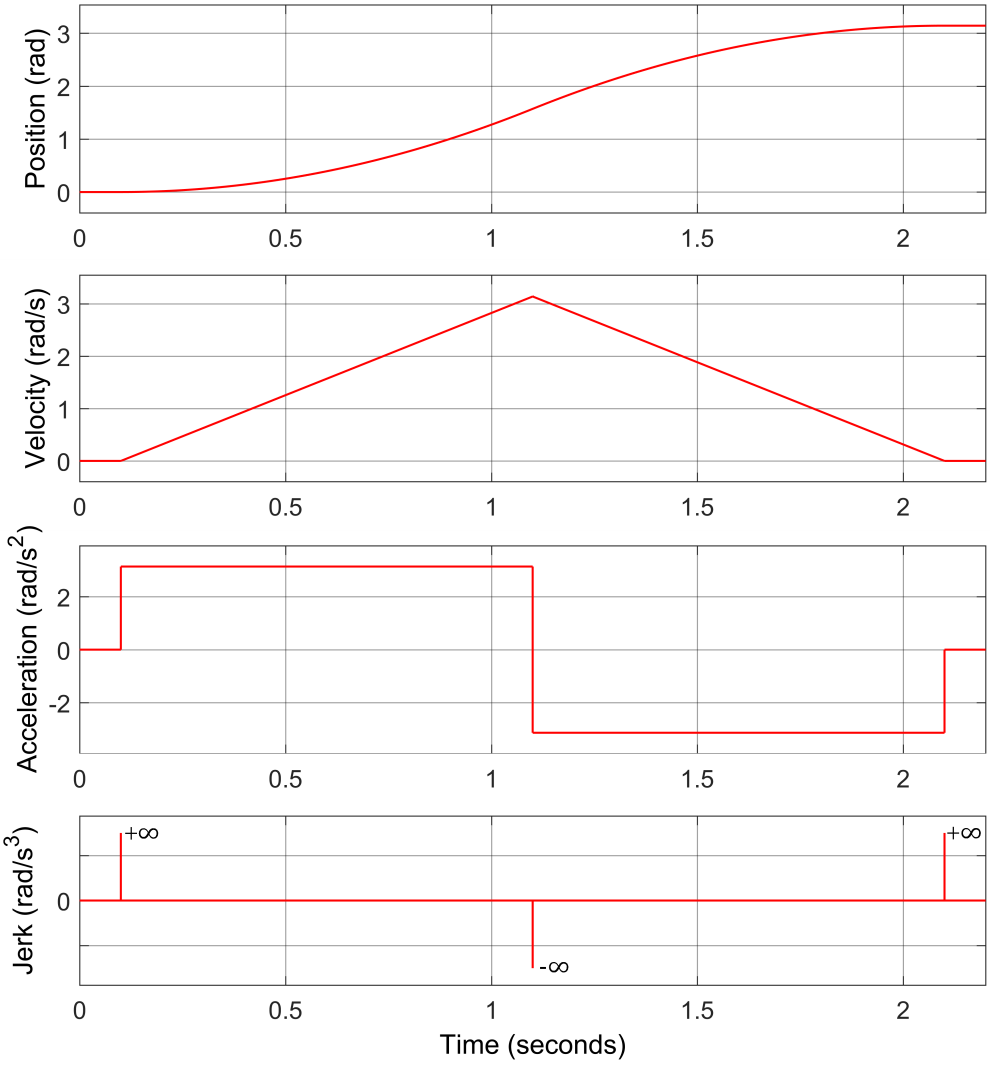

Figure 2.3: Constant acceleration kinematic profiles

which is the jerk, is still not limited. This situation is not desired for a good motion profile.

Reference with a constant acceleration, that is given in Fig. 2.3, changes the load's position from $0°$ to $180°$ in 2 seconds. These values are selected as example and independent from the system used in the study. Fourier's analysis for this reference is calculated and results are shared in Fig. 2.4. Comparison of the spectrum and the controller's bandwidth can give better results but it is important to not forget that having a transient acceleration change requires an inverter with a very high bandwidth.

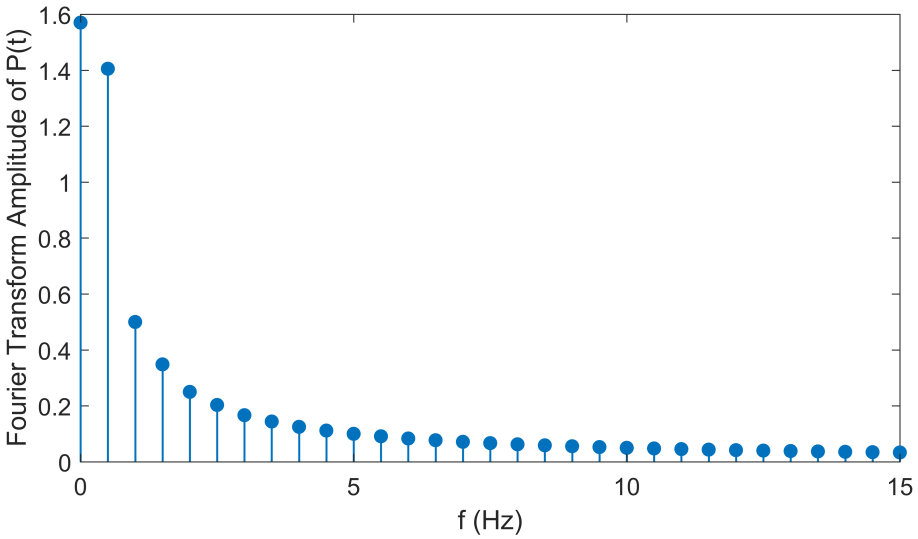

Figure 2.4: Single-sided amplitude spectrum of the trapezoidal velocity reference

2.3 Motion with Limited-Jerk Sinusoidal Trajectory

Instantaneous position change is considered as teleporting and that is not possible even for a photon of light. Accelerating directly to a certain velocity is not possible for the objects that have mass due to the need of infinite force. Physical explanations behind these phenomenas are easy to be understood. It is also important to have a continuous and smooth waveform for the acceleration to create a smooth electromechanical torque for the system which reduces vibration and increases lifetime in return [8, 9]. Smooth acceleration can be achieved by selecting a special shape for the change of jerk. As one of the optimal solutions of both time optimality and jerk continuity, sinusoidally limited-jerk trajectory is proposed in this chapter.

Selecting a sinusoidal jerk waveform as given in Eq.(2.3) guarantees to have a limited-jerk for the desired motion [11].

$$J(t) = \widehat{J} \sin\left(\frac{2\pi}{T}t\right) \tag{2.3}$$

where $\widehat{J}$ is the jerk coefficient, t is the real time of the motion and T is the duration of acceleration period.

Integrating the jerk in Eq.(2.3) gives the acceleration of the load:

$$Acc(t) = \frac{\widehat{J}T}{2\pi}\left(1 - \cos\left(\frac{2\pi}{T}t\right)\right) \tag{2.4}$$

Since it is important to keep continuity of the acceleration both at the staring and at the end of acceleration periods, the first term in the Eq.(2.4) is selected as a constant for the integral operation.

Integrating the acceleration over the speeding up period gives the velocity of the load and its change by the time is given in Eq.(2.5).

$$V(t) = \frac{\widehat{J}T}{2\pi}t - \frac{\widehat{J}T^2}{4\pi^2}\sin\left(\frac{2\pi}{T}t\right) \tag{2.5}$$

At the end of the period T, the velocity of the motor reaches to its final value as given in Eq.(2.6).

$$V(T) = \frac{\widehat{J}T^2}{2\pi} \tag{2.6}$$

If the position of the motor is also needed to be controlled, by integrating the velocity of the motor, the change of the position during the acceleration period becomes as in the equation below:

$$P(t) = \frac{\widehat{J}T}{4\pi}t^2 - \frac{\widehat{J}T^3}{8\pi^3}\left(1 + \cos\left(\frac{2\pi}{T}t\right)\right) \tag{2.7}$$

At the end of the acceleration period, the position of the motor becomes equal to the value that is given in Eq.(2.8). At this point velocity of the motor is different from zero and motion is not finalized. To reach the desired final position, the velocity is needed to be reduced to be zero.

$$P(T) = \frac{\widehat{J}T^3}{4\pi} \tag{2.8}$$

For decelerating the system, the jerk gets a negative sign. This change affects all of the equations as given in (2.9-2.12).

$$J(t) = -\widehat{J}\sin\left(\frac{2\pi}{T}t\right) \tag{2.9}$$

$$Acc(t) = \frac{\widehat{J}T}{2\pi}\left(\cos\left(\frac{2\pi}{T}t\right) - 1\right) \tag{2.10}$$

$$V(t) = \frac{\widehat{J}T^2}{2\pi} - \frac{\widehat{J}T}{2\pi}t + \frac{\widehat{J}T^2}{4\pi^2}\sin\left(\frac{2\pi}{T}t\right) \tag{2.11}$$

$$P(t) = \frac{\widehat{J}T^2}{2\pi}t - \frac{\widehat{J}T}{4\pi}t^2 + \frac{\widehat{J}T^3}{8\pi^3}\left(1 - \cos\left(\frac{2\pi}{T}t\right)\right) \tag{2.12}$$

Using the suggested sinusoidal limited-jerk trajectory, final values of the jerk, acceleration and the velocity become zero as shared in Fig. 2.5.

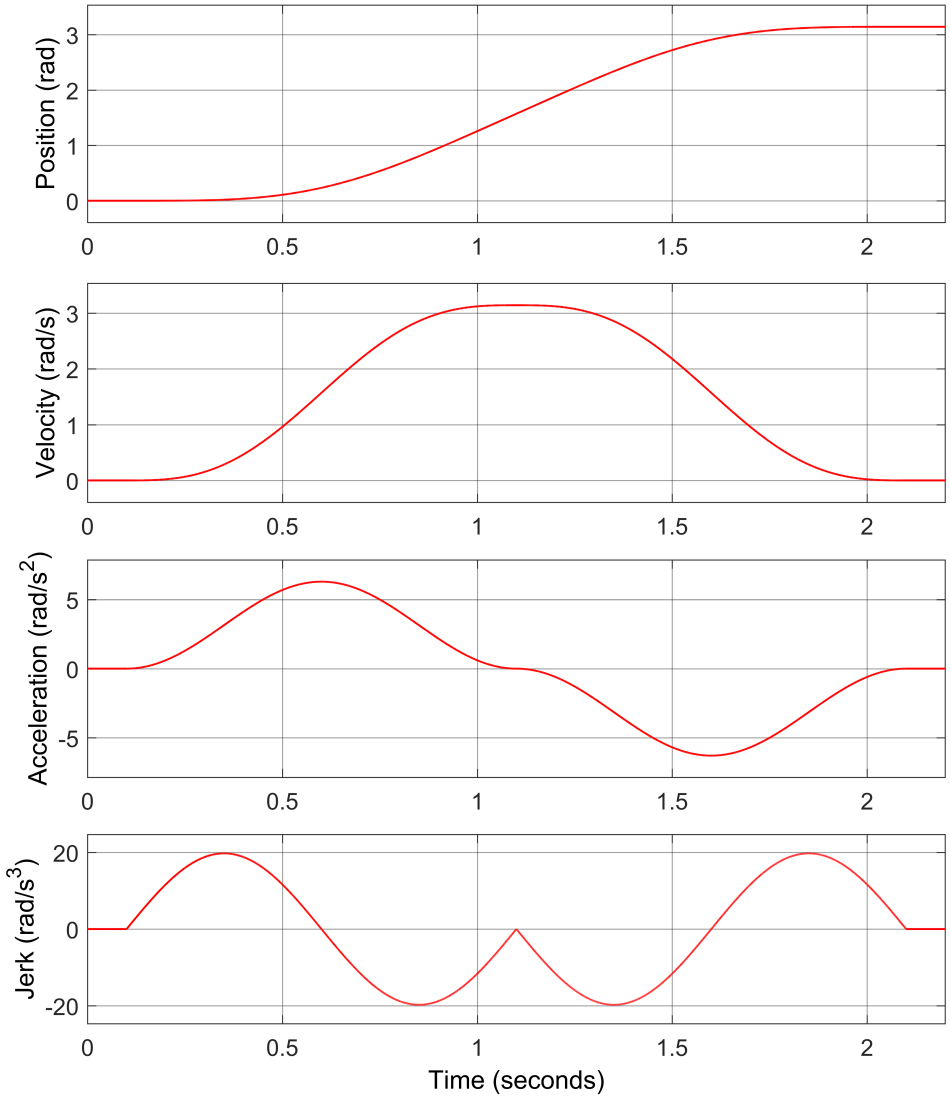

Figure 2.5: Limited-jerk sinusoidal trajectory kinematic profiles

The position equality defined in Eq. (2.12) can be updated by adding another term that represents the duration of the constant velocity motion:

$$P(t) = P^* + \frac{\widehat{J}T^2}{2\pi}t - \frac{\widehat{J}T}{4\pi}t^2 + \frac{\widehat{J}T^3}{8\pi^3}\left(1 - \cos\left(\frac{2\pi}{T}t\right)\right) \tag{2.13}$$

If this interval is zero, P^* becomes equal to the term in Eq. (2.8). In all cases it becomes equal to the definition in Eq. (2.14), where T^* is the duration of the constant velocity.

$$P^* = \frac{\widehat{J}T^2}{2\pi}T^* + \frac{\widehat{J}T^3}{4\pi} \tag{2.14}$$

After defining the motion, the final position of the system is calculated as in Eq. (2.15).

$$P(2T + T^*) = \frac{\widehat{J}T^2}{2\pi}T^* + \frac{\widehat{J}T^3}{2\pi} \tag{2.15}$$

By using the defined equations for the motion, Fig. 2.6 is prepared and continuity of the jerk is guaranteed to minimize torque ripples and vibrations of the system.

The key factor for deciding the jerk coefficient $\widehat{J}$ is the comparison of the position control closed-loop system characteristic with the frequency spectrum of the designed position trajectory. If this trajectory's frequencies are inside of the position closed-loop H_∞ controller's bandwidth, there cannot be any discontinuity in the jerk. As the spectrum approaches to the cut-off frequency of the position control, time optimality is also achieved. Fig. 2.7 is the frequency spectrum of P(t) up to 15 Hz that changes rotor angle from 0° to 180° in 2 seconds. Numerical values in this profile are selected as example and independent from the system used in this study.

In comparison of all three methods, smoothness of the motion is increased as higher derivative of the position is limited. With the first profile, velocity is limited with a constant value but acceleration is not controlled. Parabolic profile offers constant acceleration but still jerk is discontinuous. Both of these options create impulsive jerks in the mechanical system which is bad for the lifetime of the components [8].

Fourier's analyses of the different position references also show that as the limitation of the jerk is increased, amplitudes of the harmonics with lower frequencies in the spectrum are getting greater. This difference can be used to indicate that the motion with sinusoidal limited-jerk can be controlled better compared to the others since the required bandwidth of the controller is lower. To reduce the negative effect of the controller and to have a system with better accuracy, H_∞ controller is chosen to be used for this study and system identification is used to create preliminary information about the system for controller design. Details of these steps are given in Chapter 3.

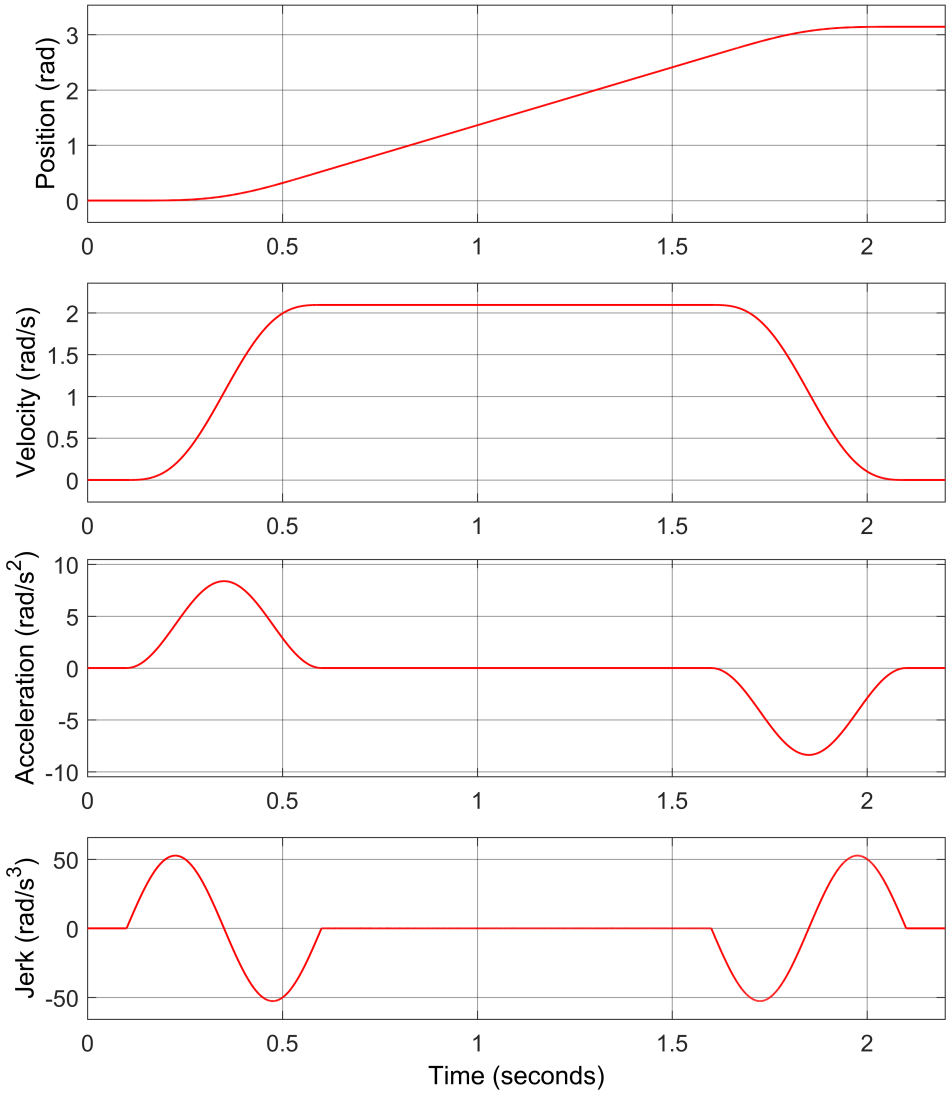

Figure 2.6: Kinematic profiles for limited-jerk sinusoidal trajectory with constant velocity region

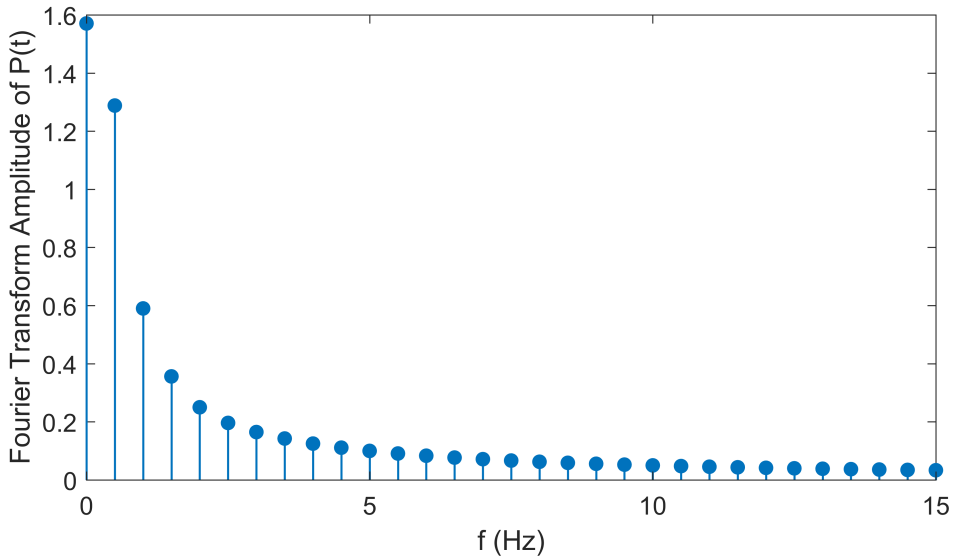

Figure 2.7: Single-sided amplitude spectrum of the sinusoidal limited-jerk position reference

CHAPTER 3

SYSTEM IDENTIFICATION AND H_∞ CONTROLLER DESIGN

Moving a mechanical load with an electrical machine consists of different steps such as creating a reference signal, converting it to the electrical domain and creating the electromechanical torque in the motor. Details of trajectory selection for creating the reference and the field oriented control method as an electromechanical motor control technique are already given in the previous chapters; now in this chapter, controller design is going to be defined to complete all the necessary steps to create a motion. In this study, H_∞ controller is chosen for the velocity and the position loops and system identification is used to provide preliminary information for controller design process.

3.1 Introduction to Identification

Model building through observations is not only applicable for living species but also plays a very important role in many branches of science. Despite the observations through our senses, scientific observations are often made via measurement instruments or sensors [25].

Identification is the exercise of developing a mathematical relationship between the inputs and the outputs of a system based on observed or measured data. In another words, identification establishes a mathematical map between the input and output spaces determined by the data as shown in Fig. 3.1. The input and output terms in identification have generic meanings for most of the processes. Outputs are all of those signals that are measured or observed. However, inputs collectively refer to all variables that are considered to influence the outputs [26].

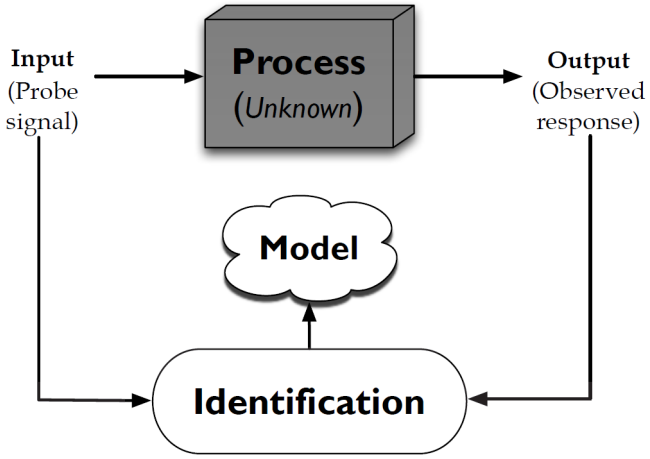

Figure 3.1: Illustration of identification

It is possible to consider the system identification (SI) as a bridge between the real world and the mathematical world of systems used in controls [26]. From the motor control point of view, system identification is an indispensable approach to define the system's open-loop characteristic that plays an important role in the optimal controller design [6]. Even if all parameters of the motor and the mechanical load are known, still a very complex work is required to calculate an open-loop system characteristic from the mathematical equations. Once parasitic effects and unexpected variations are included, the difference between the open-loop characteristics of the real and modeled systems would be much higher. In fact, accurately estimating the certain motor parameters is difficult [27]. For this reason, the system identification's feedback to the controller design plays an important role in the control theory.

3.1.1 Facts of Identification

The SI algorithm has a natural flow: first observe or measure as much as data, then choose a set of models and then pick the best one in this set. It is necessary to go back and check the steps of the procedure if the created model does not satisfy the expectations. The model may be insufficient for a variety of reasons [28]:

• Criterions were not appropriate enough to meet the expectations.

• The numerical procedure could not find the best model according to the criterations.

• The measured data set was not informative enough to provide guidance in selecting a good set of models.

• The model set was not good enough and it did not contain any appropriate model that describes the system.

The real-life actual system is a different kind of object than our mathematical models. Even if the outcomes of a mathematical model is very close to the outcomes of the real system, there are always inevitable differences between them. These differences might be reduced using true identification approaches but can never be fully eliminated. Therefore, from the system identification point of view, the target is creating an useful system model rather than the true one. This fiction is very helpful for designing the identification methods and understanding their properties. In such a case, it is assumed that obtained data have been collected with well defined mathematical codes and idealization rules [28].

Concerning the precision and accuracy of builded mathematical model, there are three universal facts of identification which provide guide for identification paths [26]:

1. Building an accurate model is not usually possible using finite-sample data for the systems with high order. It is also not possible to establish a proper model using data contaminated with errors. Mismatch of model and process is another important factor. Defining the specifications in an inappropriate way leads to systematic errors in model estimates and predictions. These kind of estimations and predictions are considered as *biased* and the biggest effort in the estimation is to produce the *unbiased* estimates. The successful way to this target passes from correctly specifying the model structure, using very large observations and choosing the estimation method properly. When all of these targets are achieved, the model is considered as *asymptotically unbiased*.

2. Variety of the data is a critical fact for estimating a precise model. A single set of data that is collected from the same experiment is only one of the several possible data sets. Therefore estimated model might not cover the various other possible realizations. Repeating an experiment produces different sets of data and it helps to minimize the negative effects of disturbances and measurement noises. The models that are builded with a wide range of data can have a high randomness property and

they can cover more states of the real process. Thus, the variability in data manifests as *impreciseness* in estimates. It is possible to model the variability statically using the term of variance. It is expected from each proper model to decrease the variance to zero. But it can be hardly never possible to have it using finite-length data. However, it can be achievable under asymptotic conditions and this is a highly desirable property of every estimator.

3. The accuracy and precision of the optimally identified model, among other factors, is critically dependent on the **input type** and **the signal-to-noise ratio** achieved in the measurement. A generalized term capturing both of these aspects is information.

3.2 Mathematical Background of the Numerical Algorithms for Subspace State Space System Identification Method

In order to estimate the system model with unknown parameters, a subspace identification algorithm namely the numerical algorithms for subspace state space system identification (N4SID) [29] is selected for this study.

3.2.1 Subspace Identification

The dynamic subspace identification methods are commonly used in linear time invariant systems which are operating in discrete time [30]. It is possible to describe these systems in the following form:

$$x(k+1) = Ax(k) + Bu(k) + Ke(k) \tag{3.1}$$

$$y(k) = Cx(k) + Du(k) + e(k) \tag{3.2}$$

where $u(k)$ is the input, $y(k)$ is the output, $x(k)$ is the state and K is the Kalman filter gain, $e(k)$ is independent of past input and output matrices since it is zero-mean Gaussian white noise. A, B, C, D are the state space representation matrices.

In the subspace identification method, it is aimed to determine the A, B, C, D system matrices using a set of input-output measurements.

3.2.2 Subspace Matrix Equation

After performing sequential iterations in Eq. (3.1) and Eq. (3.2), following matrix equation can be derived [30]:

$$Y_f = \Gamma_i X_f + H_i^d U_f + H_i^s E_f \tag{3.3}$$

where the matrices with sub-index f represents future for the input matrix U, the output matrix Y and the noise innovation matrix E; Γ_i is the extended observability matrix and H matrices are defined as in the following form:

$$H_i^d = \begin{bmatrix} D & 0 & \dots & 0 \\ CB & D & \dots & 0 \\ \vdots & \vdots & \ddots & \vdots \\ CA^{i-2}B & CA^{i-3}B & \dots & D \end{bmatrix} \tag{3.4}$$

$$H_i^s = \begin{bmatrix} I & 0 & \dots & 0 \\ CK & I & \dots & 0 \\ \vdots & \vdots & \ddots & \vdots \\ CA^{i-2}K & CA^{i-3}K & \dots & K \end{bmatrix} \tag{3.5}$$

The past and future input block-Henkel matrix can be defined as

$$U_p = \begin{bmatrix} u_0 & u_1 & \dots & u_{j-1} \\ u_1 & u_2 & \dots & u_j \\ \vdots & \vdots & \ddots & \vdots \\ u_{i-1} & u_i & \dots & u_{i+j-2} \end{bmatrix} \tag{3.6}$$

The required states can be defined as in the following form:

$$X_p = X_0 = \begin{bmatrix} x_0 & \dots & x_{j-1} \end{bmatrix} \tag{3.7}$$

$$X_f = X_i = \begin{bmatrix} x_i & \dots & x_{i+j-1} \end{bmatrix} \tag{3.8}$$

The extended observability matrix Γ_i is given by

$$\Gamma_i = \begin{bmatrix} C \\ CA \\ \vdots \\ CA^{i-1} \end{bmatrix} \tag{3.9}$$

3.2.3 Orthogonal Projection

The orthogonal projection of row spaces of A_x and B_x is

$$A_x/B_x = A_x B_x (B_x B_x^t)^\dagger B_x \tag{3.10}$$

where $(B_x B_x^t)^\dagger$ denotes the Moore-Penrose pseudo-inverse of the matrix $B_x B_x^t$. The projection of the row space of A_x into the orthogonal complement of the row space of B_x is given in Eq. (3.11).

$$A_x/B_x^\perp = A_x - A_x/B_x \tag{3.11}$$

3.2.4 Oblique Projection

The oblique projection of the row spaces of G along with H into the J is,

$$G/H^J = (G/H^\perp)(J/H^\perp)^\dagger J \tag{3.12}$$

Properties of the orthogonal and the oblique projections are given below. Their proof can be found in [29].

$$A_x/A_x^\perp = 0 \tag{3.13}$$

$$A_x/{}_{A_x}C_x = 0 \tag{3.14}$$

3.3 Details of N4SID Method

The N4SID method helps to solve the problem in the Section 3.2.2 by using the past and future Kalman filter state sequence. Equation (3.15) can be written using the theorems in [29].

$$\tilde{X}_i = \Gamma_i^{\dagger}\Theta_i \tag{3.15}$$

where $\Theta_i = Y_f/_{U_f}W_p$ which is achieved by performing an oblique projection of Eq. (3.3), along row space U_f onto the row space of W_p:

$$Y_f/_{U_f}W_p = \Gamma_i X_f/_{U_f}W_p + H_i^d U_f/_{U_f}W_p + H_i^s E_f/_{U_f}W_p \tag{3.16}$$

Using the second property of the oblique projection that is given in Eq. (3.14), it is possible to eliminate the second term of Eq. (3.16) since it is equal to zero. The last term of Eq. (3.16) can also be eliminated with the assumption that the noise is not correlated with input and output past data [29], and Eq. (3.16) can be simplified to:

$$Y_f/_{U_f}W_p = \Gamma_i \tilde{X}_i \tag{3.17}$$

where $\tilde{X}_i = X_f/_{U_f}W_p$ and $W_p = [U_p^t Y_p^t]^t$. By using this information, it is possible to rewrite the Eq. (3.17) as

$$\Theta = \Gamma_i \tilde{X}_i \tag{3.18}$$

Eq. (3.18) shows that the column space of Γ_i can be calculated by the singular-value decomposition (SVD) of Θ and Γ_i can be calculated as in the following form:

$$\Gamma_i = U_1 S_1^{1/2} \tag{3.19}$$

Knowledge of Θ and Γ_i is enough to calculate $\tilde{X}_i$ by using the Eq. (3.6) it becomes possible to calculate $\tilde{X}_{i+1}$ as

$$\tilde{X}_{i+1} = \Gamma_{i-1}^{\dagger}\Theta_{i+1} \tag{3.20}$$

where $\Theta_{i+1} = Y_f^-/_{U_f^-}W_p^+$ and Γ_{i-1} represents the matrix Γ_i without the last l rows [30].

By using the past and future, input and output matrices LQ decomposition of the big

matrix can be performed as in 3.21. [26].

$$\begin{bmatrix} U_f \\ W_p \\ Y_f \end{bmatrix} = \begin{bmatrix} L_{11} & 0 & 0 \\ L_{21} & L_{22} & 0 \\ L_{31} & L_{32} & 0 \end{bmatrix} \begin{bmatrix} Q_1^T \\ Q_2^T \\ Q_3^T \end{bmatrix} \tag{3.21}$$

where L is the lower triangular matrix and Q is the orthogonal matrix.

Oblique projection can be computed using the following equation:

$$\Gamma_i = L_{32} L_{22}^{\dagger} W_p \tag{3.22}$$

SVD of the oblique projection can be performed to obtain estimates of state sequence X_f and extended observability matrix $\mathcal{O}_i$:

$$X_f = T^{-1} \Sigma_1^{1/2} V_1^T \tag{3.23}$$

$$\mathcal{O}_i = U_1 \Sigma_1^{1/2} T \tag{3.24}$$

where T is the controllability matrix, U and V are the left and right singular vectors corresponding to the user-identified insignificant singular value in Σ_1. The right hand side matrices are obtained from the SVD of Γ_i.

$$\Gamma_i = \begin{bmatrix} U_1 & U_2 \end{bmatrix} \begin{bmatrix} \Sigma_1 & 0 \\ 0 & 0 \end{bmatrix} \begin{bmatrix} V_1 \\ V_2 \end{bmatrix} \tag{3.25}$$

Using estimated state space sequence as a least squares solution, state space matrices can be computed:

$$\begin{bmatrix} \tilde{X}_{i+1} \\ \tilde{Y}_i \end{bmatrix} = \begin{bmatrix} A & B \\ C & D \end{bmatrix} \begin{bmatrix} \tilde{X}_i \\ \tilde{U}_i \end{bmatrix} \tag{3.26}$$

where,

$$\tilde{X}_{i+1} = \begin{bmatrix} x[i+1] & \dots & x[i+N-1] \end{bmatrix}$$

$$\tilde{X}_i = \begin{bmatrix} x[i] & \dots & x[i+N-2] \end{bmatrix}$$

$$\tilde{Y}_i = \begin{bmatrix} y[i] & \dots & y[i+N-2] \end{bmatrix}$$

$$\tilde{U}_i = \begin{bmatrix} u[i] & \dots & u[i+N-2] \end{bmatrix}$$

As the final step of the system identification process, a very useful system model can be obtained in the state space representation form. This model can be used for any purpose since it is the representative of the real system. For most of the real life examples, system models are used in the simulations to reduce the costs of the experimental studies and to have opportunity for trying different scenarios which are not suitable for real systems.

In this study, system identification is performed for the velocity and the position open-loops. The identified models are used as input to the velocity and the position controller design phases which are H_∞ optimal method for loop shaping control synthesis.

3.4 Introduction to H_∞ Controller Design

The robust stability problem of closed-loop systems has been receiving attention since 1980s. Exclusively, the H_∞ approach to optimal control system design and analysis has proved promising outcomes in robust stabilization of systems with unstructured uncertainties. Unstructured uncertainty is lack of information available except that boundaries on its magnitude [31]. In the design of H_∞ optimal controller, it is important to model uncertainty as another transfer function of the nominal plant model.

Generic H_∞ controller design techniques assume unity signals and aim to calculate a feasible controller that makes the closed-loop system input-output H_∞ gain less than one. Fig. 3.2 shows the closed-loop system with the plant G and the controller K that generic design algorithm assumes.

In this representation, w is the input reference and the disturbances, u is the control signal, y is the measured sensor output of the plant and z is the output signal to be minimized. For a plant G, generic H_∞ control algorithm calculates a controller K that makes closed-loop H_∞ gain from w to z less than one [32].

In this study, H_∞ optimal control method for loop shaping synthesis is used to compute a stabilizing H_∞ controller (K) for linear time-invariant plant G to shape the frequency response of the loop transfer function GK to have desired loop shape G_d.

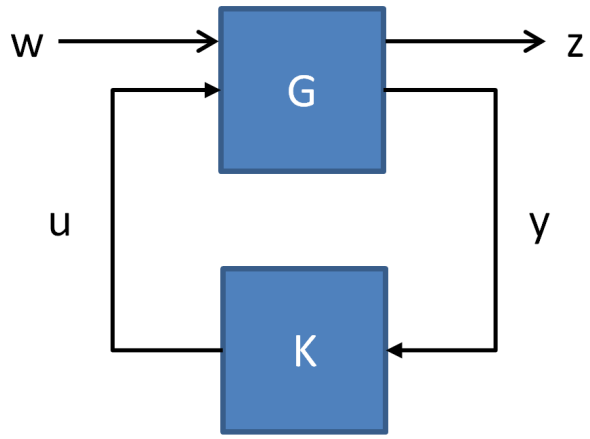

Figure 3.2: Closed-loop system representation for a generic H_∞ synthesis algorithm

3.4.1 H_∞ Optimal Method for Loop Shaping Control Synthesis

Using the greatest common divisors (GCD's) formula given in [33], H_∞ optimal controller design method first computes a stable, minimum-phase loop-shaping, squaring-down prefilter W such that the shaped plant is square. The desired shape G_d is achieved with very good accuracy in the $\{\omega_{min}, \omega_{max}\}$ frequency range by the shaped plant as in Eq. (3.27).

$$\sigma(G_d) \approx \sigma(G_s) \text{ for all } \omega \in \{\omega_{min}, \omega_{max}\} \tag{3.27}$$

Once this step is completed, normalized coprime-factor control synthesis theory, as defined in [31], is used to compute an optimal loop shaping controller for the shaped plant. If the plant G is a continuous time, linear time-invariant system such as in electrical motor control applications, then for having a GW that achieves a perfect accuracy fit for all frequencies ω, G has to have following properties;

1) It is needed to have a full rank D matrix which is in state space representation,

2) G should not have finite zeros on the $j\omega$ axis,

3) Frequency range of G is needed to be in the right-hand side of the $j\omega$ axis.

Otherwise, a bilinear pole-shifting transformation is required such as defined in [34].

All of these required properties of G are achievable for the open-loop electrical motor control applications. Therefore this method can be applied to the controller design phases for the velocity and the position loops during the simulation and the experimental tests of the system with PMSM. Since open-loop system transfer function provides input for the controller design phase, N4SID method works in harmony with the H_∞ optimal controller design method.

Throughout the simulation and the experiment phases of the study, system identification and controller design methods given in this chapter are applied by using the related tools of MATLAB. For both of these domains transfer functions of the velocity and the position loops are identified as post-processing actions and corresponding controllers are calculated. Details of these actions are shared in the following two chapters.

CHAPTER 4

SIMULATION RESULTS AND COMPARISON

After all necessary steps to develop an electromechanical system are defined, now a simulation setup in the Simulink environment is going to be established to create the links between these different steps and results of the simulations are going to be compared for the system which its block diagram is given in the Fig 4.1. After the the field oriented control is achieved for the open-loop voltage control of the system, the current loop is going to be tuned and then the velocity and the position loops are going to be identified one by one and their controllers are going to be designed.

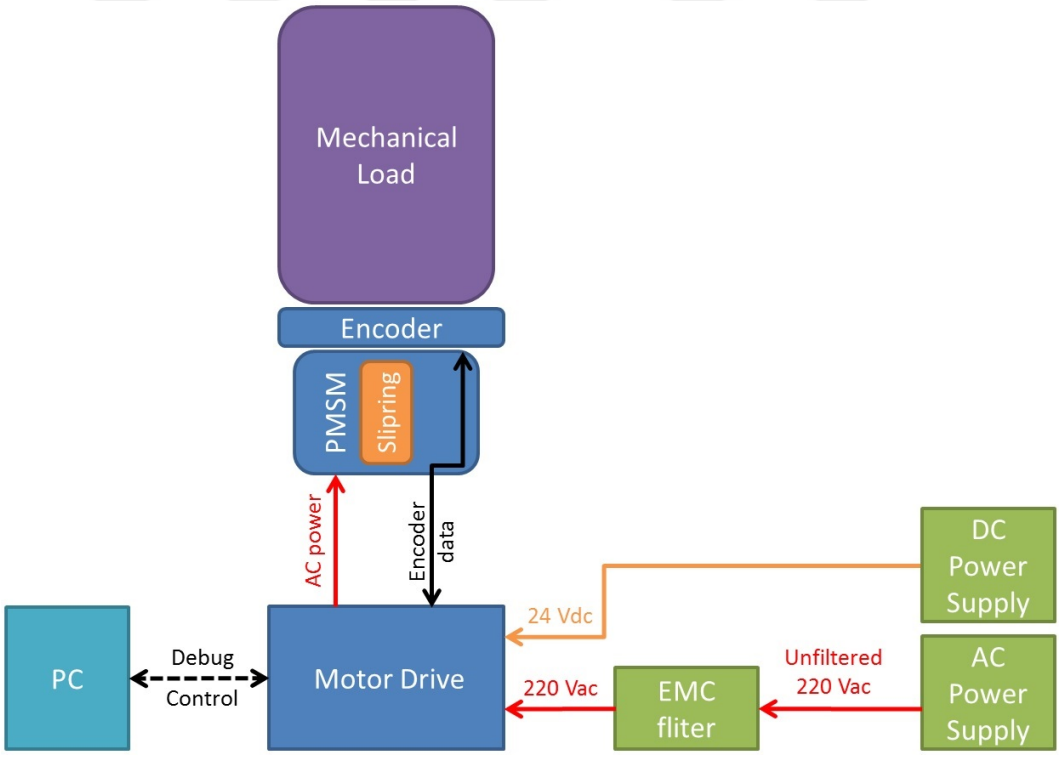

Figure 4.1: Block diagram of the experimental test setup

The electromechanical prototype, which is developed for a radar motion control system, is established as in the Fig 4.2 and real values in Table (4.1) are also used for the simulation of the system that controls a direct drive permanent magnet synchronous motor with a custom design motor drive. The electronic system is supplied from an AC source and motor drive rectifies the AC input voltage to charge inverter's DC bus capacitance. Since a direct drive motor is preferred with a large inner hallow shaft and it has 16 pole pairs, any additional gears are not required to cover torque demand of the mechanical system. Static and dynamic frictions are related with the slip ring that is located inside the inner gap of the motor. The inertia value is calculated through the mechanical design environment of the system.

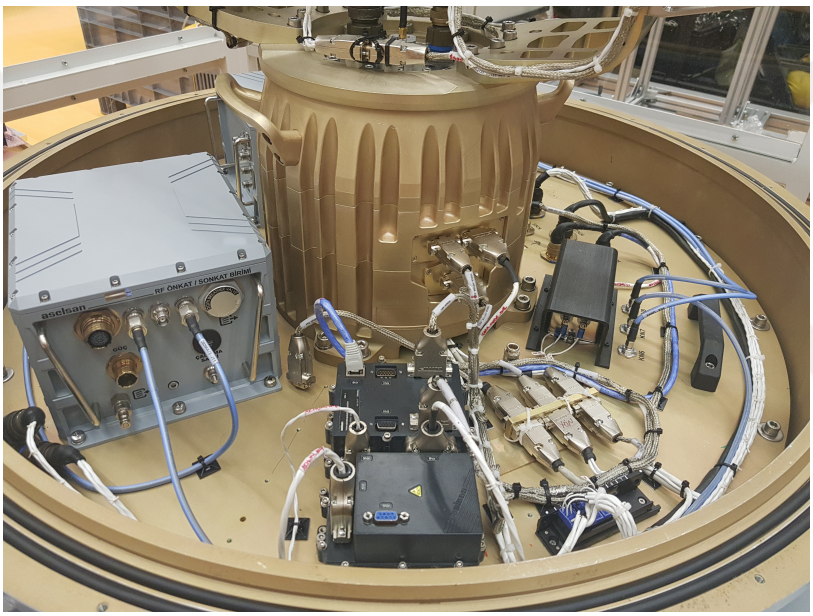

Figure 4.2: Experimental test setup (only the inverter and the motor)

Importance of the jerk limitation even for a system with low inertia is already studied in [35]. Even if the acceleration is smooth for the system, discontinuous jerk can still create vibration for the mechanical system and it may effect the service life and the quality of the motion [8]. In this chapter, simulation parameters are selected from a real industrial system and a similar electromechanical system is defined according to the selected system. The velocity and position control loops are identified, required controllers are tuned using the related techniques defined in the previous chapters. Closed-loop position control is achieved for three different trajectories that are defined in the Chapter 2 and results are shared at the end of the chapter.

Table 4.1: Motor, power electronics and load specifications

Parameter	**Value**
Rated continuous output power	2385 W
Speed at rated power	730 RPM
Starting torque of motor	0.407 Nm
Phase resistance	4.2 Ω
Stator d-axis inductance	46 mH
Stator q-axis inductance	46 mH
Number of poles	32
Continuous current	4.95 Arms
Back EMF constant	536 Vrms/kRPM
Switching frequency	20 kHz
DC bus voltage	311 V_{DC}
Motor and Load combined inertia	2.9 kg.m^2
Damping	1.1 Nm/(rad/s)
Static friction	5.3 N
Dynamic friction	4.5 N

4.1 Basic Control Loops and Tuning Processes

Details of the FOC is already given in the Section 1.1. In this part, all control loops are established, the velocity and the position open-loops are identified and required controllers are designed to successfully follow the reference values of different trajectories.

4.1.1 Open-Loop Voltage Control Simulation

Electromechanical system's simulation starts with the open-loop voltage control of the PMSM using the FOC method as defined in the Section 1.1.1. Motivation of this part is to see that all power electronic components are integrated, conversions between three phase rotating and two phase stationary domains are constructed and all of these parts work in a harmony with mechanical load as given in the Fig 4.3.

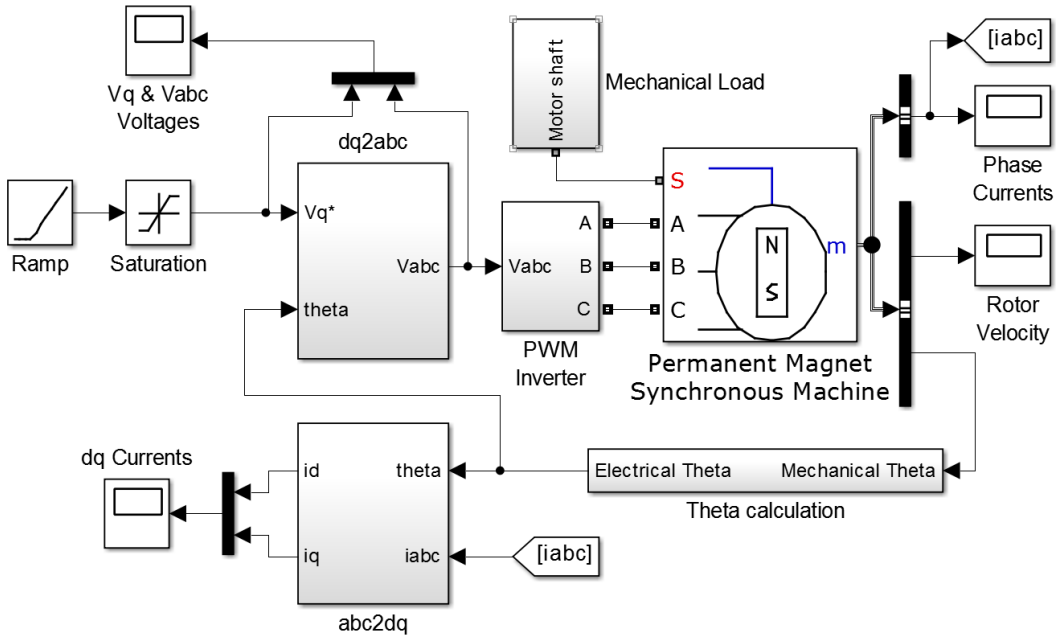

Figure 4.3: The model used in the open-loop voltage control simulation

Since a positive voltage value is applied as a reference to the q axis of the motor, it is expected to have three phase sinusoidal voltages as the input for the inverter. The inverter compares these references with the carrier signal and determines the gate signals of the switches. Sinusoidal voltages create sinusoidal phase currents since the motor is an inductive electrical load.

Q axis voltage reference is generated by a ramp and a saturation block to have a changing reference from 0 to 167 volts in 75 milliseconds as in Fig 4.4 together with the three phase a, b, c voltages. The reason for applying the sinusoidal references with a ramp function is to limit the instantaneous electromechanical torque demand at the beginning of the motion.

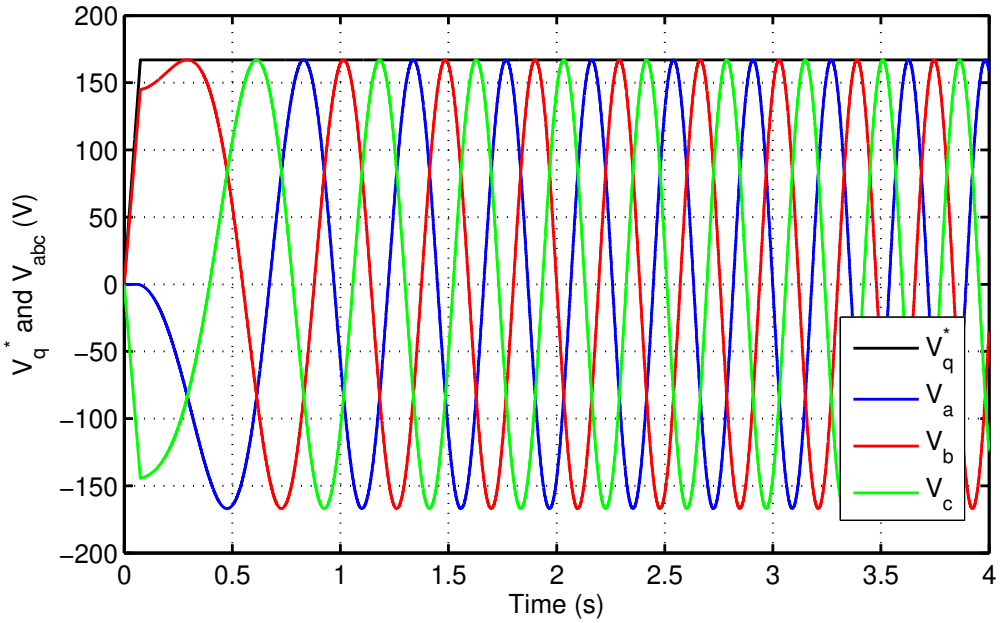

Figure 4.4: Quadrature and abc voltages of voltage loop simulation

As a result of the rotating magneto motive force (MMF) in the air gap of the motor, the rotor accelerates synchronously to the MMF and the position of the mechanical load changes by time as it is in the Fig 4.5.

The first graph in the Fig 4.5 yields to the position change of the load where the second one is for the electrical load angle change of the system. Difference between these two signals are directly related with the number of magnetic pole pairs of the motor.

The shared values until now are actually enough to complete the open-loop voltage simulation. However, the three phase currents are also monitored and $d-q$ axis currents are calculated using the electrical load angle information in the Clarke and Park's transformations. Both of these monitored and calculated currents are shared in the Fig 4.6 and they have components with higher frequencies which can be considered as oscillation. Not controlling these currents is the main reason for this situation. Sinusoidal voltages applied to the system do not create a perfectly smooth rotating MMF in the air gap of the motor due to the mechanical parts and the characteristics of the electrical machine.

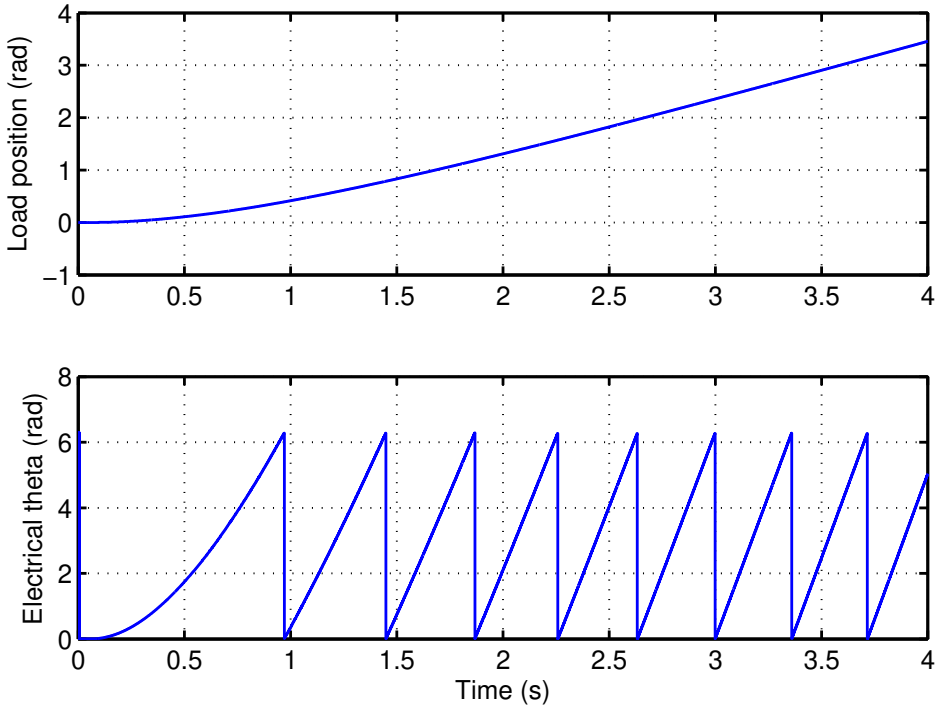

Figure 4.5: Mechanical and electrical rotor position of voltage loop simulation

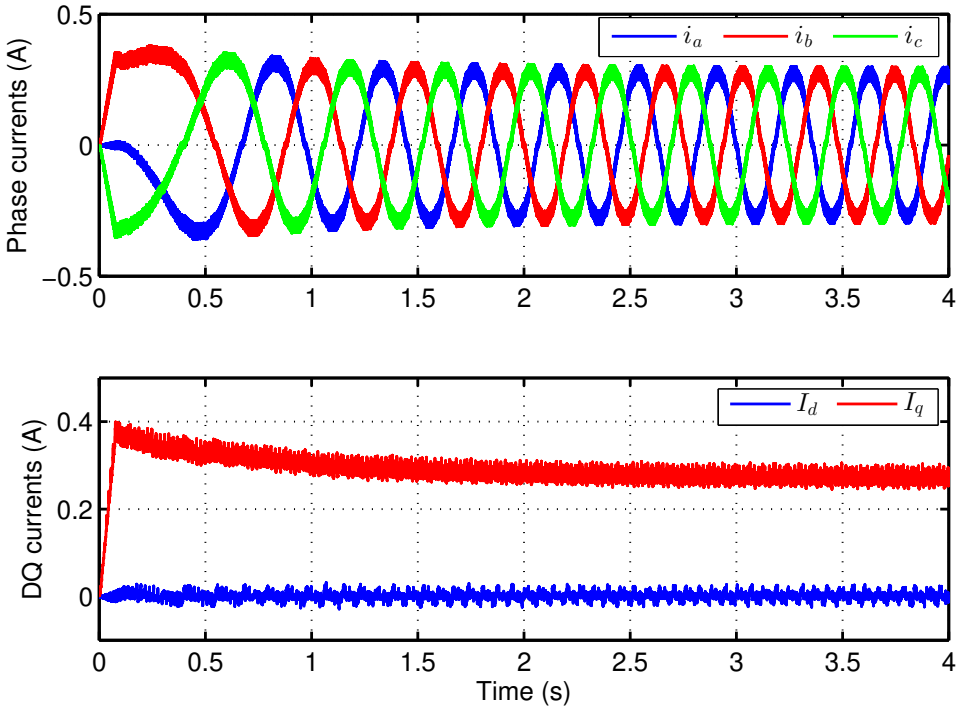

Figure 4.6: Voltage loop simulation quadrature and phase currents

Since the created torque greater than the mechanical torque in the opposite direction, the velocity of the motor changes as in the Fig 4.7. The motor stops its acceleration the motion continues with a constant velocity after the electrical and the mechanical torques are equal.

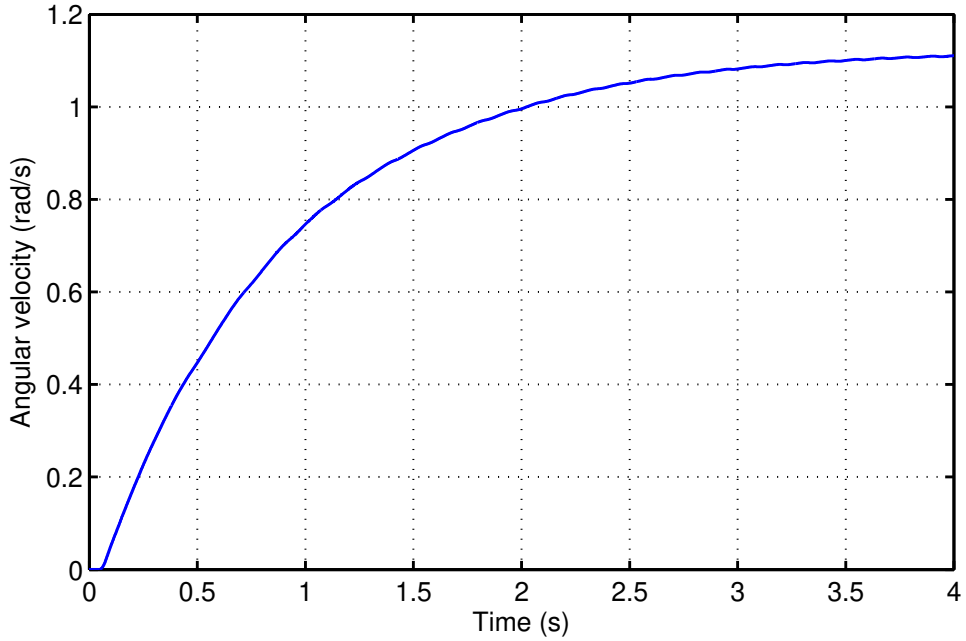

Figure 4.7: Angular velocity of the load for the voltage loop simulation

4.1.2 Closed-Loop Current Control Simulation

Current control loop is the first closed-loop control in the Field Oriented Control technique that its details are given in the Section 1.1.2. Controlling the quadrature current yields to the torque control of the motor, therefore this loop is also called as torque control loop. In addition to the voltage control loop, three phase current measurements and two phase synchronously rotating current calculations are also required in this level of control. To minimize the difference between the reference and the feedback values of the currents, current controllers are needed to be used for both direct and quadrature currents. The model that is created in the MATLAB - Simulink environment is used in the simulation of the closed-loop current control is given in the Fig 4.8.

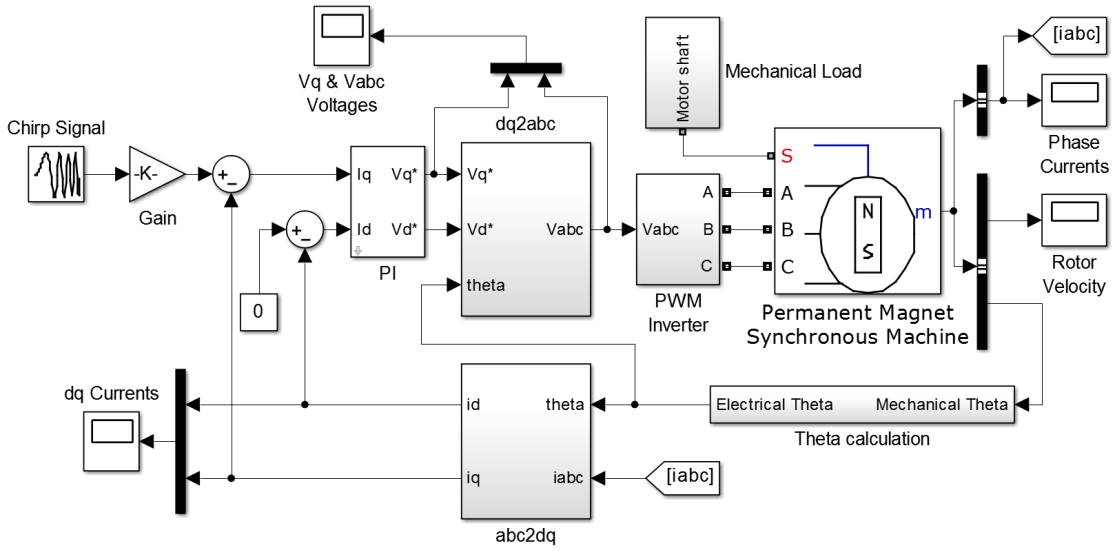

Figure 4.8: The model used in the closed-loop current control simulation

A standard PI controller is used in the simulation of the closed-loop current control and it is tuned with the Ziegler-Nichols tuning rules which its details are given in [4]. The controller that is designed with this method is given in Eq. 4.1 and used in the closed-loop current control simulation.

$$K_c(s) = \frac{1200(s + 0.011)}{s} \tag{4.1}$$

After the controller given in Eq. 4.1 is added to the loop, a sinusoidal chirp signal with increasing frequency from 0 to 100 Hz is used as the reference to the quadrature axis current. As it can be seen from the Fig 4.9, calculated values for the quadrature axis follows its reference either without any decrease in the magnitude or delay in time. Since the preferred motor is not salient, direct axis current does not help to the electromechanical torque and its reference is always zero. Therefore the reference of the direct axis is not plotted in the Fig 4.9. Even if the quadrature axis currents changes, the I_d current does not change thanks to the current decoupling application.

To be able to highlight the success of the current controller better for the targeted frequency, the last two periods of the direct and quadrature currents are given in the Fig 4.10. Even at 100 Hz, current controller achieves to make real current to follow reference current without any phase delay and magnitude difference.

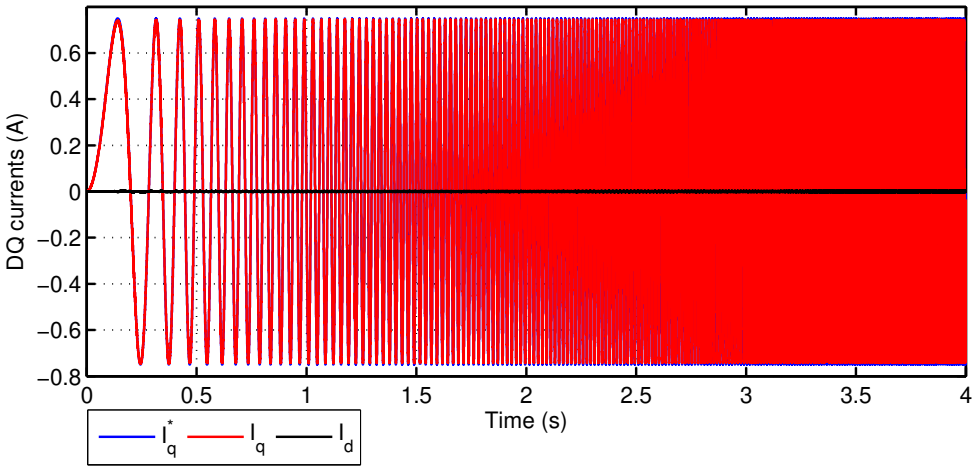

Figure 4.9: Current loop simulation quadrature and phase currents

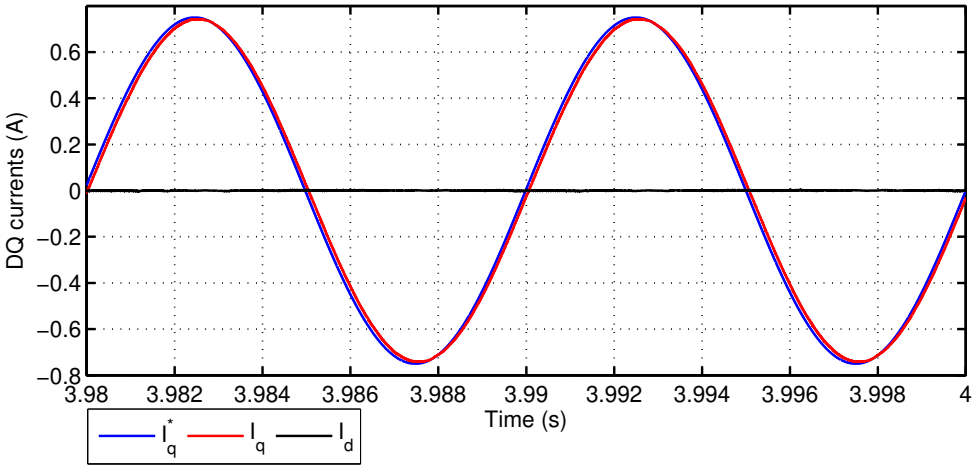

Figure 4.10: Current loop simulation quadrature and phase currents for 100 Hz

Once the electrical torque is greater than the static friction, the motor starts to rotate and accelerates as long as the difference is greater than zero. Once the magnitude of the reference starts to reduce, the motor slows down and accelerates in the opposite direction. As the frequency of the reference increases, the inertia of the load becomes more dominant and the magnitude of the velocity starts to decrease as it can be seen in the Fig 4.11.

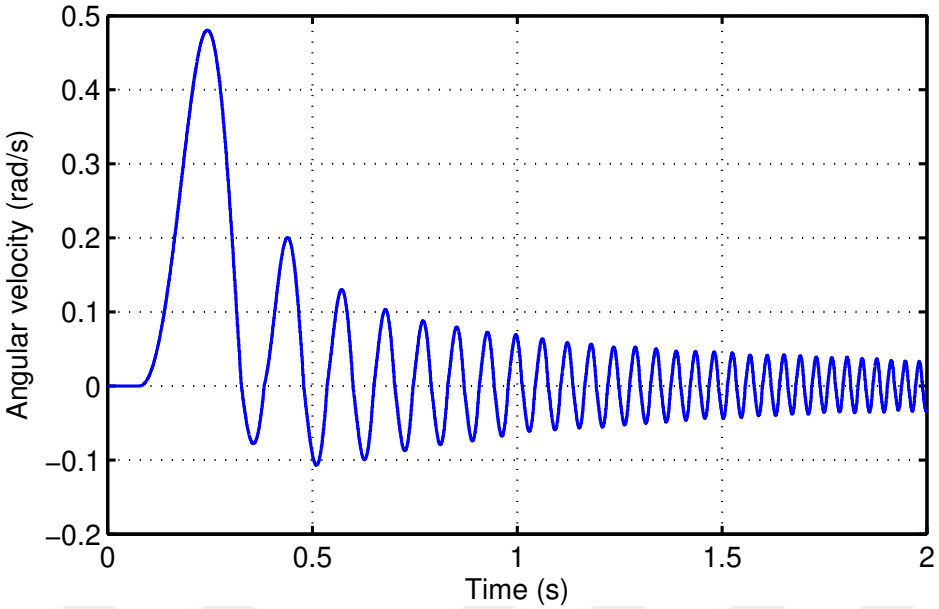

Figure 4.11: Angular velocity of the load for the current loop simulation

4.1.3 Closed-Loop Velocity Control Simulation

Closed-loop velocity control is one outer loop of the current control loop and its details are given in the Section 1.5. The target of this loop is to make electrical machine to follow the reference velocity within the targeted bandwidth of the closed-loop system. Basically, the velocity controller adjust the reference point of the current controller, depending on the error between the reference velocity and the measured system velocity, afterwards current control loop takes the responsibility for the rest. The MATLAB - Simulink simulation model that is used for the velocity control loop is given in the Fig 4.12.

4.1.3.1 Identification of Velocity Open-Loop

Identification of the velocity control loop is completed using the N4SID algorithm method which is described in Section 3.3. Since the velocity controller is not designed yet and since it is an open-loop identification, instead of using the model given in the Fig 4.12, the one that is used for the current control is used for the system identification process of the velocity loop.

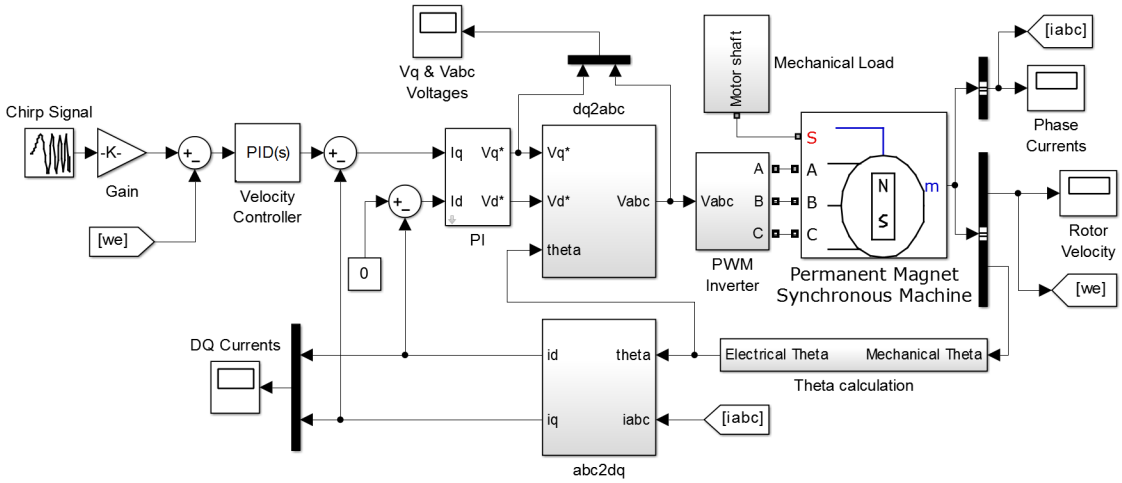

Figure 4.12: The model used in the closed-loop velocity control simulation

Co-sinusoidal chirp signal, between 0.5 Hz and 12.5 Hz frequencies, is applied as the input signal and velocity outputs are collected from the model given in the Fig. 4.8. Each frequency value is applied as a whole period to avoid having a non-zero averaged input signal. Sampling time of the simulation is selected as 250 nanoseconds to increase the number of samples in the dataset. After collecting the input/output data of the simulation as in Fig. 4.13, they are used in the N4SID algorithm.

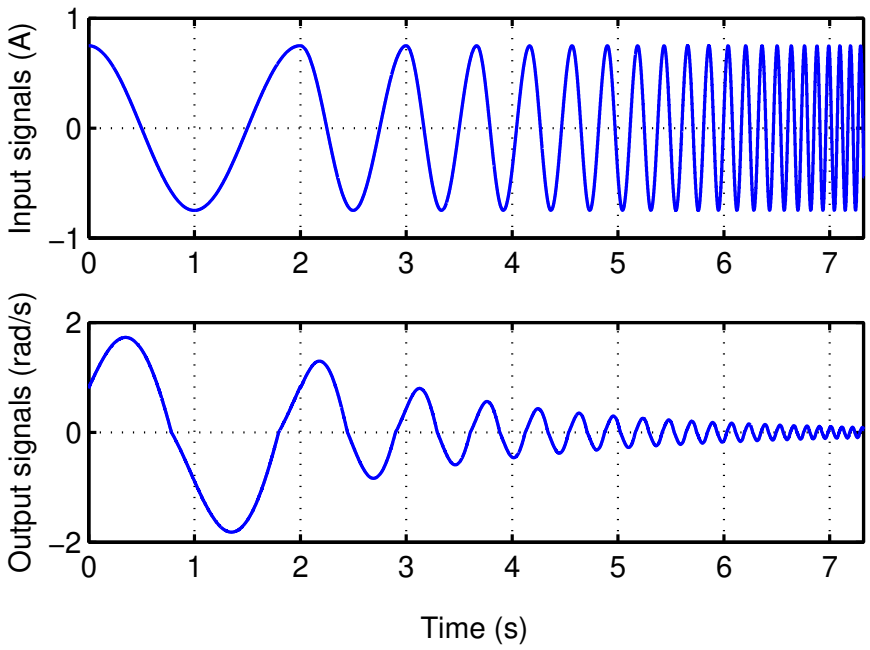

Figure 4.13: Input / output data of the open-loop velocity control

After the input and the corresponding output signals are obtained for different frequency levels, this dataset is used to obtain lower triangular matrix L and the orthogonal matrix Q, as the details of the steps are given in Section 3.3. By following the next steps in the same section, open-loop velocity state space model matrices are calculated as in the same form of Eq. (3.26) and results are given in Eq. (4.2):

$$A = \begin{bmatrix} -1.9 & 1.342 & 7.731 \\ -0.1061 & 632.1 & 6402 \\ -9.811 & -9032 & -2267 \end{bmatrix}, B = \begin{bmatrix} 107.7 \\ 89715 \\ -20973 \end{bmatrix} \tag{4.2}$$

$$C = \begin{bmatrix} 109.5 & -0.00208 & 0.0139 \end{bmatrix}, D = \begin{bmatrix} 0 \end{bmatrix}$$

Conversion between the state space model and the transfer function starts with the Laplace transformation of Eq. (3.26).

$$sX(s) = AX(s) + BU(s) \tag{4.3}$$

$$Y(s) = CX(s) + DU(s) \tag{4.4}$$

Since the desired transfer function is the ratio of $Y(s)$ and $U(s)$, $X(s)$ is needed to be removed from the equation. Solving the state Eq. (4.3) and putting the solution into the output Eq. (4.4) gives the transfer function of the same system.

$$X(s) = (sI - A)^{-1}BU(s) \tag{4.5}$$

$$Y(s) = C(s)[(sI - A)^{-1}BU(s)] + DU(s) \tag{4.6}$$

$$G(s) = \frac{Y(s)}{U(s)} = C(sI - A)^{-1}B + D \tag{4.7}$$

Open-loop velocity transfer function is obtained by putting the state space matrices into Eq. (4.7):

$$G_v(s) = \frac{1.13e4s^2 + 3.49e6s + 4.63e8}{s^3 + 1637s^2 + 5.64e7s + 1.07e8} \tag{4.8}$$

Comparison of the estimated model and the real system outputs are shared in the Fig. 4.14. The match between these two output waveforms is 96.37%.

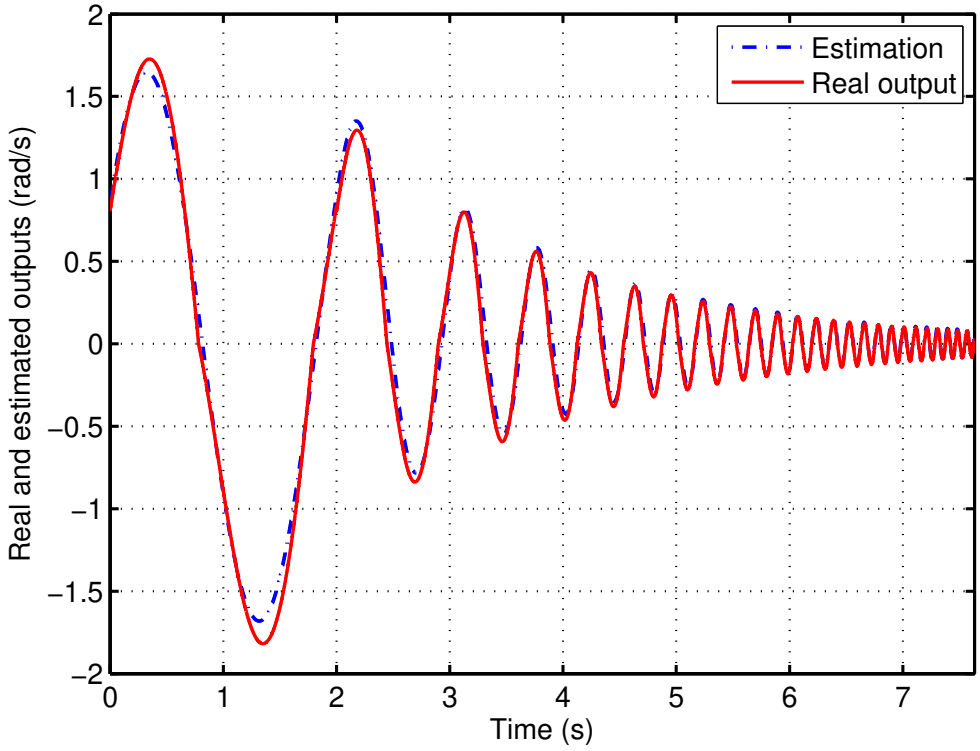

Figure 4.14: Identified system data of the velocity loop simulation

The open-loop system characteristic of the velocity loop that is shared in the Eq. (4.8). This transfer function is going to be used as a preliminary information for the controller design algorithm.

4.1.3.2 Velocity Loop Controller Design

The Fig. 4.14 shows that system identification that is given in Eq. (4.8) can be used as input to the H_∞ controller design process since it is a good representation of the real system. Details of this process are given in Chapter 3.4.1. Calculated velocity controller is given in Eq. (4.9) with a target close-loop control bandwidth of 10 Hz.

$$K_v(s) = \frac{32022(s+4096)(s+1.901)}{s(s+4096)(s+4220)} \tag{4.9}$$

Even if this controller can achieve a good performance in the closed-loop system, its high order requires complex processing for MCU in the real world and its simplification might bring advantages in the operation time of the control loop. After some pole-zero cancellations, order of the transfer function is reduced and updated version of Eq. (4.9) is given below:

$$K_v(s) = \frac{7.59(s + 1.901)}{s} \tag{4.10}$$

These two controllers have same characteristics until a certain frequency and their difference does not effect the performance of the closed-loop system in the focused bandwidth. Frequency responses of these two controllers are given in the Fig. 4.15.

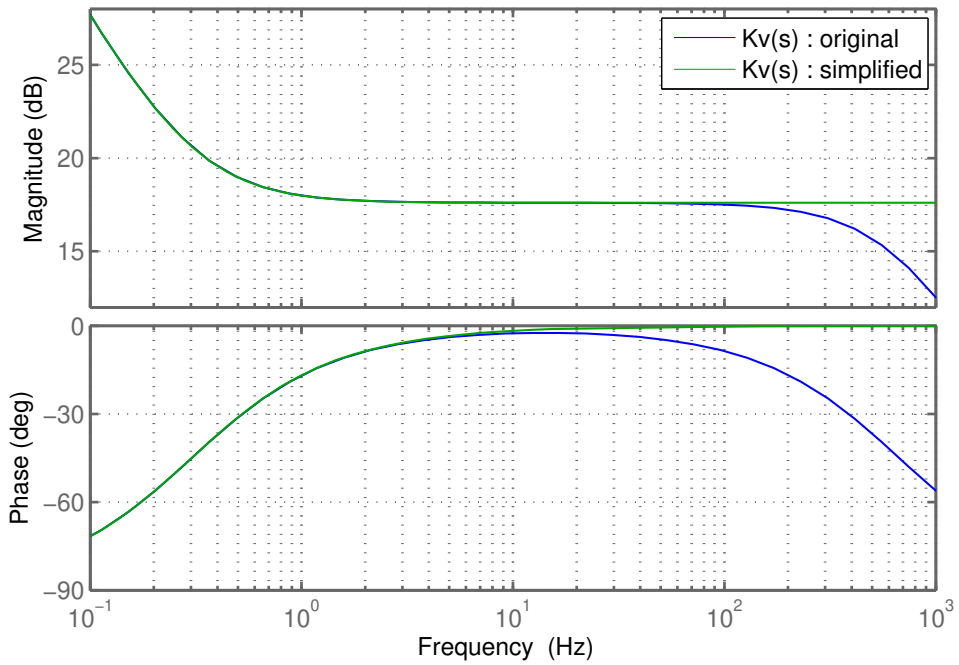

Figure 4.15: Comparison of original and simplified controllers

Original and simplified controllers are identical in the targeted bandwidth of the closed-loop system. Starting from 20 Hz, phase response of the simplified controller starts changing. Its magnitude margin is effected only after 100 Hz and it does not create a disadvantage for the closed-loop velocity control.

Controller that is given in the Eq. (4.10) corresponds to a PI controller. By integrating this controller into the simulation model given in the Fig 4.12, closed-loop velocity control is achieved and corresponding results are given in the Fig. 4.16 for the frequencies from 0.5 Hz to 12.5 Hz.

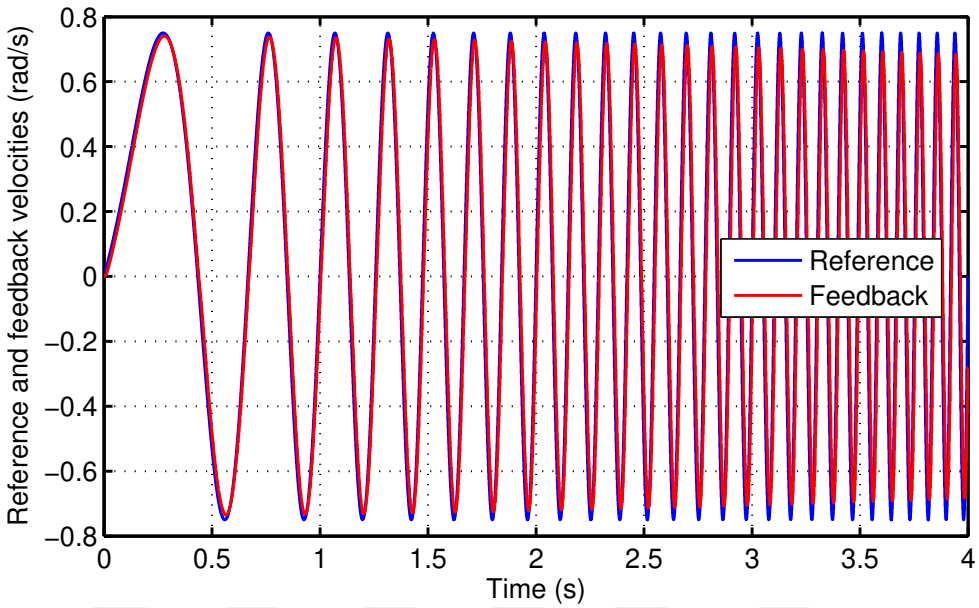

Figure 4.16: Closed loop velocity control of the tuned system

Since the targeted bandwidth of the closed-loop system is set as 10 Hz, performance of the controller is as expected for the selected bandwidth. Gain margin of the closed-loop system starts to drop as the frequency increases.

4.1.4 Closed-Loop Position Control Simulation

The last loop of the PMSM control series is the closed-loop position control. As defined in the Section 1.1.4, position control loop is the extended version of a velocity control loop with an additional position controller. In this section, design of the position controller is going to be completed after the open-loop position control system is identified. Final version of the position control loop, that can be used for different trajectories, is given in the Fig. 4.17.

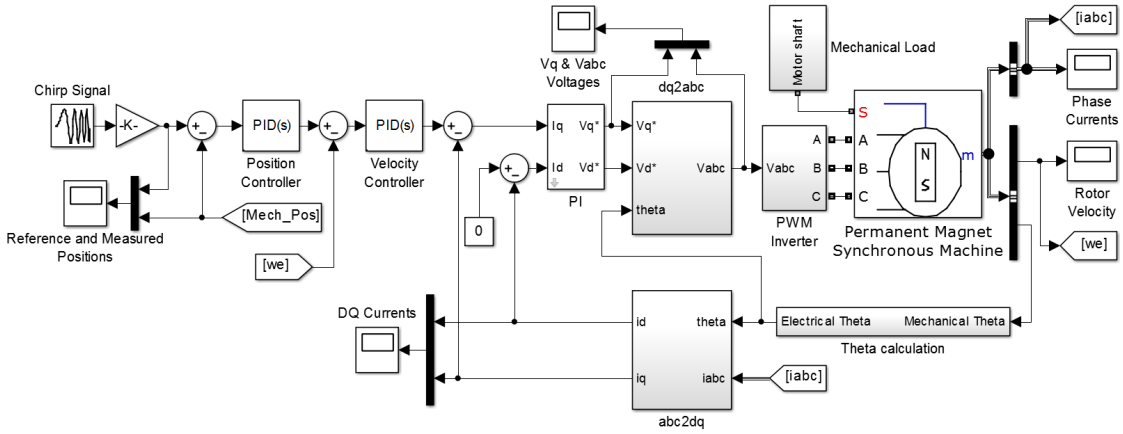

Figure 4.17: The model used in the closed-loop position control simulation

4.1.4.1 Identification of Position Open-Loop

Identification of the position open-loop is completed by using the N4SID method. During the identification process, the MATLAB - Simulink model given in the Fig 4.12 is used as the simulation environment and position of the load is sampled as the output of the open-loop system. These simulation results are shared in the Fig 4.18.

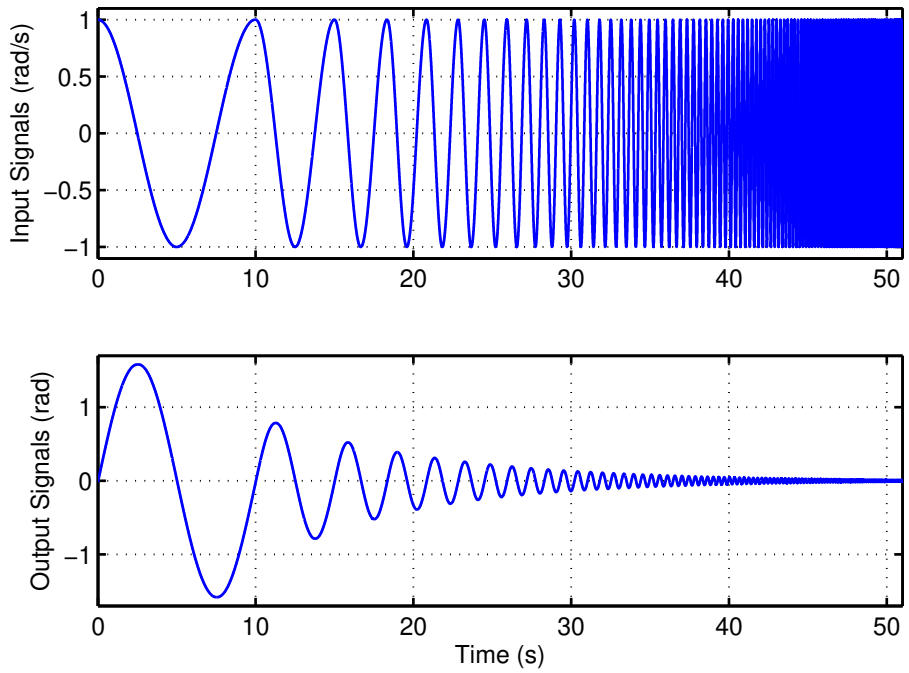

Figure 4.18: Input / output data of the open-loop position control

A periodic chirp signal between 0.1 Hz and 10 Hz is applied as the input to the system. During the frequency sweep of the input signal generation, each frequency is applied as the whole co-sine waveform to eliminate the DC average of the input signal and 0.1 Hz is used as the increase step. As the frequency of the input signal increases, response of the system decreases.

After the open-loop system data is obtained for different frequency levels, this dataset is used in the MATLAB's system identification tool, as its details and internal steps are given in Section 3.3. By following the next steps in the same section, open-loop position state space model matrices are calculated as in Eq. (4.11) in the same form of Eq. (3.26):

$$A = \begin{bmatrix} 0.007145 & -0.02563 & -0.0001664 \\ 3.669 & -23.34 & -53.22 \\ 3.318 & -2.58 & -111.3 \end{bmatrix}, B = \begin{bmatrix} -0.001179 \\ -36.06 \\ -58.81 \end{bmatrix}$$
$$C = \begin{bmatrix} 122.3 & -0.001547 & 0.000048 \end{bmatrix}, D = \begin{bmatrix} 0 \end{bmatrix} \tag{4.11}$$

Once the state space model is defined, by putting the matrices into the Eq. (4.7), open-loop position transfer function can be obtained as below:

$$G_p(s) = \frac{-0.09122s^2 + 96.08s + 2447}{s^3 + 134.7s^2 + 2461s - 11.63} \tag{4.12}$$

Simulation outputs and the response of the identified system, which is given in Eq. (4.12), are shared in Fig 4.19. Match between these two systems are 99.5% and therefore, calculated transfer function of the position open-loop can be used as an input for the position controller design phase.

Calculated transfer function of the open-loop position system shows that this is an unstable system since one of the poles is in the right-half side of the s-plane. If a step input, which corresponds to a constant velocity, is applied to the open-loop system, position of the load continuously changes. But in fact for any other inputs with periodic characteristic at any frequency, it behaves like a stable system. Even so this instability is going to be compensated with the position controller.

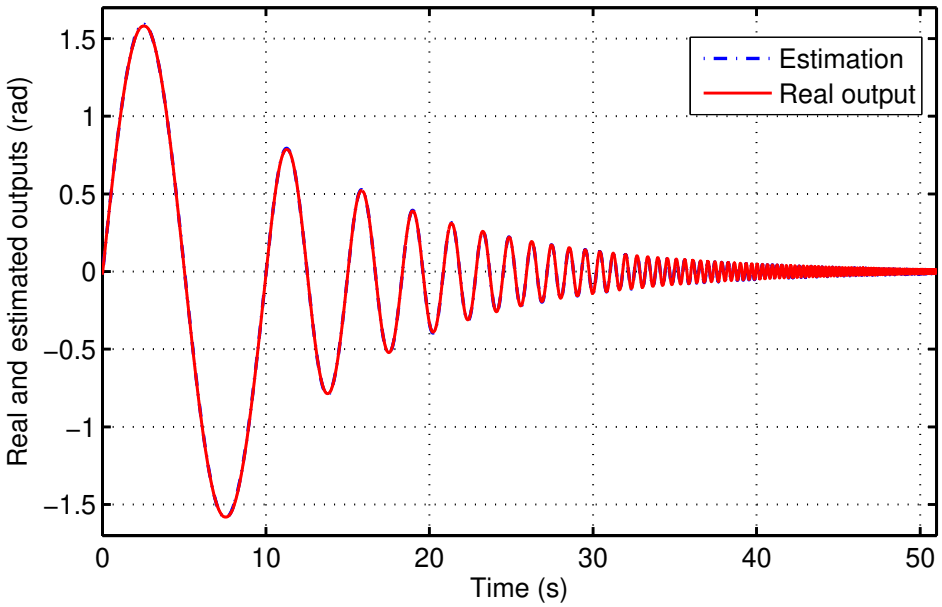

Figure 4.19: Identified system data of the position loop simulation

4.1.4.2 Position Loop Controller Design

The Fig. 4.19 shows that system identification that is given in Eq. (4.12) can be used as input to the H_∞ controller design process since it is a good representation of the real system. Details of this process are given in the Chapter 3.4.1. Calculated position controller is given in Eq. (4.13) with a target bandwidth of 7.5 Hz.

$$K_p(s) = \frac{3.49x10^5(s+4096)(s+22.64)(s+0.0042)^2}{s(s+4189)(s+4096)(s+4442.1)(s+0.0042)} \tag{4.13}$$

Pole-zero cancellation helps to reduce order of the transfer function. Updated version of Eq. (4.13) is given below:

$$K_p(s) = \frac{0.19(s+22.64)(s+0.0042)}{s} \tag{4.14}$$

Simplified position controller, given in Eq. (4.14), corresponds to a PID controller. After this controller is implemented to the open-loop system converting it to the closed-loop control which is given in Fig. 4.17, position change of the load with respect to the sinusoidal chirp signals with the targeted frequency is given in Fig. 4.20.

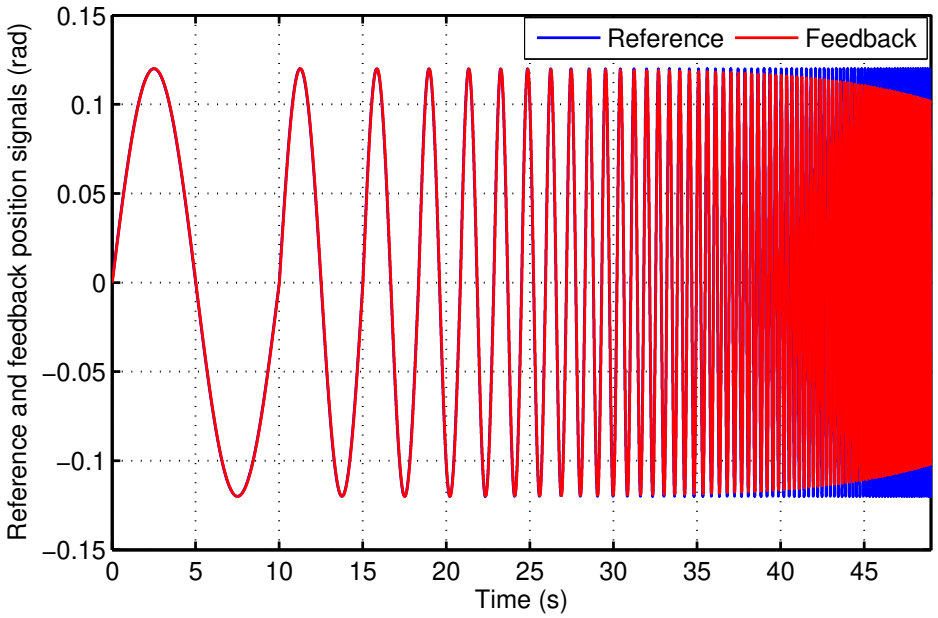

Figure 4.20: Closed loop position control of the tuned system

For a better understanding of the capability of the controller and the performance of the closed loop system, frequency response of the position control loop is calculated and given as a bode plot in the Fig. 4.21.

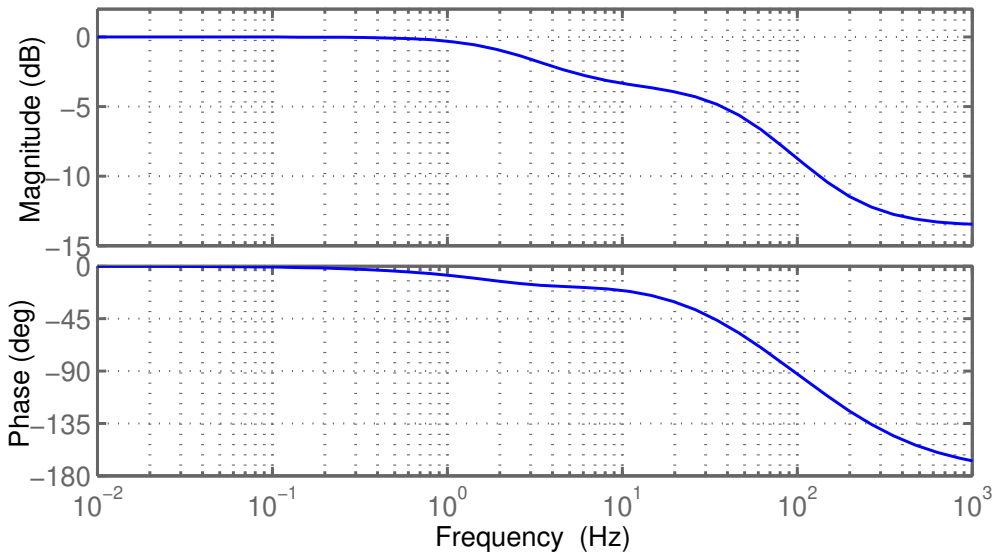

Figure 4.21: Bode plot of tuned closed loop position control

4.2 Position Control Applications with Different Trajectories

After all required processes are completed for the basic control loops, predetermined different trajectories are applied to the same system to highlight their advantages and disadvantages over each other.

4.2.1 Motion with a Constant Velocity

The first trajectory is selected as the motion with a constant velocity. Unlike the other simulations that rotates the load $180°$ in 1 second, for this simulation, the load is rotated $180°$ in 1.5 seconds as given in the Fig. 4.22. When the same motion is performed with constant velocity in the same duration, the performance of the control is dramatically worse than the others due to the limitations in the current controller.

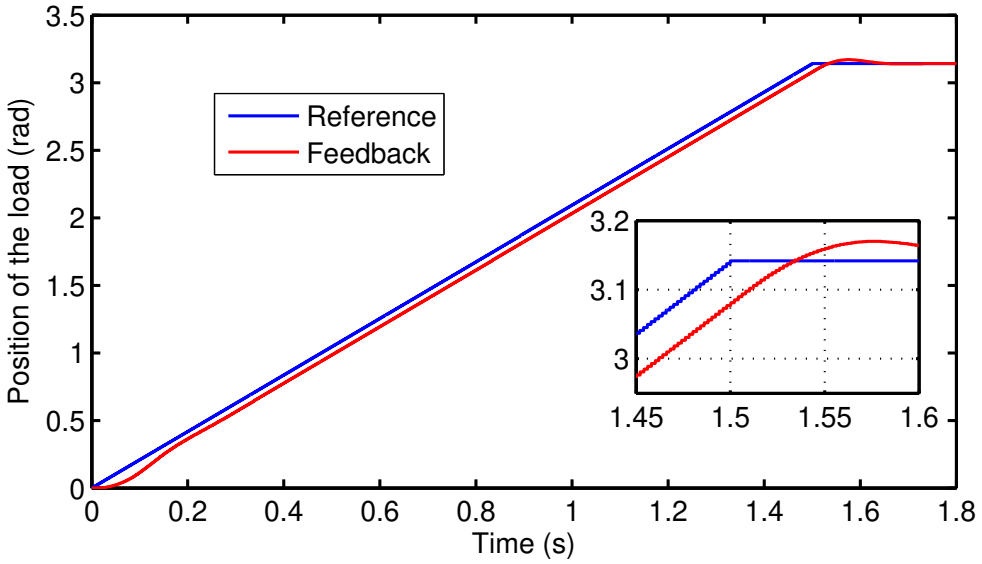

Figure 4.22: Position change with constant velocity motion

At the beginning of the movement, the load position starts to follow the reference with a delay. This delay makes the load to settle its final position later than the expected time and creates an overshoot at the final approach. Difference between these two signals are used as the input to the velocity controller loop and velocity change of the system is given in the Fig. 4.23.

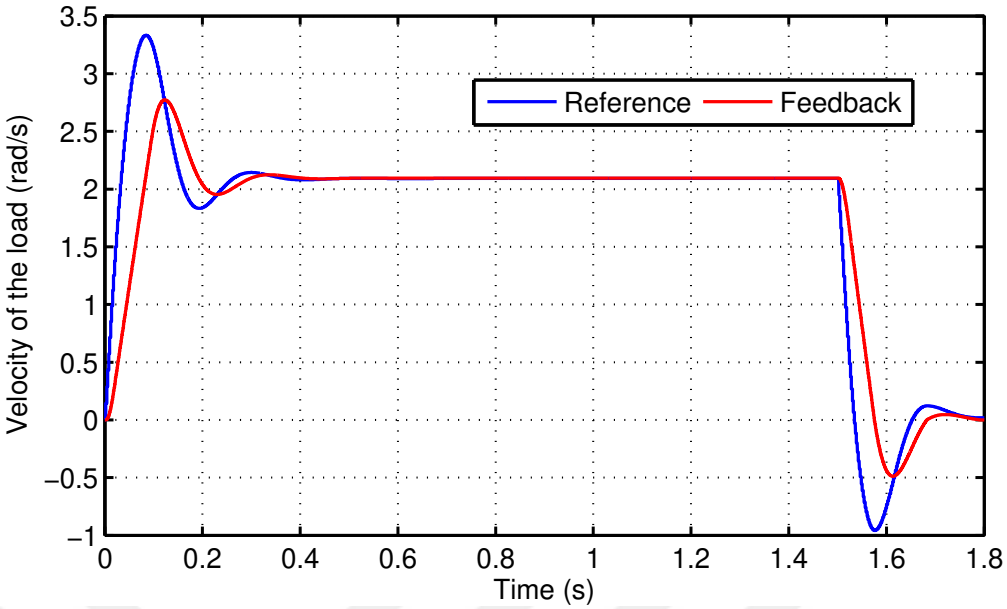

Figure 4.23: Velocity change with constant velocity motion

Even if the velocity controller is tuned well, the closed-loop system is unable to follow the reference signal during some parts of the movement. The reason for this situation is directly related with demanding a rapid velocity change from the load. Since it requires an infinite current that is not realistic, velocity of the load changes by time with the limits of the power electronics circuitry. In this simulation, output of the velocity controller is limited to 7.5 A to have completely same situation in the experimental test.

Differences between the reference and the feedback value of the velocity signals provide input to the velocity controller which determines the I_q reference for the current control loop. For the constant velocity motion profile, corresponding current waveforms are shared in the Fig. 4.24.

At the beginning and at the end of the movement there are high current demands from the motor drive. As seen from the Fig. 4.24, these currents are not sinusoidal waves and crest factor is also high due to the ratio between the RMS and the peak values of the currents. As a result of these currents, change of electromechanical torque of the motor is given in the Fig. 4.25.

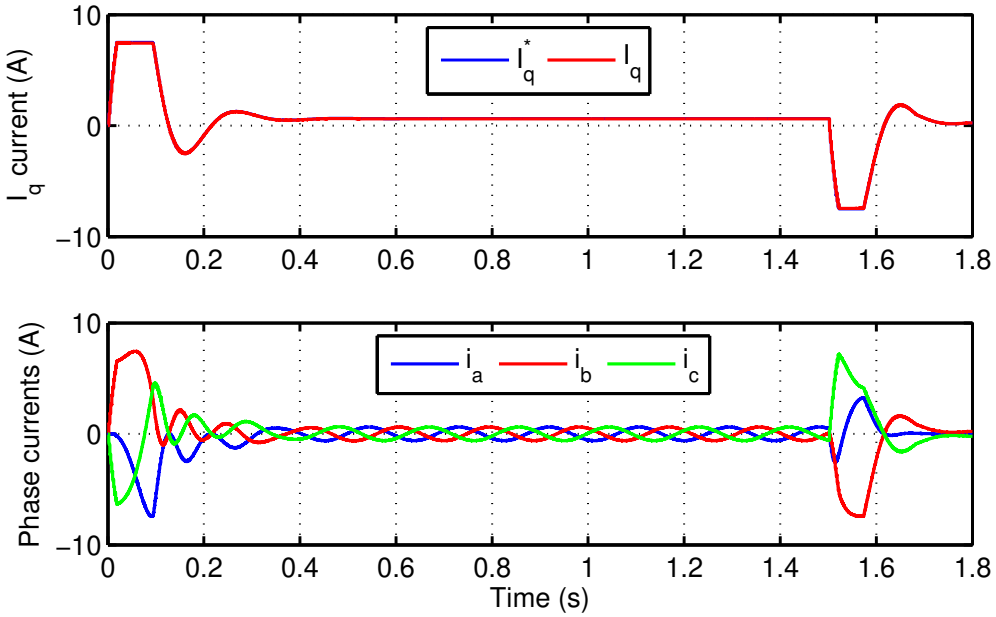

Figure 4.24: Change of currents with constant velocity motion

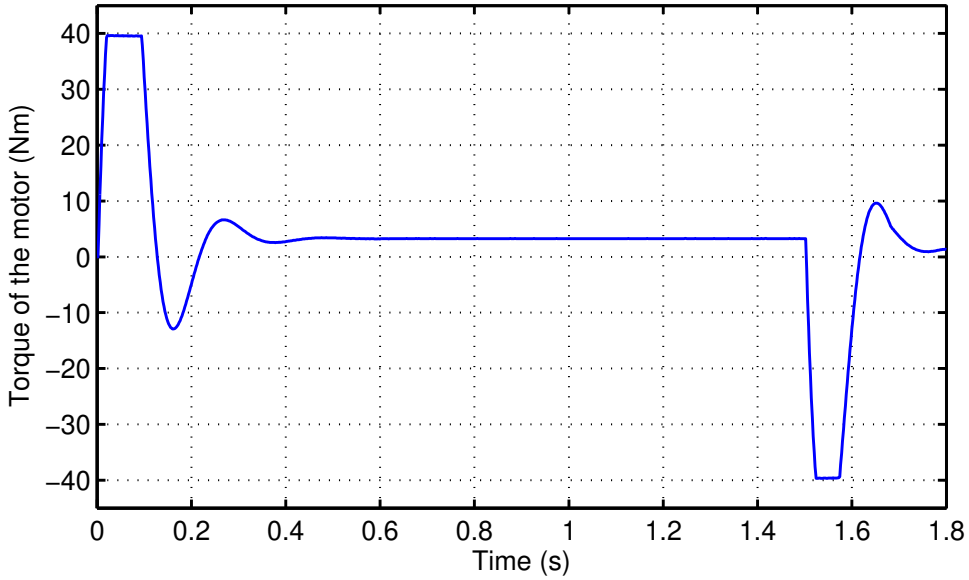

Figure 4.25: Change of torque with constant velocity motion

4.2.2 Motion with a Constant Acceleration

As the second trajectory, a parabolic position profile which rotates the mechanical load $180°$ in 1 second is applied to the same system and results are given starting

from the Fig. 4.26. In this type of a motion, acceleration of the load is limited to a constant value resulting a finite current demand from the power electronics circuitry.

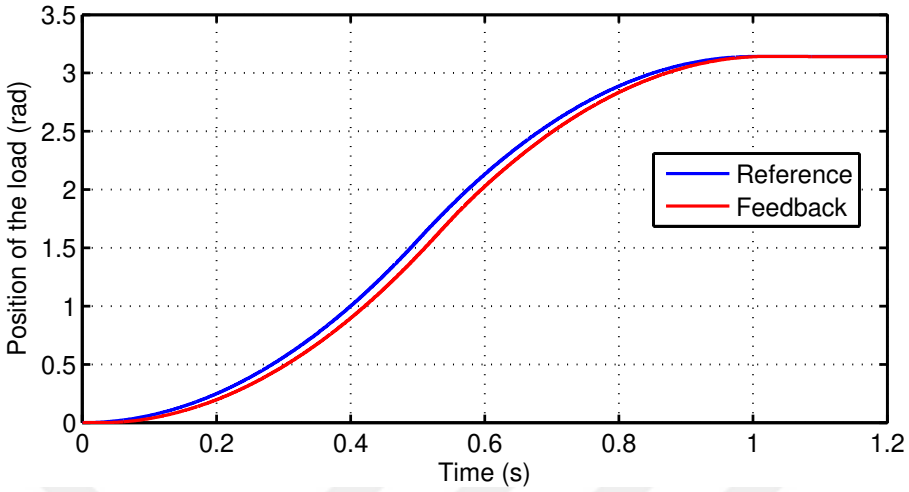

Figure 4.26: Position change with constant acceleration motion

Since it is a smoother profile compared to the case with constant velocity, the position of the load changes with a much more smaller overshoot. The velocity change of the system which is linear in time is given in the Fig. 4.27.

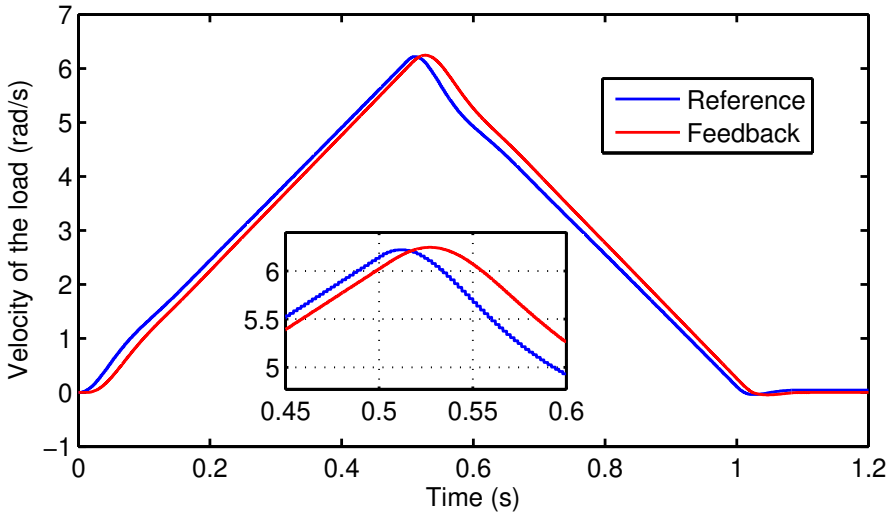

Figure 4.27: Velocity change with constant acceleration motion

The velocity of the system follows its reference with a small delay and the PMSM completely stops after the expected time. This delay is more visible with the currents' change of time which is in the Fig. 4.28.

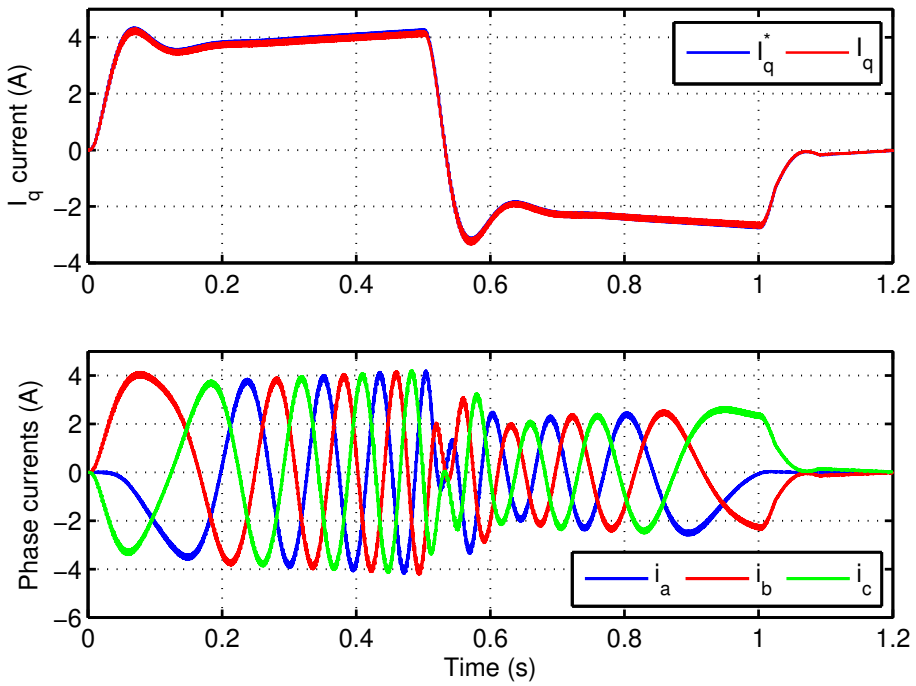

Figure 4.28: Change of currents with constant acceleration motion

Due to the overshoot in the position, non-zero velocity reference demands current from the controller even after the end-time of the motion. This duration takes around 60 ms and corresponding torque change of the motor is given in the Fig. 4.29.

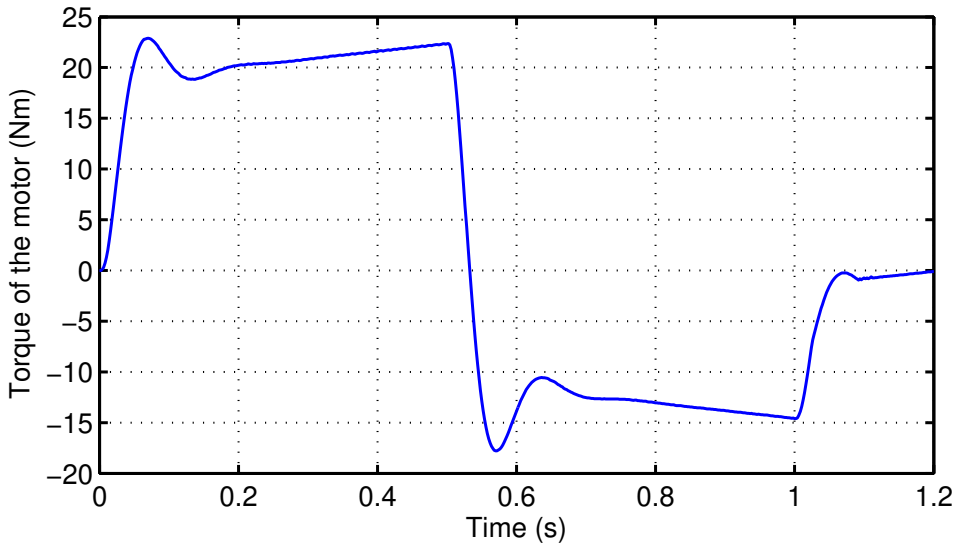

Figure 4.29: Change of torque with constant acceleration motion

4.2.3 Motion with a Limited-Jerk Sinusoidal Waveform

The last trajectory that is applied to the system is the one with a limited-jerk sinusoidal waveform which its details are given in the Section 2.3. In this trajectory, the jerk which is the derivative of the acceleration is limited with a sinusoidal signal and position reference is obtained by integrating this waveform. The reference signal that rotates the load $180°$ in 1 second and the resulting position of the system is given in the Fig. 4.30.

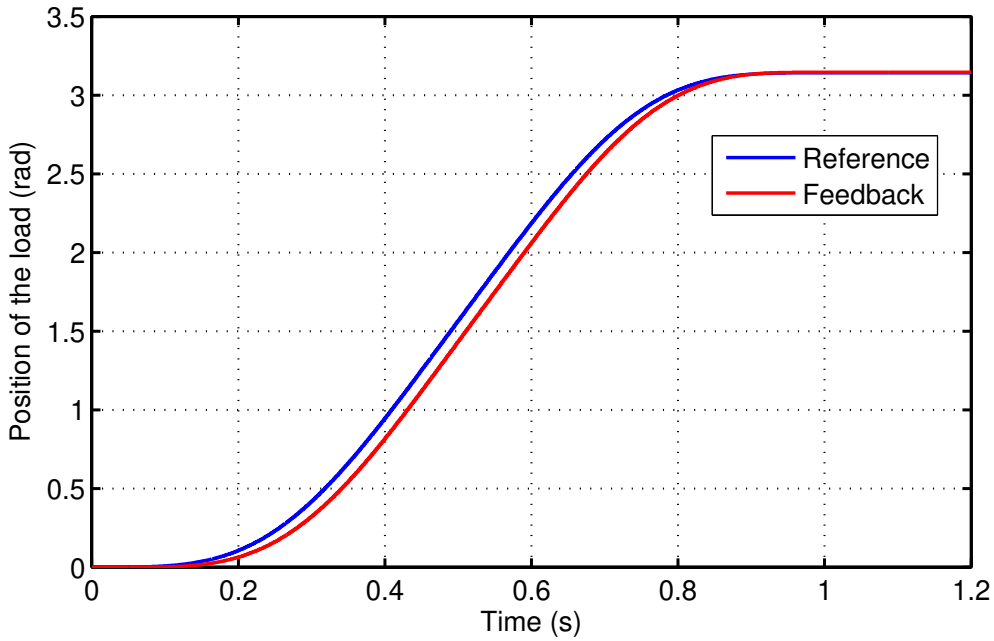

Figure 4.30: Position change with limited-jerk sinusoidal motion

With this trajectory, the position of the system changes without any overshoot and the movement of the load is finished in the desired time. Velocity change of the system is given in the Fig. 4.31 together with the velocity reference that is the output of the position controller.

Change of the velocity with a limited-jerk sinusoidal trajectory is smoother compared to others and the movement is completely finished within the defined duration as one of the most important differences. Smoother currents as the result of the velocity loop is given in the Fig. 4.32.

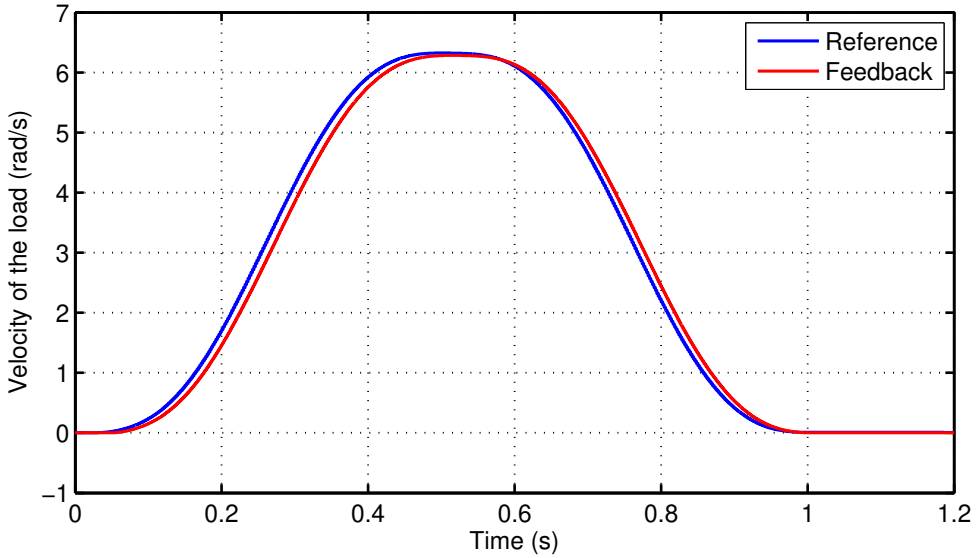

Figure 4.31: Velocity change with limited-jerk sinusoidal motion

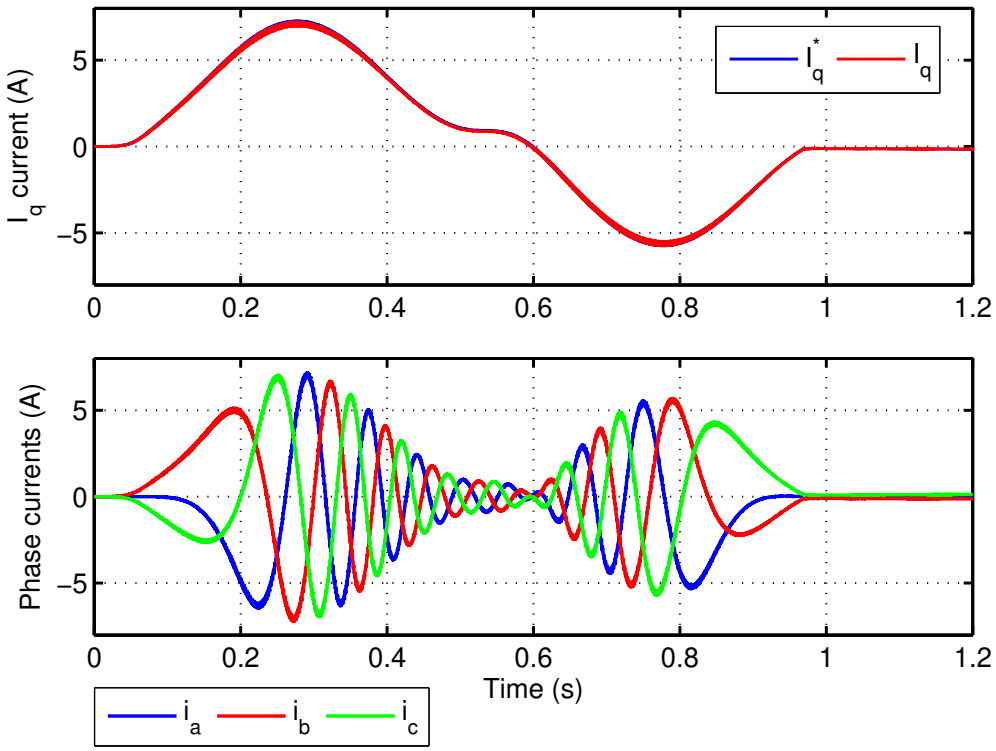

Figure 4.32: Change of currents with limited-jerk sinusoidal motion

Different from the other two trajectories, the demand for the current after the load reaches to its final position does not exist. Therefore the system is completely ready and in an idle state for the next operation.Torque change is given in the Fig. 4.33.

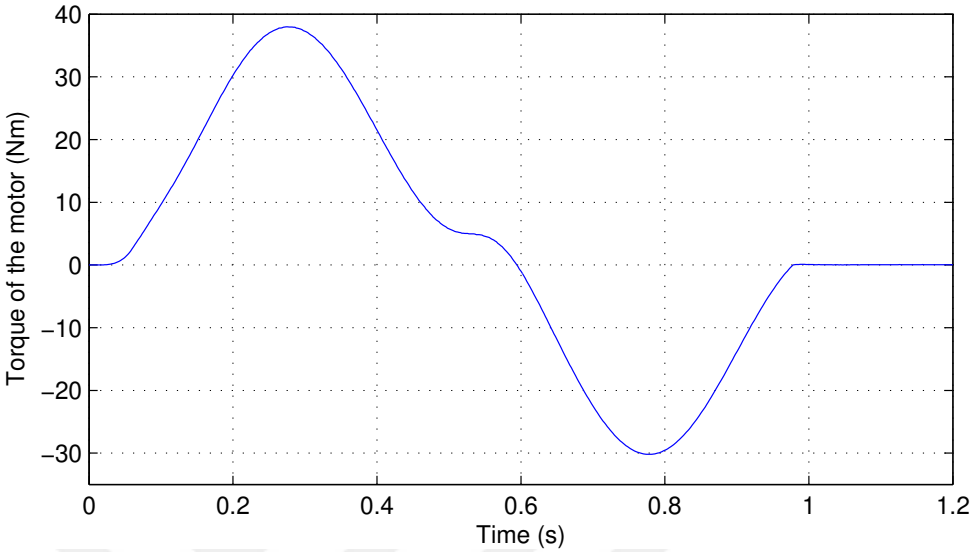

Figure 4.33: Change of torque with limited-jerk sinusoidal motion

4.3 Comparison of the Results of the Simulations

As the position reference gets smoother, the waveform of the velocity and the currents also get smoother as seen from the outcomes of the simulations. By this way the load follows the reference with less overshoot and chance of completing the motion within the defined time target increases. For the motion with the sinusoidally limited-jerk, the load reaches to the destination in desired time without any overshoot and time delay.

Another advantage of the smoothness of the position reference is noticeable by checking the derivative of the torque as given in the Fig. 4.34 and Fig. 4.35.

Transients in the change of torque for the constant velocity motion profile creates very high derivatives as given in the Fig. 4.34. The load can fully stop after around 200 ms than the targeted time and derivative of torque shows the root cause for the undesired vibrations in the mechanical system.

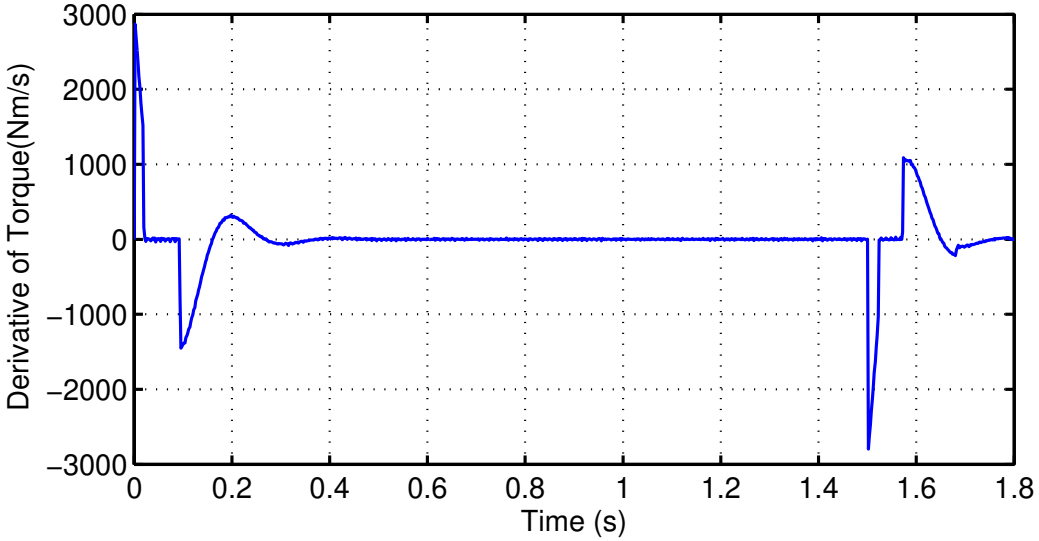

Figure 4.34: Derivative of torque with constant velocity motion

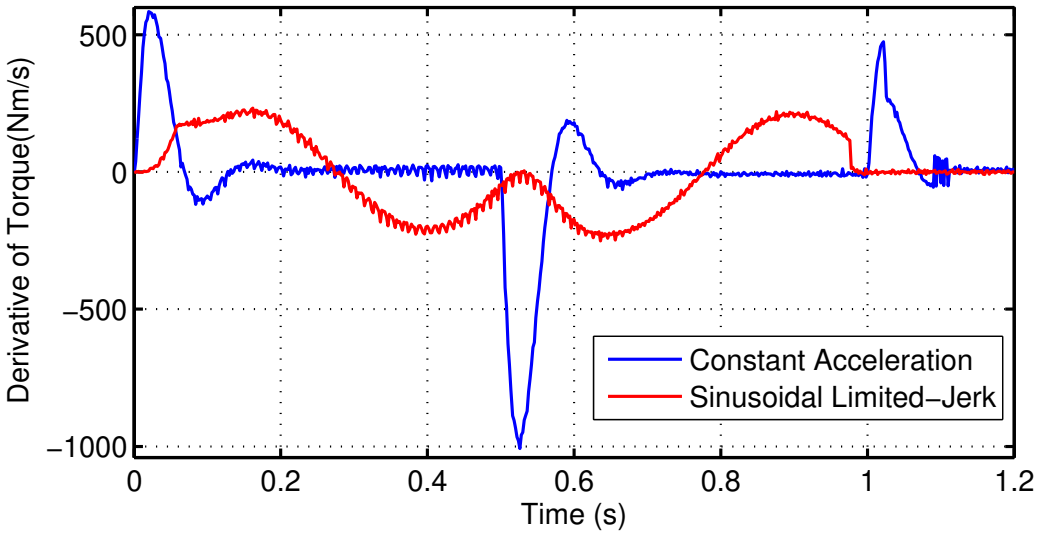

Figure 4.35: Derivative of torque with other trajectories

The results for the constant acceleration and the limited-jerk sinusoidal waveforms are given together in the Fig. 4.35 for a better comparison. The result with the sinusoidal limited-jerk completes the motion within the expected time and with 4 times smaller torque derivative compared with the constant acceleration case which requires around 100 ms extra time to settle. Oscillations in the Fig. 4.35 are result of the derivation operation and they are not filtered out to keep the original results.

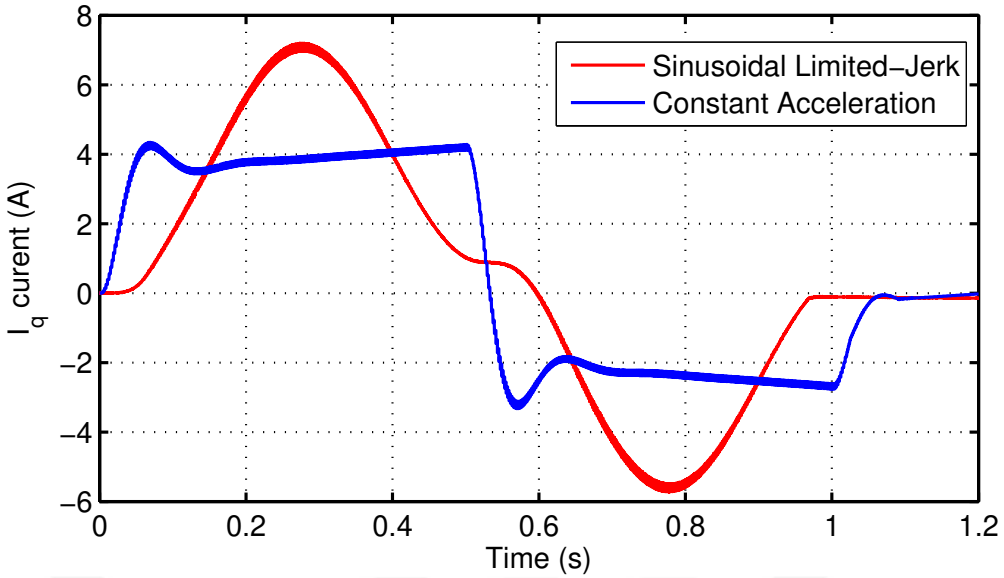

Figure 4.36: I_q currents for the motions with constant acceleration and limited-jerk

Punctuality of the motion with sinusoidal limited-jerk can also be detected in the Fig. 4.36 which is the comparison of the I_q currents of these two motion profiles. Even if the peak current of the motor and the peak torque of the motion with sinusoidal limited-jerk is high; by means of other parameters, Table (4.2) shows that proposed trajectory is better for time optimality and undesired transient jerks.

Table 4.2: Comparison of the simulation results

Simulation results	**Constant velocity**	**Constant acceleration**	**Sinusoidal limited-jerk**
Settling time	200 ms	100 ms	0
Peak torque	40 Nm	23 Nm	38 Nm
RMS of I_q current	2.36 A_{rms}	2.93 A_{rms}	3.58 A_{rms}
Copper losses	94.9 Wh	63 Wh	80.7 Wh
Peak of torque derivative	2867 Nm/s	1008 Nm/s	277 Nm/s

Completed steps and results given in this chapter show that a system that controls a permanent magnet synchronous motor with field oriented control is established and controllers for the velocity and the position loops are designed after their open-loop system identifications are completed. Simulation results for different trajectories also show that proposed motion type bring certain advantages which are beneficial to the system performance and the lifetime. As the next step of the study, this electromechanical system, which its parameters are being used in the simulations, is going to be used in an experimental test setup and same steps are going to be repeated to see the same advantages of the proposed trajectory.

CHAPTER 5

EXPERIMENTAL RESULTS AND COMPARISON

After the simulations for the electromechanical system, which is given in the Fig. 4.2 together with the parameters in the Table (4.1), is completed, experimental test setup is established as in the Fig. 5.1 and the same steps for the system identification and the controller design processes are repeated.

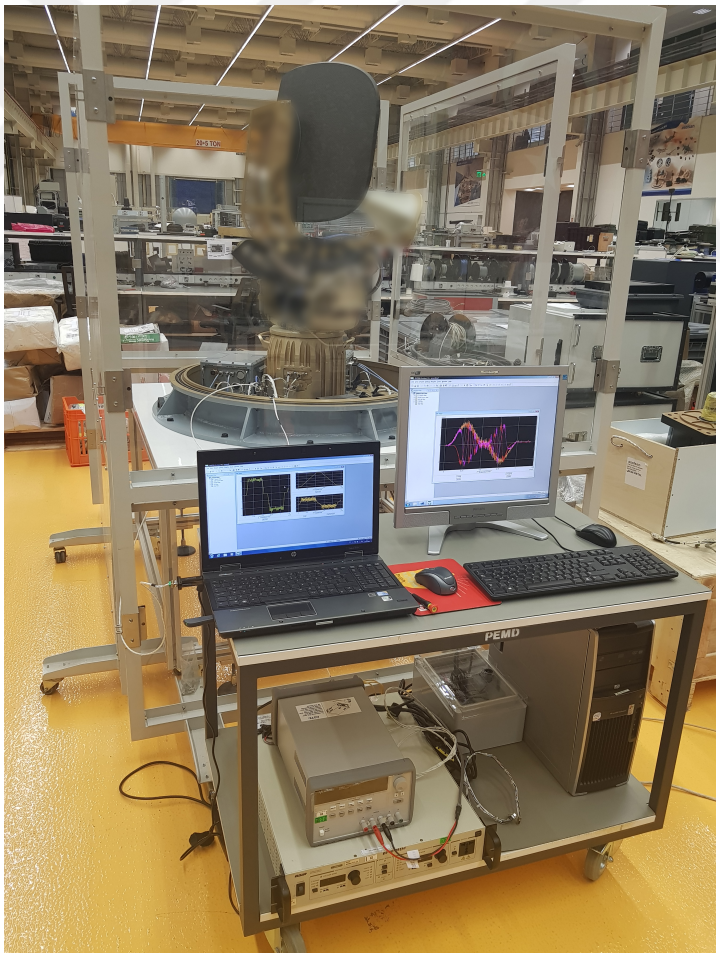

Figure 5.1: Experimental test setup (some parts are blurred for confidentiality)

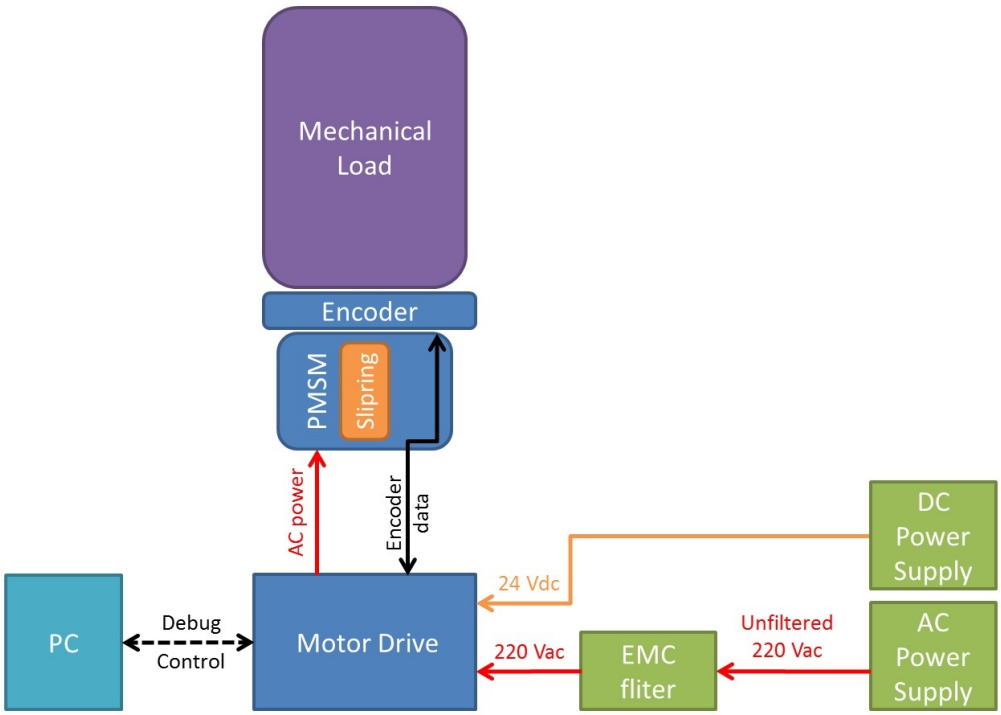

Figure 5.2: Block diagram of the experimental test setup

More detailed structural block diagram of the system is given in the Fig. 5.2. Custom design AC motor drive is powered by a DC power supply with 24 V of input voltage. This input is further converted to lower voltages which micro controller and other electronic components require. AC power supply is used to create the main power demand of the system after it is filtered with an EMC filter. This voltage is internally rectified and a DC bus voltage is created for the inverter. Software of the motor drive is uploaded through the computer and the same interface is used for debugging purposes.

A slip ring and a rotary joint are also integrated inside the hollow shaft of the motor to be able to connect the rotating electrical and RF modules to the stationary frame. Even if it is not focus of this study, the electromechanical system has also a freedom in pitch axis. To control the movement in this direction, another PMSM and motor driver module are located in the rotating frame. Central of gravity is statically and dynamically balanced before this study, therefore azimuth motor only sees a balanced inertia and an extra friction that comes from the slip ring. Details of this second axis are not given in the block diagram.

Motor drive unit is capable of measuring the position of the rotor by reading the quadrature incremental encoder located in the motor frame. This position information is used to calculate the electrical angle between the rotor and the magnetic axis of phase-A of the stator. Same position information is also used to calculate the position and the velocity of the mechanical system. Phase currents are also measured by the sensing resistors located inside the motor drive unit and together with all of these measured values, required loops of the field oriented control are constructed and position references for different trajectories are followed. Parameters related with these measurements are given in the Table (5.1).

Table 5.1: Measurement and sensor specifications

Parameter	**Value**
Resolution of the encoder	32768 bits/rev
Position accuracy	0.0027 °
Velocity accuracy	0.46 RPM
Resolution of the current sensor	11702857 bits/A
Current accuracy	0.09 μA

5.1 Basic Control Loops and Tuning Processes

The details of the field oriented control is already given in the Section 1.1 and the related simulations are completed in the Chapter 4. In this part all control loops are established on the experimental setup, the velocity and the position open-loops are identified and required controllers are designed to successfully follow the reference values.

5.1.1 Voltage Control Loop

Control of the electromechanical system starts with the open-loop voltage test of the PMSM using the Field Oriented Control method as defined in the Section 1.1.1 and as

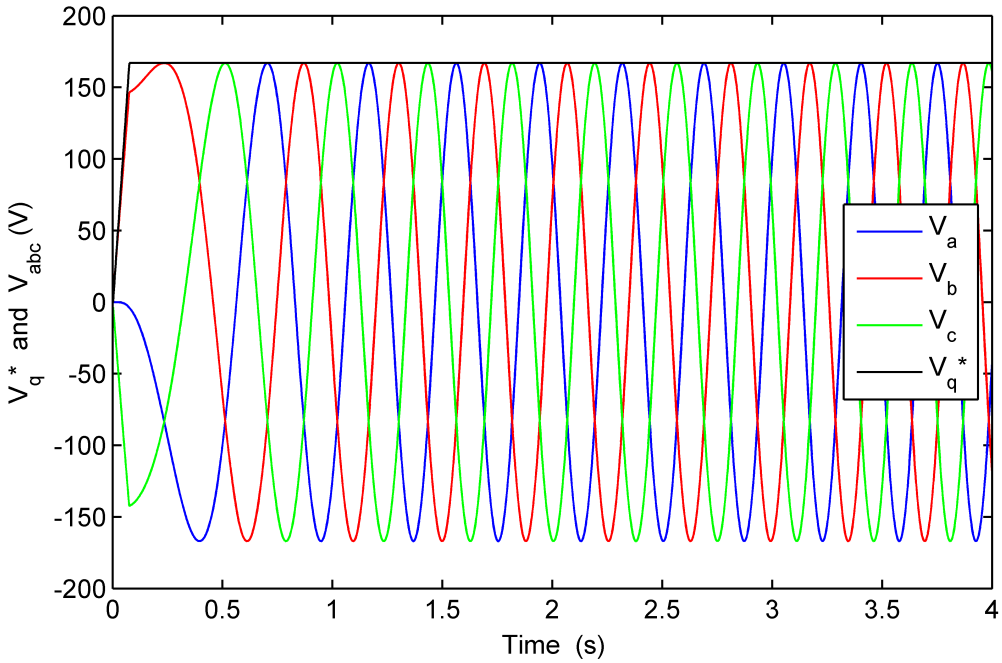

Figure 5.3: Quadrature and abc voltages of experimental voltage test

simulated in the Section 4.1.1. Motivation of this test, same as the simulation part, is to see that the power electronic circuitry is working without any problem, conversions between three phase rotating and two phase stationary domains are constructed and direction of the position sensor is in a harmony with the three phase motor winding connection. Since this control is not closed-loop, unexpected situations do not create unstable situations and it is completely harmless from the electromechanical system point of view.

During the open-loop voltage control, a V_q^* reference voltage is applied to the dq to abc transformation block and three phase voltages are obtained as the input reference to the PWM inverter as given in the Fig. 5.3. The direct axis reference voltage, V_d^*, is not given in the graph since it is zero.

The FOC technique guarantees to have a force in the rotor of the motor in the tangential axis and if this force is greater than the friction the rotation is created. Keeping the force in the same axis requires the electrical rotor position and this information can be obtained using the position sensor in the system.

Data in the Fig. 5.3 is enough to complete the open-loop voltage control of the system but further calculations are also completed in this part to avoid any possible future mistakes. For this purpose, phase currents of the motor are measured through the sensing resistances located in the inverter and results are shared in the Fig. 5.4. These currents are also converted to the two-phase stationary dq domain to be used in the current control loop. Since the torque creating current is the i_q and the reference value of the d-axis voltage is zero, the amplitude of the i_q is greater than the i_d current. The deviation in the i_d current stands since current decoupling between these two axis is not handled in the voltage control loop.

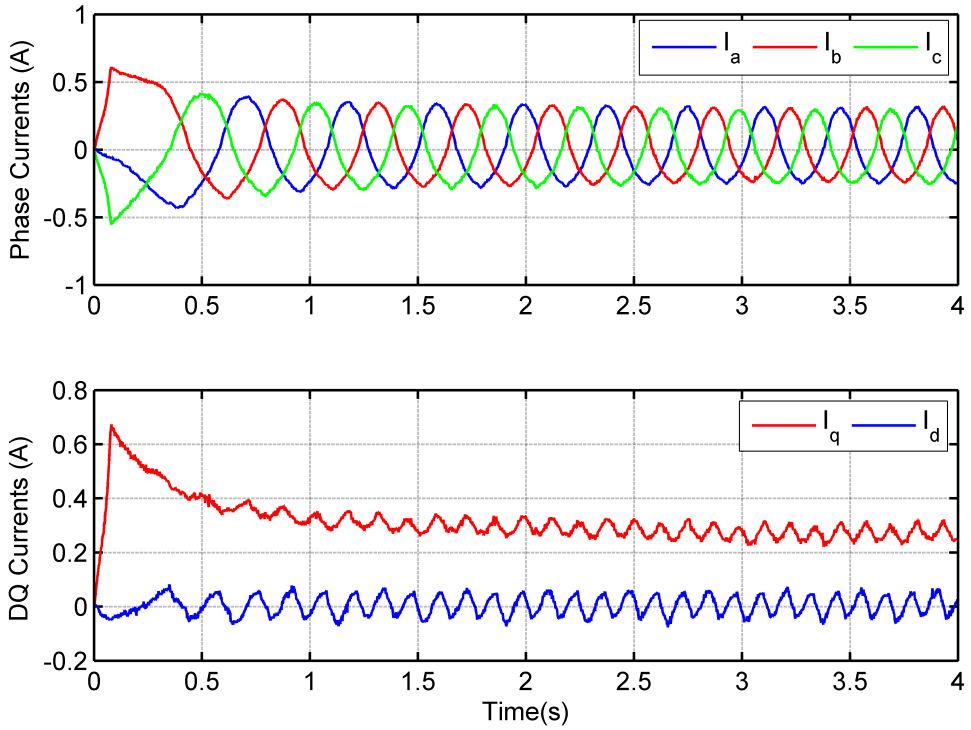

Figure 5.4: Experimental voltage test quadrature and phase currents

The last data calculated in this phase is the velocity as shared in Fig. 5.5. The system has a position sensor located in the frame of the PMSM and the velocity of the rotor is needed to be calculated using its data. The most appropriate way to calculate the rotor velocity is to derivate the output of the position sensor.

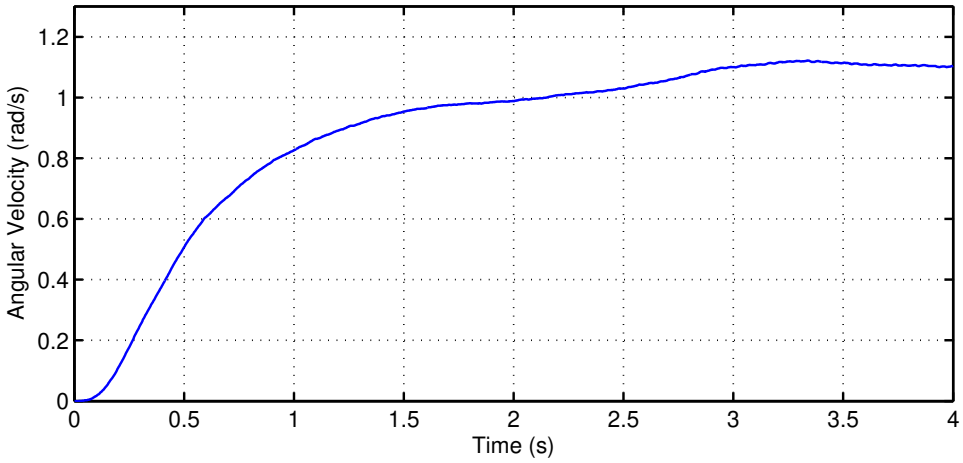

Figure 5.5: Experimental voltage test rotor velocity

5.1.2 Current Control Loop

After the open-loop voltage control is achieved and all other calculations are completed, the current control loop for PMSM is constructed as defined in the Section 1.1.2. Unlike the voltage control loop, here a controller is needed to be created and used in the control of the direct and the quadrature currents. As it is done in the Section 4.1.2, also in the experimental setup, controllers are designed following the standard PID controller design steps as defined in [4]. As an experimental approach, tuning can start with setting the proportional gain. While applying a square wave to the system, proportional controller gain can be increased until the system creates an overshoot in its output. Once it is set, half of this value can be taken as the proportional gain. The integral gain of the PI controller can be found by dividing the proportional gain to the oscillation period of the output. After fine tuning of the controller, the selected parameters are given in Eq. 5.1 and used for control of both direct and quadrature currents.

$$K_c(s) = \frac{12(s + 83.33)}{s} \tag{5.1}$$

Transfer function given as K_c corresponds to a PI controller. By using it as the controller for both direct and quadrature currents, current decoupling also achieved and results of the test are given in the Fig. 5.6.

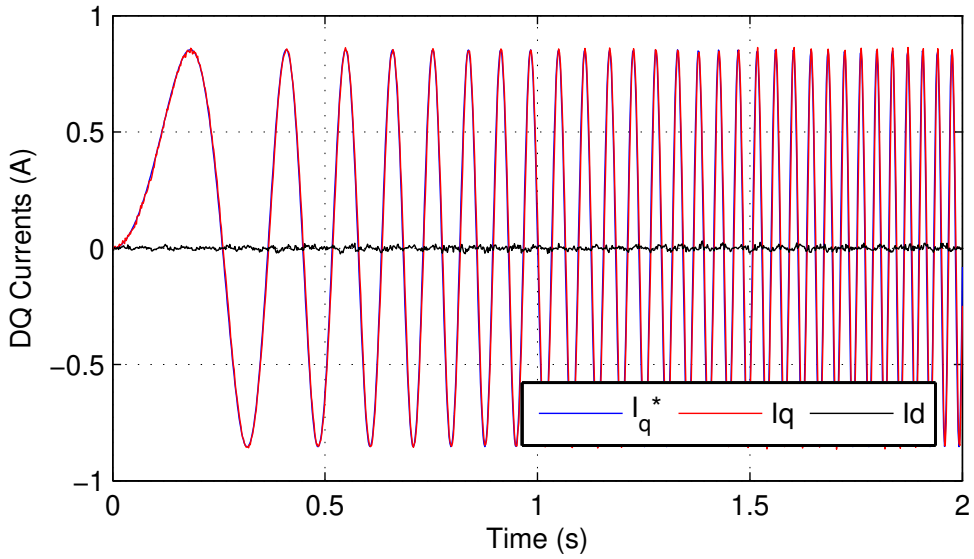

Figure 5.6: Experimental current test DQ currents

Here, the reference of the direct axis current is always zero and it is not represented in the figure. Quadrature axis current is a sinusoidal chirp signal with a linearly increasing frequency from 1 to 30 Hz. For this frequency range, both dq currents follow their references as it is expected. Monitoring the angular velocity of the load is not needed for this loop but it is calculated and given in Fig. 5.7. Here, it understood that low frequencies create a meaningful rotation but as frequency goes up magnitude of the velocity reduces and only a vibration is stayed in the system.

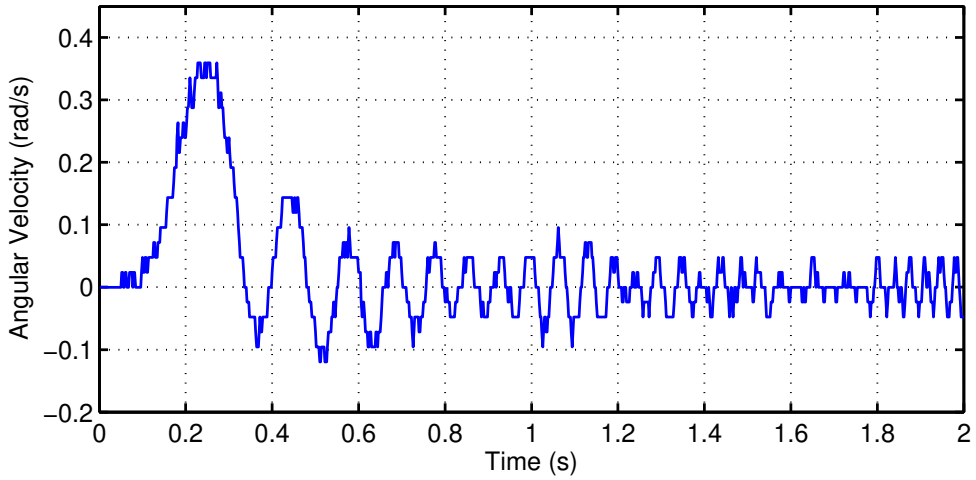

Figure 5.7: Angular velocity of the load for the experimental current test

5.1.3 Velocity Control Loop

The velocity control loop is one outer loop of the current control and the main parts are the same except for the velocity controller. This loop is desired to be constructed as defined in the Chapter 1.1.3 but before that, the controller is needed to be selected according to the process defined in the Section 3.4.1. To provide input to the H_∞ controller design, system identification is needed to be performed according to the mathematical approach defined in the Section 3.2. It is known that the amount of data used in the system identification determines the achievement level of the process.

5.1.3.1 Identification of Velocity Open-Loop

To improve the efficiency of the identification, different cosinusoidal references are applied to the velocity control loop and output velocities are collected from the system. Frequency range of this work is selected as 0.1 Hz to 12.5 Hz and this band is scanned with the steps of 0.1 Hz. Measured velocity values are given in Fig. 5.8 together with the input signals.

Applying a sinusoidal input signal creates a DC offset in the output of the measured system and it reduces accuracy of the system identification. By following the steps of the N4SID algorithm, the velocity open-loop's identified state space representation is calculated as in Eq. 5.2.

$$A = \begin{bmatrix} -0.4242 \end{bmatrix}, B = \begin{bmatrix} 0.02242 \end{bmatrix}$$
$$C = \begin{bmatrix} 233.8 \end{bmatrix}, D = \begin{bmatrix} 0 \end{bmatrix} \tag{5.2}$$

By using Eq. (4.7), open-loop transfer function can be obtained as given in Eq. (5.3).

$$G_v(s) = \frac{5.243}{s + 0.4242} \tag{5.3}$$

Once same input signals are applied to the transfer function of the velocity loop, harmony between the real values and the estimates is 98.16 $\%$. Both real and estimated values are shared in Fig.5.9.

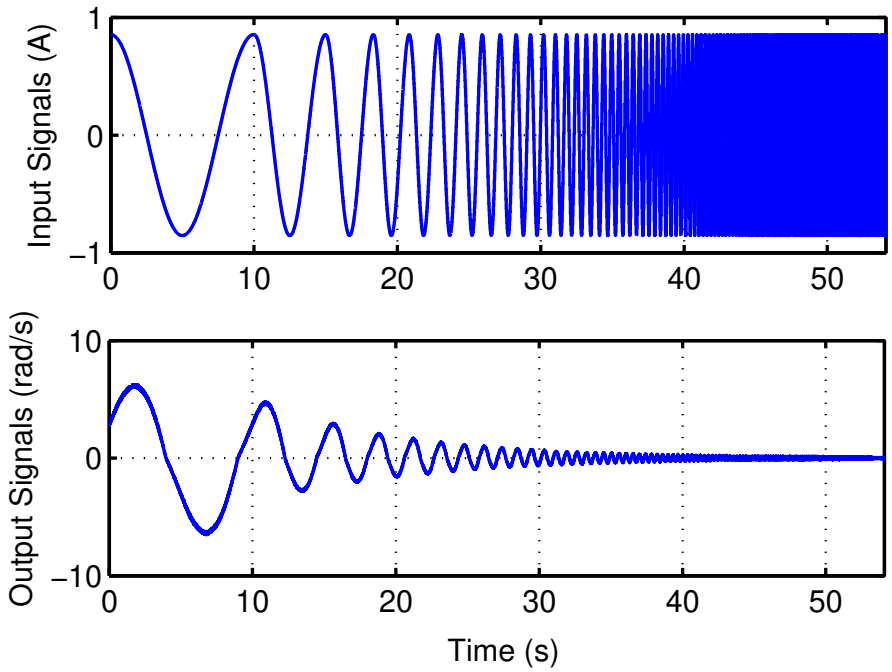

Figure 5.8: System identification data of experimental velocity loop

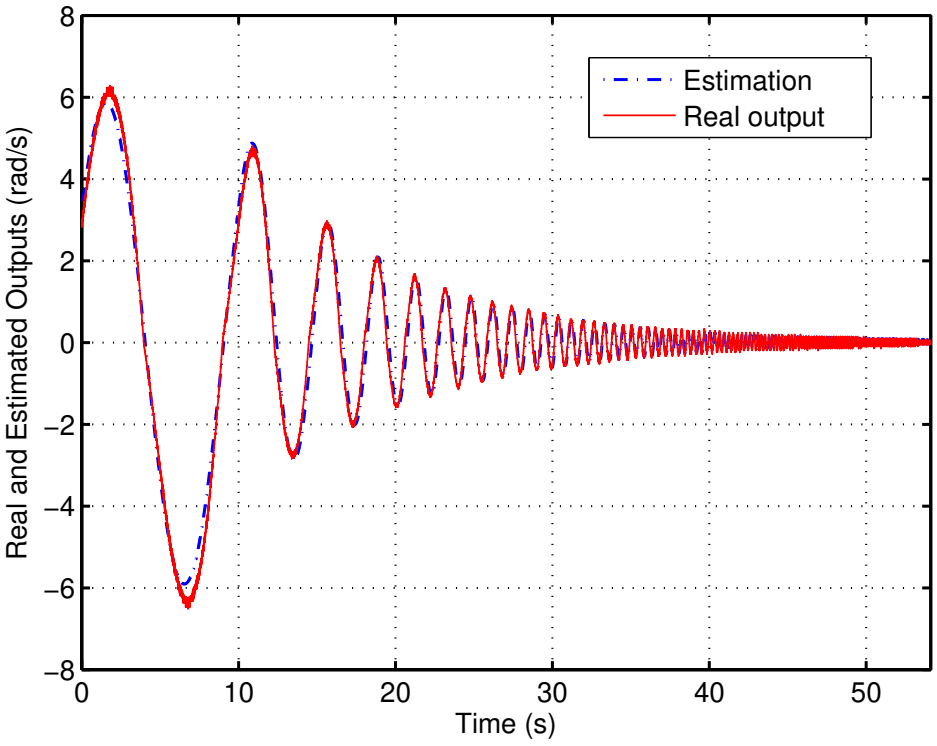

Figure 5.9: Identified system data of the experimental velocity loop

5.1.3.2 Velocity Loop Controller Design

After Eq. (5.3) is cross checked, it can be used as input the H_∞ controller design process. Details of this process are given in the Chapter 3.4.1. Calculated velocity controller is given in Eq. (5.4) with a target of 10 Hz of close-loop control bandwidth.

$$K_v(s) = \frac{49443(s + 0.4242)(s + 4096)}{s(s + 4096)(s + 4220)} \tag{5.4}$$

After some pole-zero cancellations, order of the transfer function can be reduced and updated version of Eq. (5.4) is given below:

$$K_v(s) = \frac{11.72(s + 0.4242)}{s} \tag{5.5}$$

Controller given in Eq. (5.5) corresponds to a PI controller. By integrating this controller into the system, closed-loop velocity control is achieved and corresponding results are given in the Fig. 5.10 for the frequencies from 0.1 Hz to 12.5 Hz.

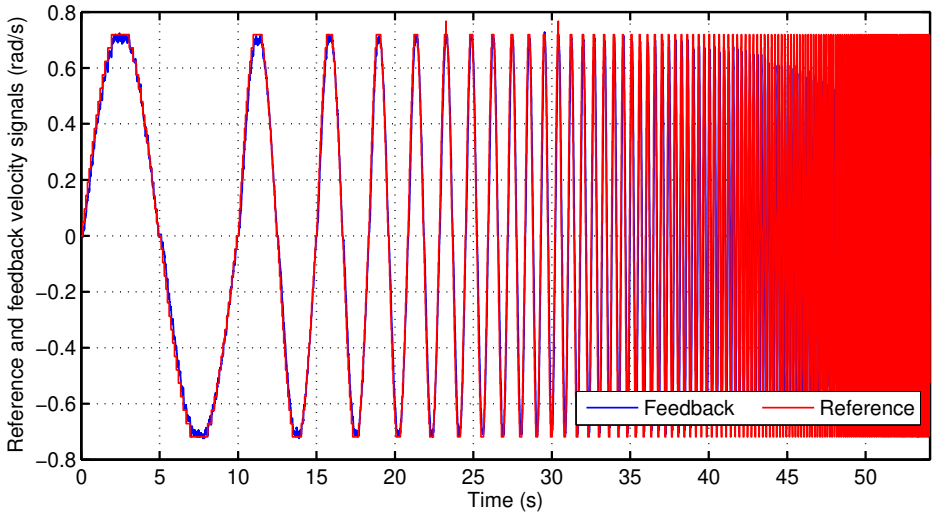

Figure 5.10: Closed loop velocity control of the tuned system

For a better understanding of the capability of the controller and the performance of the closed loop system, frequency response of the velocity control loop is calculated and given as a bode plot in the Fig. 5.11.

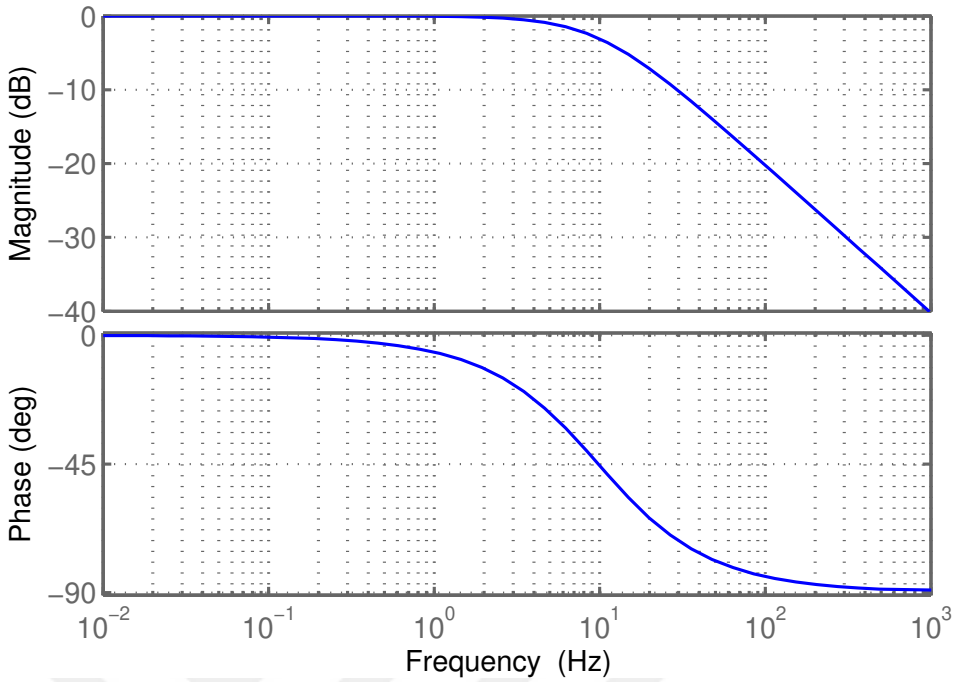

Figure 5.11: Closed loop velocity control of the tuned system for higher frequencies

5.1.4 Position Control Loop

The final loop of the PMSM control is the position loop. As defined in the Section 1.1.4, a position controller is needed to extend a velocity control loop into a position control loop.

5.1.4.1 Identification of Position Open-Loop

The first step for the controller design is the system identification of the position loop. For this purpose, 10 Hz is determined as an upper limit for identification process and cosinusoidal input signals are applied to the position control loop with 0.1 Hz of increment steps. Outputs are measured from the position sensor which is the incremental encoder and these data are given in the Fig. 5.12. Motivation behind using a cosine waveform against the sine is to eliminate the DC offset for the system identification process.

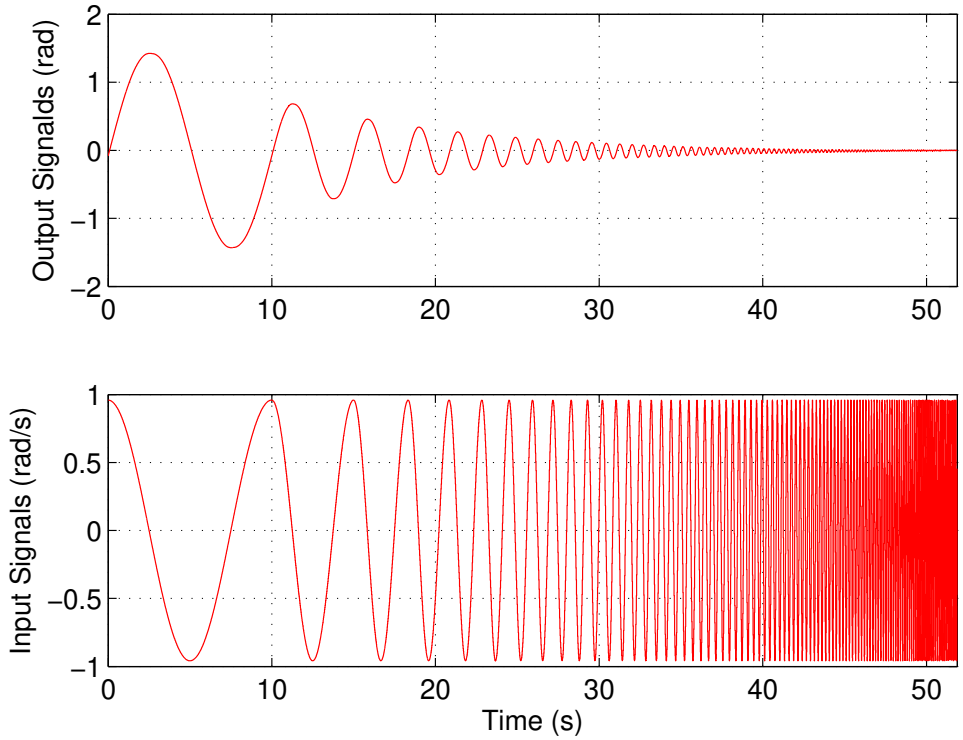

Figure 5.12: System identification data of experimental position loop

Relation between these input and output data of the system is revealed by using N4SID algorithm and SS representation of position control loop is given in Eq. (5.6).

$$A = \begin{bmatrix} 0.05578 & 0.3058 \\ -2.802 & -23.95 \end{bmatrix}, B = \begin{bmatrix} -1.56x10^{-5} \\ 1.3 \end{bmatrix}$$
$$C = \begin{bmatrix} 55.79 & 0.02464 \end{bmatrix}, D = \begin{bmatrix} 0 \end{bmatrix} \tag{5.6}$$

By using Eq. (4.7), open-loop transfer function can be obtained as given in Eq. (5.7).

$$G_p(s) = \frac{0.03117s + 22.16}{s^2 + 23.9s - 0.4793} \tag{5.7}$$

Once same input signals are applied to the transfer function of the position loop, harmony between the real values and the estimates is 99.91 %. Both real and estimated values are shared in Fig.5.13.

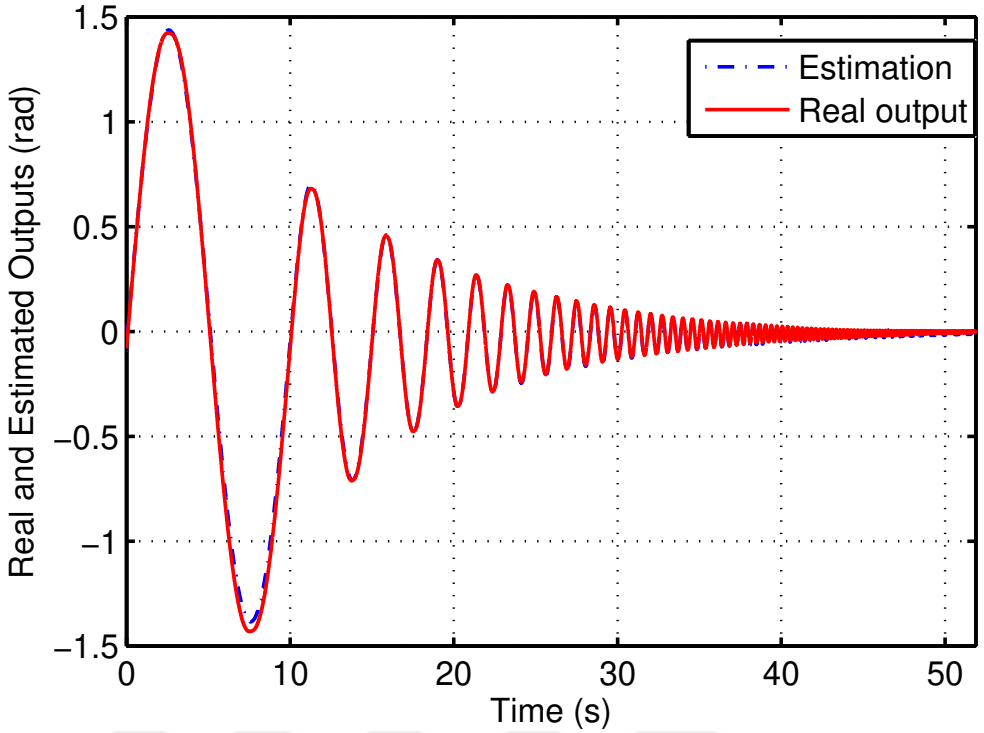

Figure 5.13: Identified system data of the experimental position loop

5.1.4.2 Position Loop Controller Design

After Eq. (5.7) is cross checked, it can be used as input the H_∞ controller design process. Details of this process are given in the Chapter 3.4.1. Calculated position controller is given in Eq. (5.8) with a target of 7.5 Hz of close-loop control bandwidth.

$$K_p(s) = \frac{4.15x10^6(s+4096)(s+23.92)(s+0.02028)(s+0.02023)}{s(s+711)(s+4096)(s+4189)(s+0.02028)} \tag{5.8}$$

After some pole-zero cancellations, order of the transfer function can be reduced and updated version of Eq. (5.8) is given below:

$$K_p(s) = \frac{1.4(s+23.92)(s+0.02023)}{s} \tag{5.9}$$

Controller given in Eq. (5.9) corresponds to a PID controller. By integrating this controller into the system, closed-loop position control is achieved and corresponding results are given in the Fig. 5.14 for the frequencies from 0.1 Hz to 8 Hz.

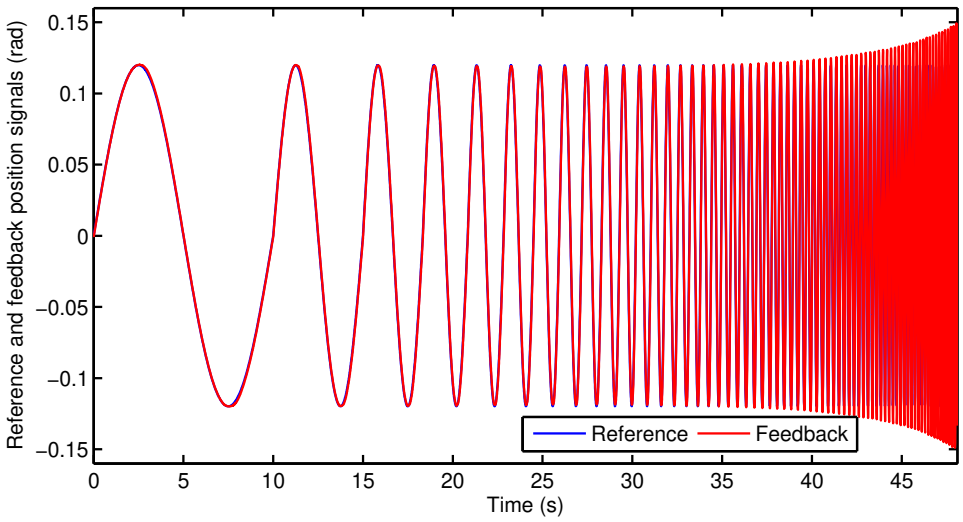

Figure 5.14: Closed loop position control of the tuned system

5.2 Position Control Applications with Different Trajectories

After all required processes are completed for the basic control loops, predetermined different trajectories are applied to the same system to highlight their advantages and disadvantages over each other.

5.2.1 Motion with a Constant Velocity

The first trajectory is selected as the motion with a constant velocity. For this experiment, the load is turned $180°$ in 1.5 seconds as given in the Fig. 5.15.

The motion with a constant velocity creates a linear position change. But since it is not possible to achieve an instantaneous velocity change with a finite power supply, errors in the starting and ending of the motion are larger than the rest of the times. These two intervals are focused in the Fig. 5.15.

The velocity of the load increases during a certain time and the load accelerates with a delay. Once the motion is performed, again some certain amount of time is needed to slow down. During deceleration, the load continues its movement and creates an overshoot in the system. To compensate this overshoot in the position, an extra

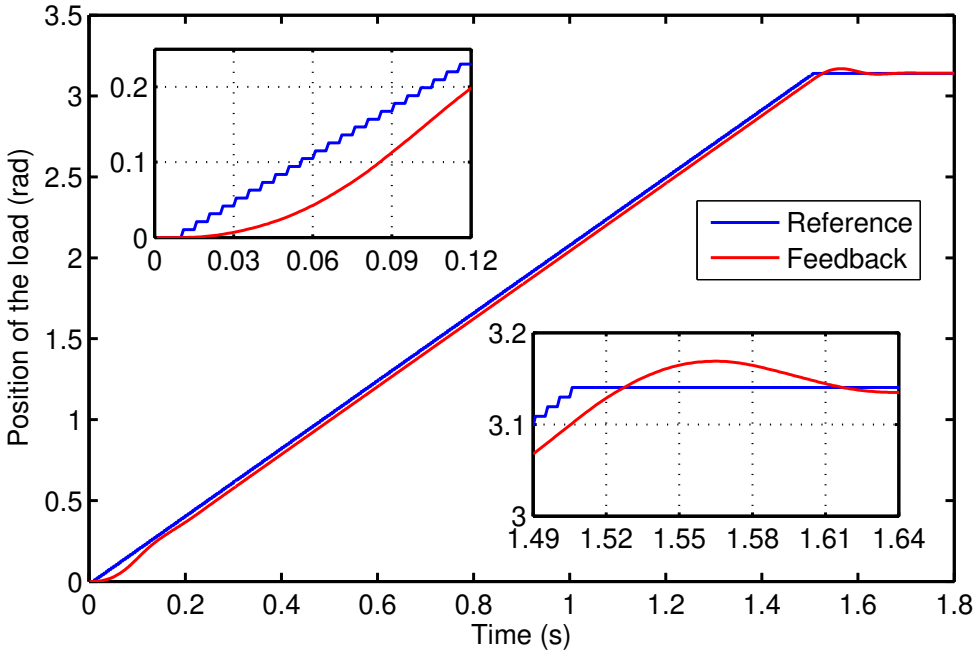

Figure 5.15: Position change with constant velocity motion

interval with negative velocity is needed to be performed to settle in the reference position. All of these intervals can be seen in the Fig. 5.16. Even if the reference saturates in 1.5 seconds, the real movement of the load takes a longer period due to the last part of the motion.

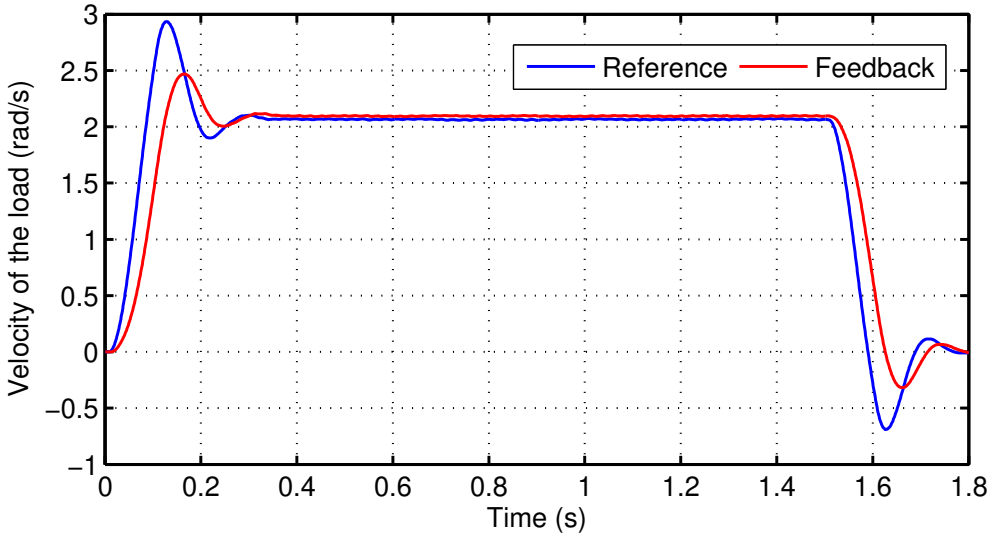

Figure 5.16: Velocity change with constant velocity motion

Errors in the velocity control loop, which are the differences between the reference and feedback signals, determines the I_q reference. For the motion profile with constant velocity, corresponding current waveforms are shared in the Fig. 5.17.

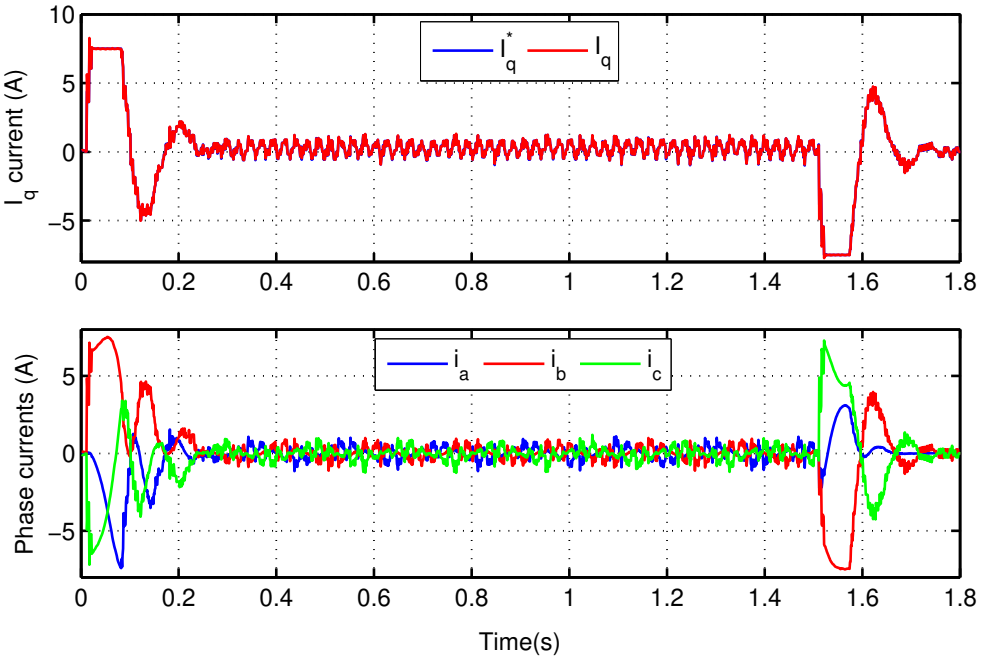

Figure 5.17: Change of currents with constant velocity motion

Output of the current controller is limited with the maximum peak current capability of the inverter which is 7.5 A in this experiment. Considering the electromechanical torque output of the system which is given in Eq. (1.3), it is possible to say that the quadrature current given in the Fig. 5.17 creates vibration and discontinuity for jerk in the system due to its rough behavior. Calculated torque change of the load is given in the Fig. 5.18.

As indicated before, with this type of a reference trajectory, the motion is not completed at the end of the targeted time. To highlight its importance, as the second part of the experiment, the reference signal is created to turn back the load to its initial position just after it has reached to the destination. The reference and the corresponding measured position values are given in the Fig. 5.19 for such a motion that first moves the load $180°$ in 1.5 seconds and then turns it back to the first position again

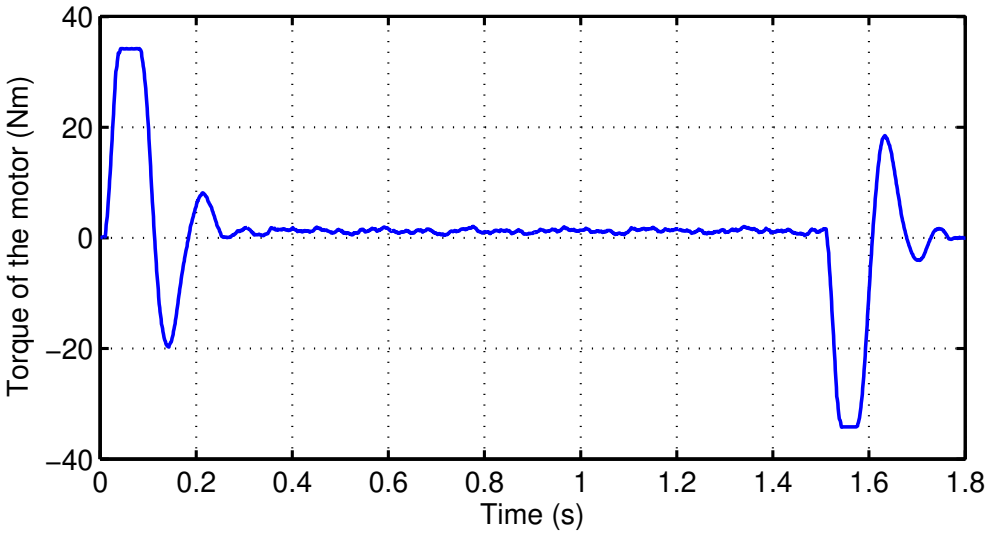

Figure 5.18: Torque change with constant velocity motion

in 1.5 seconds. After the inverter is switched off due to the safety reasons, the load keeps it movement using the stored kinetic energy in its inertia but then decelerates and stops due to the friction.

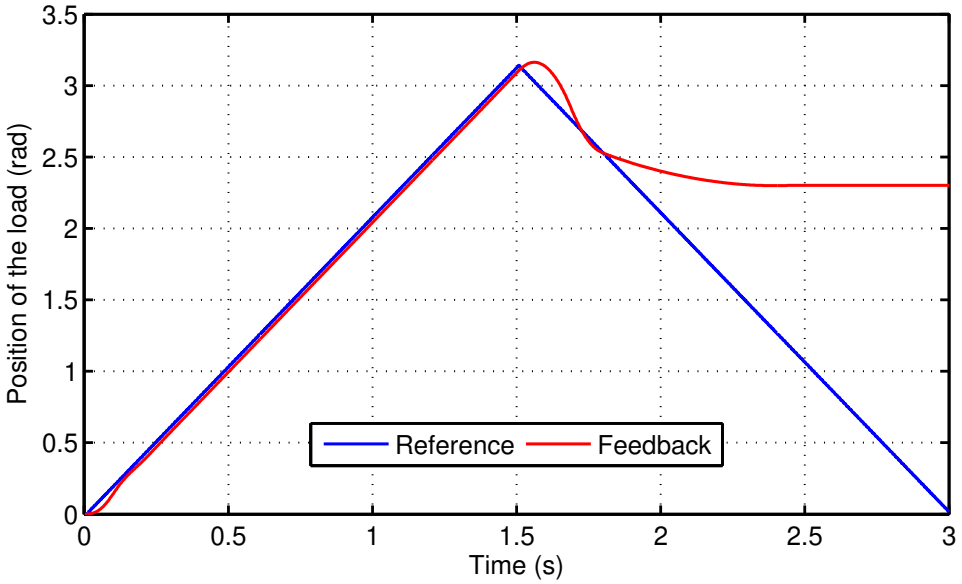

Figure 5.19: Position change with constant velocity motion for two cycles

The mechanical load follows the reference during the first half of the motion in the same characteristic as in the first part of the experiment. However, just after the direc-

tion of the system is requested to be inverted, controller creates a very large negative torque demand which is beyond the capability of the inverter. Since the output of the current controller is saturated, velocity controller starts to lose the control of the system and algorithm turns off the inverter for safety reasons due to high current demand. Velocity reference which is the output of the position controller is given in the Fig. 5.20 together with the velocity of the system.

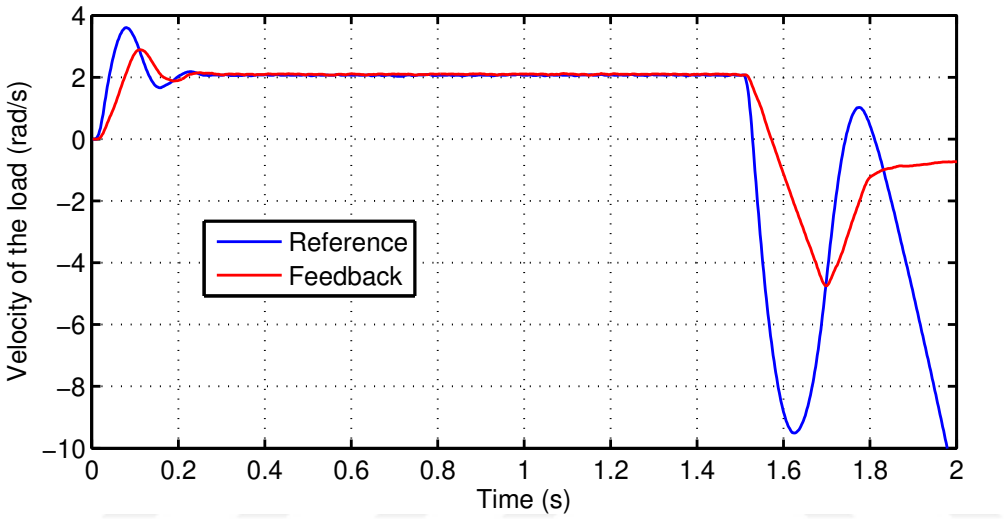

Figure 5.20: Velocity change with constant velocity motion for two cycles

The position reference expects from velocity controller to change the direction instantaneously but it is not an achievable target due to the physical limitations. In this experiment, once the direction is changed, the load slows down with the maximum possible deceleration which is governed by the current controller. The reference of the quadrature current and all other measured currents are given in the Fig. 5.21.

After the direction of the motion is changed, the velocity controller demands from current controller to work in the limits for 300 milliseconds and afterwards the system is turned-off for safety reasons. During this interval the polarity of the quadrature current changes two times. Both of these transients create high torque differences for the electromechanical system and creates undesired vibrations.

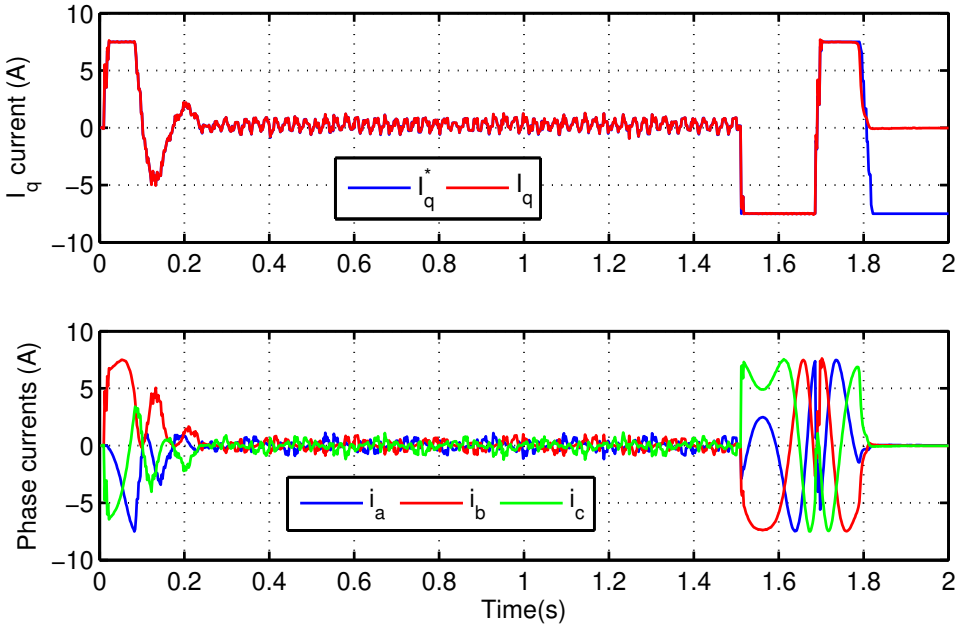

Figure 5.21: Change of currents with constant velocity motion for two cycles

5.2.2 Motion with a Constant Acceleration

The second trajectory that is selected for the experiment is the motion with a constant acceleration. For this case, the load is turned $180°$ in 1 second as given in the Fig. 5.22.

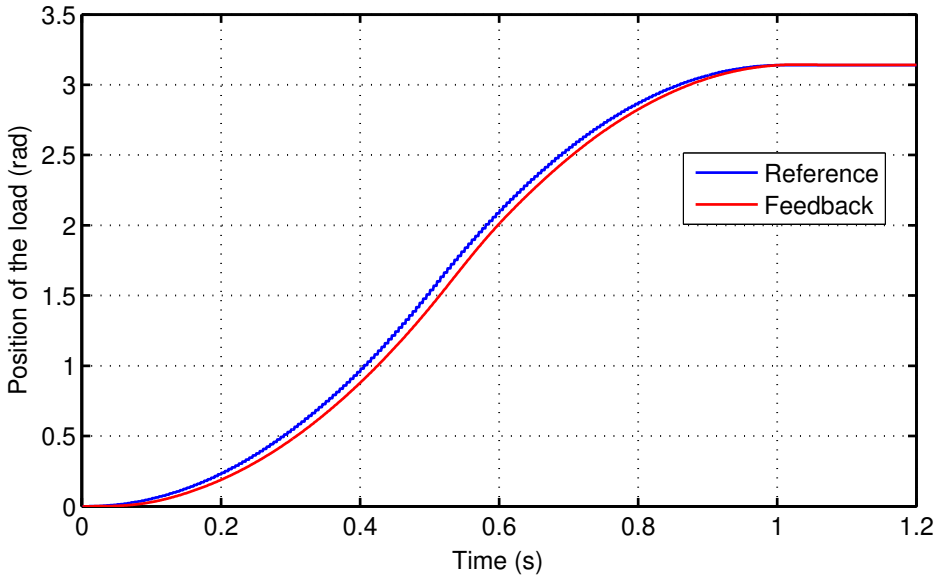

Figure 5.22: Position change with constant acceleration motion

Compared to the constant velocity case, motion with linear velocity creates a smoother movement and parabolic position change is achieved. During the first half of the motion, the load accelerates with a constant value and reaches it maximum velocity at the end of this period. During the second part of the motion, the velocity of the load reduces until the measured position reaches to the reference value. In this case, the first movement of the load starts without a delay and overshoot at the end is minimized.

Reference values for the velocity reaches to zero at the end of the motion but it takes more time for the load to completely slow down as it can be seen from the Fig. 5.23. Results of this situation can be discussed over the current values in the Fig. 5.24. Since the reaction time of the system is decreased compared to the previous motion profile, the peak value of the velocity reference is increased. Errors in the velocity control loop creates a current feedback with high frequency components, but since they are within the bandwidth of the current controller, reference current can be applied to the motor and the reference of both velocity and the position can be followed without any failure.

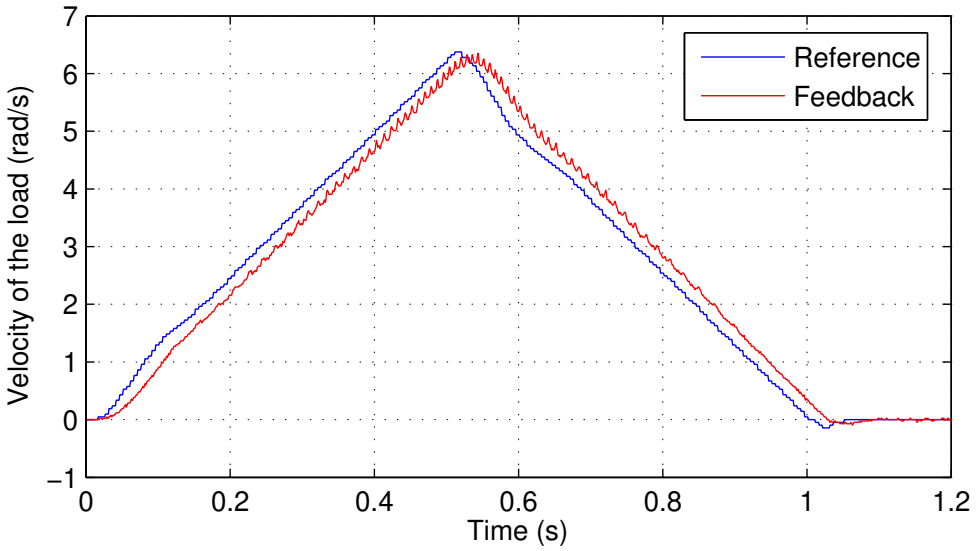

Figure 5.23: Velocity change with constant acceleration motion

Latency in the velocity loop creates a duration that quadrature current is different from zero. Even if the current controller keeps tracking its reference, this nonzero period is inevitable and create a torque for the motor as given in the Fig. 5.25.

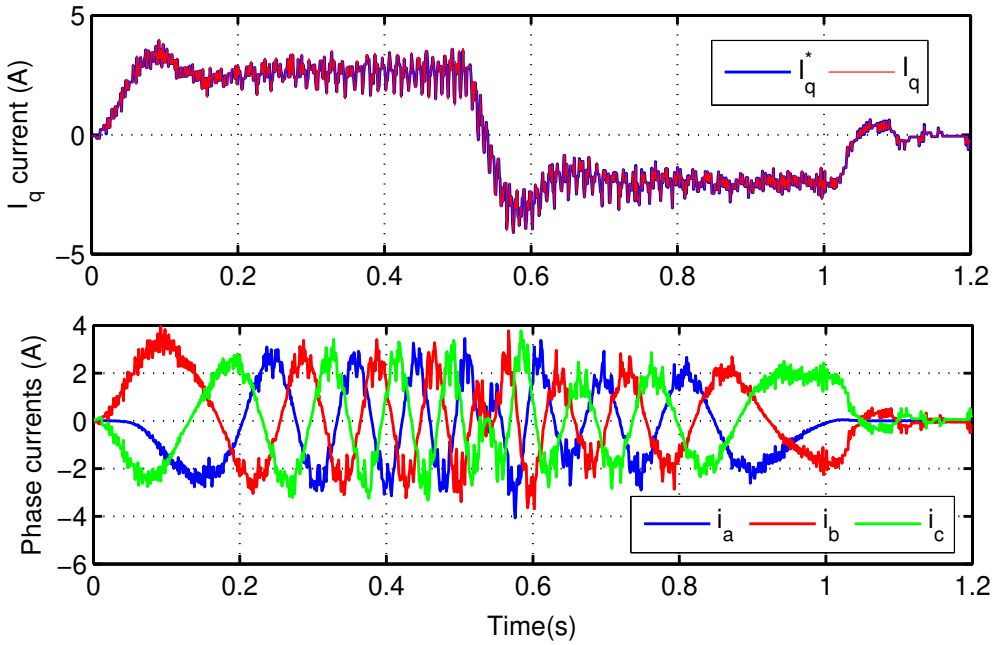

Figure 5.24: Change of currents with constant acceleration motion

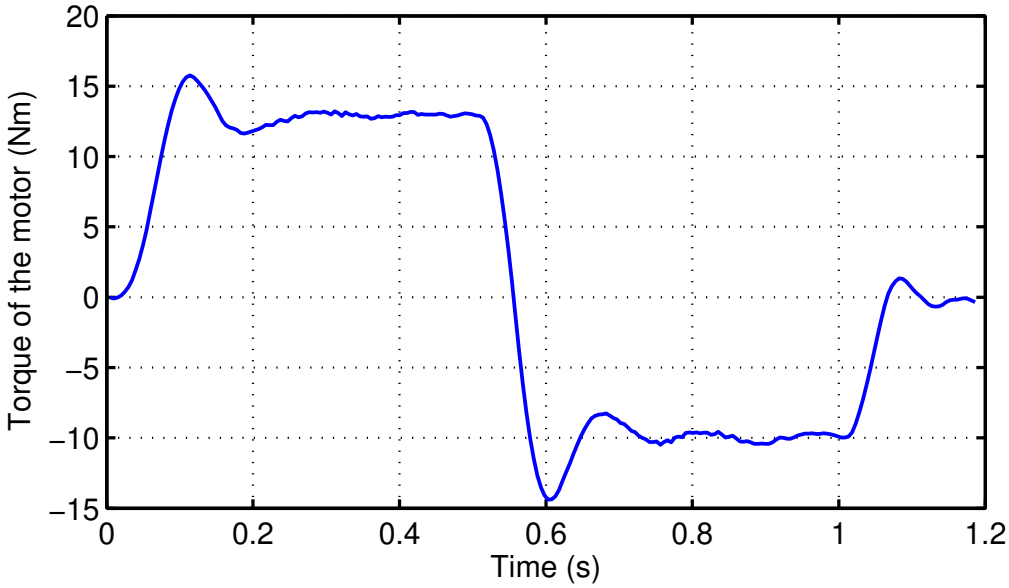

Figure 5.25: Torque change with constant acceleration motion

As the second phase of the experiment, the position reference is extended to rotate the load an extra $180°$ within the same time period. This new reference and the measured position of the load is given in the Fig. 5.26.

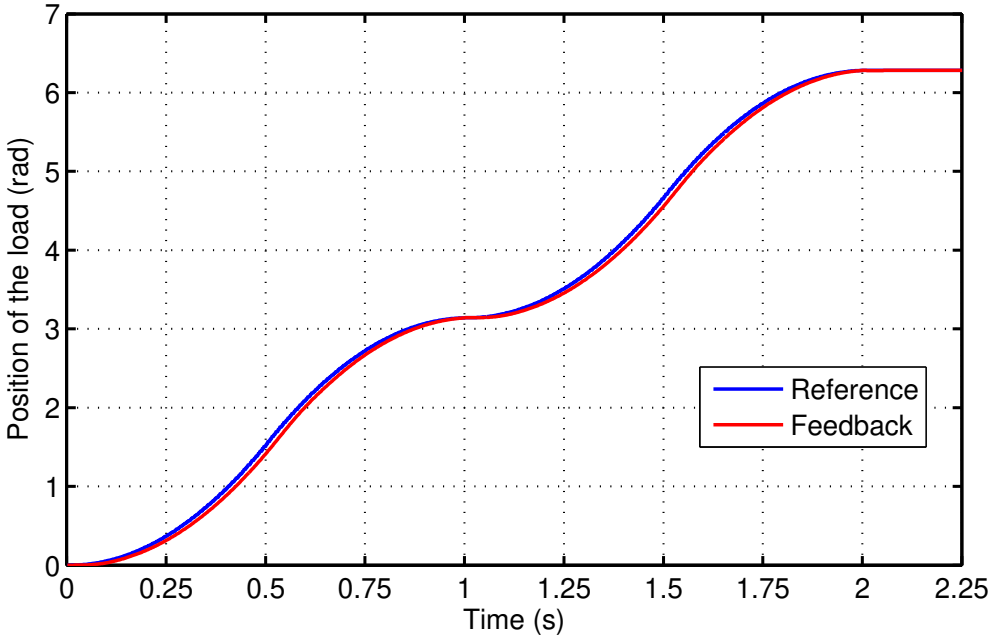

Figure 5.26: Position change with constant acceleration motion for two cycles

To follow the defined position references, velocity of the load changes as a triangular waveform as it is given in the Fig. 5.27.

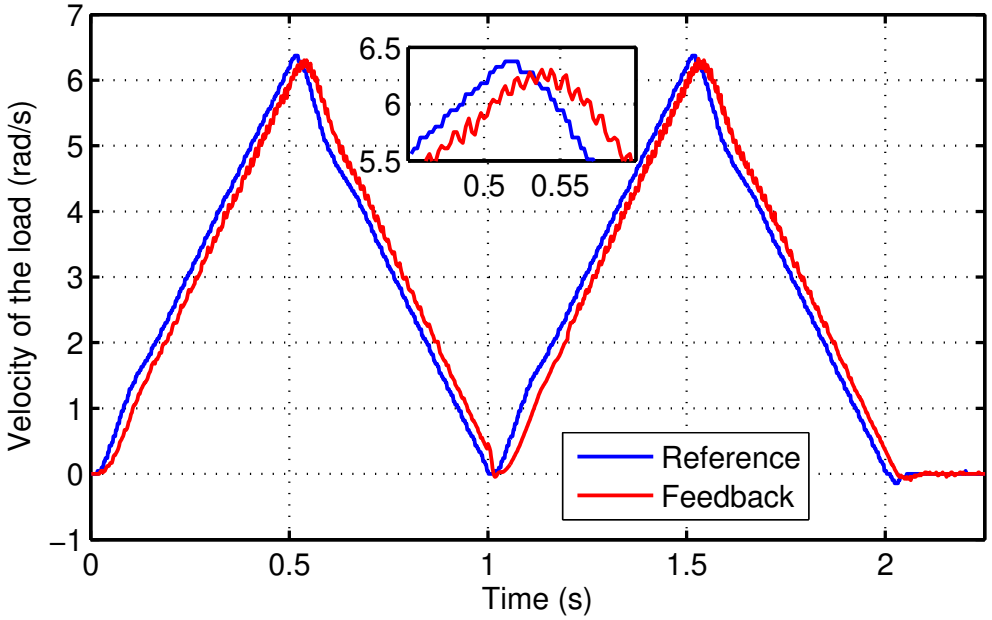

Figure 5.27: Velocity change with constant acceleration motion for two cycles

Due to the overshoot in the first part of the motion, the velocity of the motor is not completely zero before the starting time of the second part. Since the movement is in the same direction of the previous interval, it is expected from the system to accelerate again while the motor is still trying to slow down. The quadrature current, that is needed to create these velocity changes by accelerating the system, is given in the Fig. 5.28. In this figure, the reference and the measured currents are coinciding with each other. Since the motor is needed to be accelerated as it is still slowing down, the peak of the current in the second-half of the motion is greater than the initial peak value.

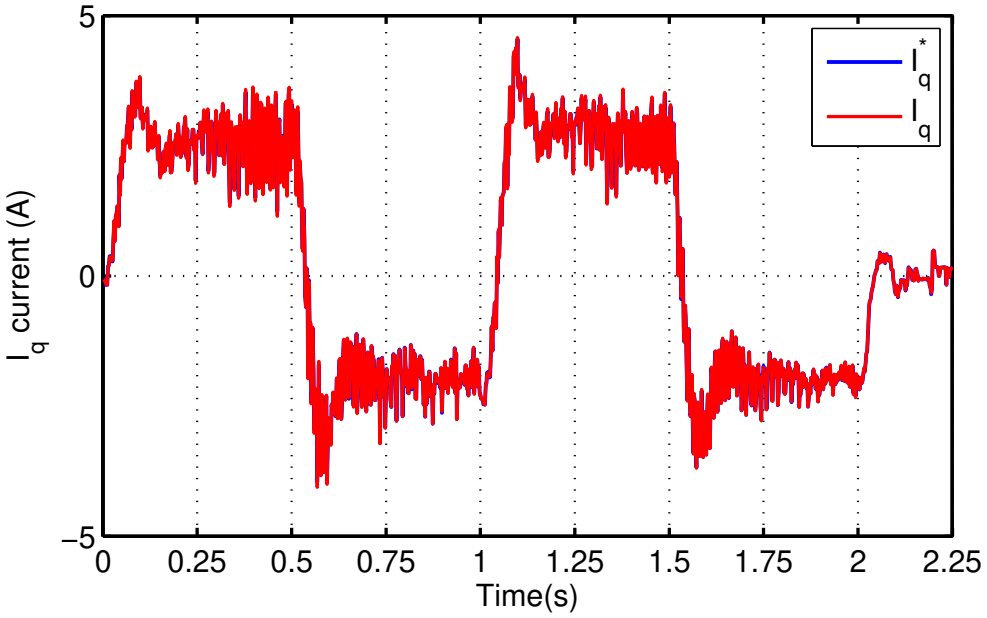

Figure 5.28: Change of currents with constant acceleration motion for two cycles

Even if the smoothness of the quadrature current is better compared to the motion with the trajectory of constant velocity, still it has transient change intervals which might create vibration in the system. As expected, it also completes the movement again after targeted time. The electromechanical torque change of the motor is given in the Fig. 5.29.

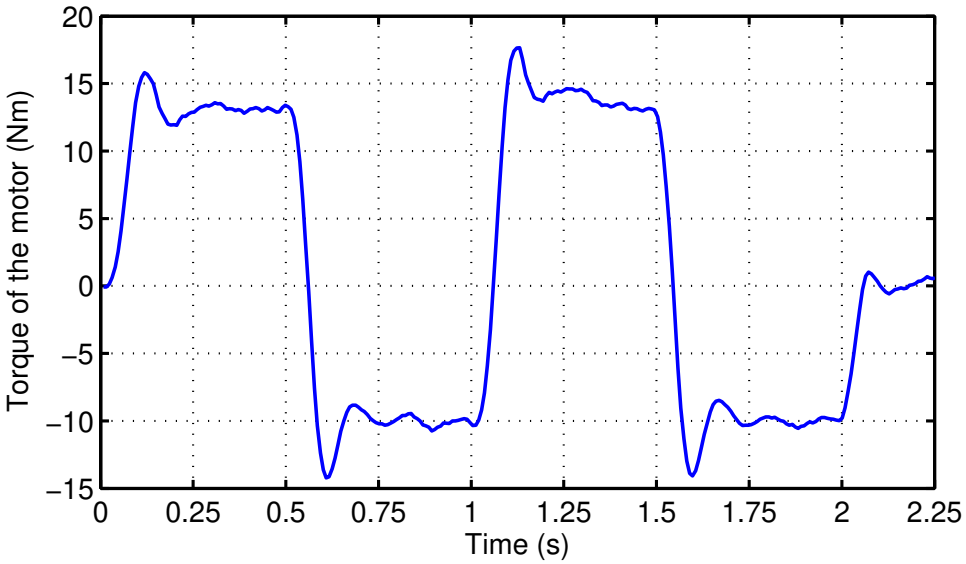

Figure 5.29: Torque change with constant acceleration motion for two cycles

5.2.3 Motion with a Limited-Jerk Sinusoidal Waveform

The last position reference waveform that is used in the experimental test setup is the limited-jerk sinusoidal trajectory. Same as the motion with constant acceleration, again the load is turned $180°$ in 1 second as given in the Fig. 5.30. Reference profile is created using the equations in the Section 2.3.

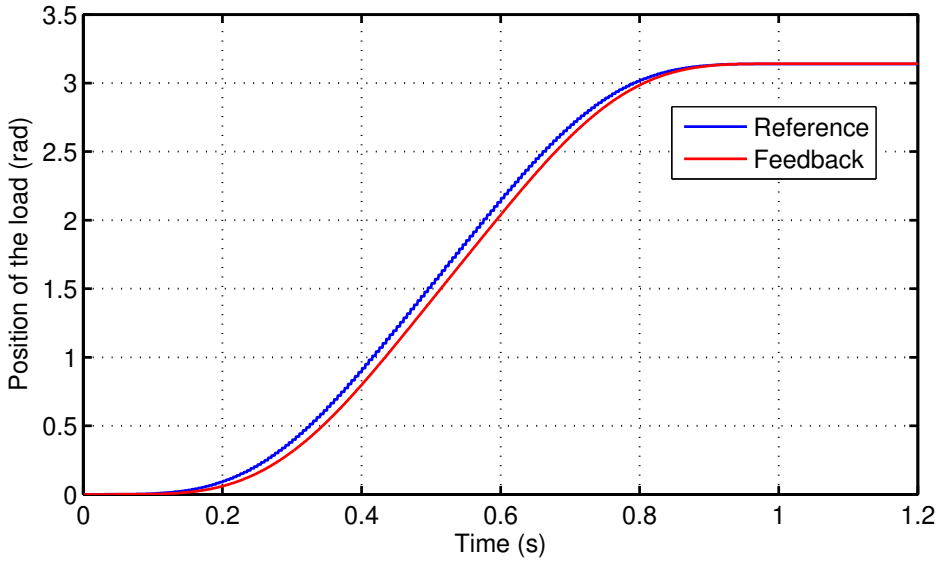

Figure 5.30: Position change with limited-jerk sinusoidal motion

In this type of a motion, the load accelerates and decelerates in a smoother waveform comparing to the other trajectories. As a result of it, the overshoot of the motion is completely eliminated and the velocity decreases to zero without any delay and the motion is completely finalized in 1 second as it is aimed. The velocity change of the motion is shared in the Fig. 5.31.

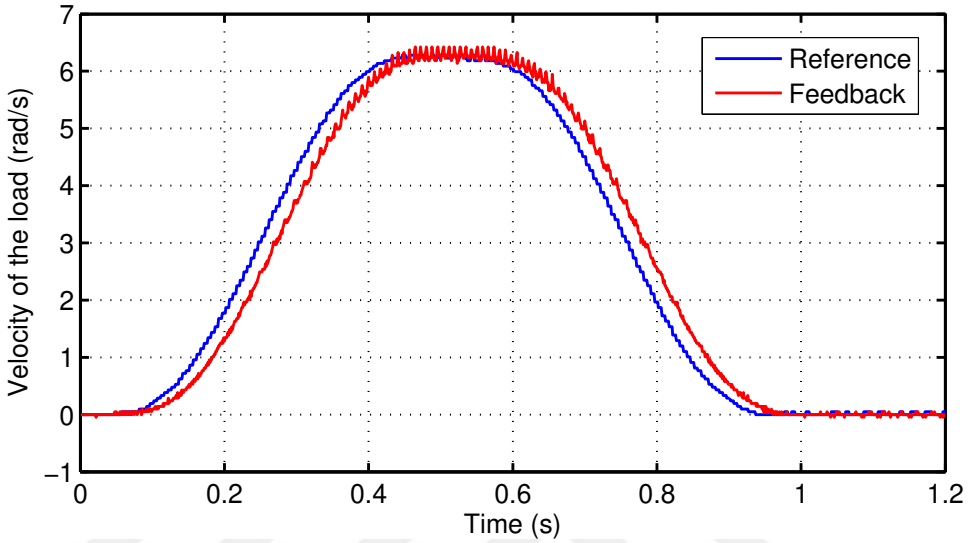

Figure 5.31: Velocity change with limited-jerk sinusoidal motion

As it is seen from the Fig. 5.31, there is a time delay between the reference and the measured velocity of the system but still the load stops in the true position within the targeted time period.

Since the load slows down in the planned duration, the quadrature current is not demanded after the load reaches to its final position. As it can be seen from the Fig. 5.32, the waveform of the I_q is very close to the acceleration profile that is given in the Fig. 2.5. This term is directly related with the electromechanical torque and smoothness of this value determines the ripples in the torque which is given in the Fig. 5.33.

As the last part of the experiment series of the position control, the limited-jerk sinusoidal trajectory is applied to the mechanical load to turn it 180° more after the first part of the motion is completed. Required reference for this motion and the feedback of the system are given in the Fig. 5.34. Reference profile is again created using the equations in the Section 2.3.

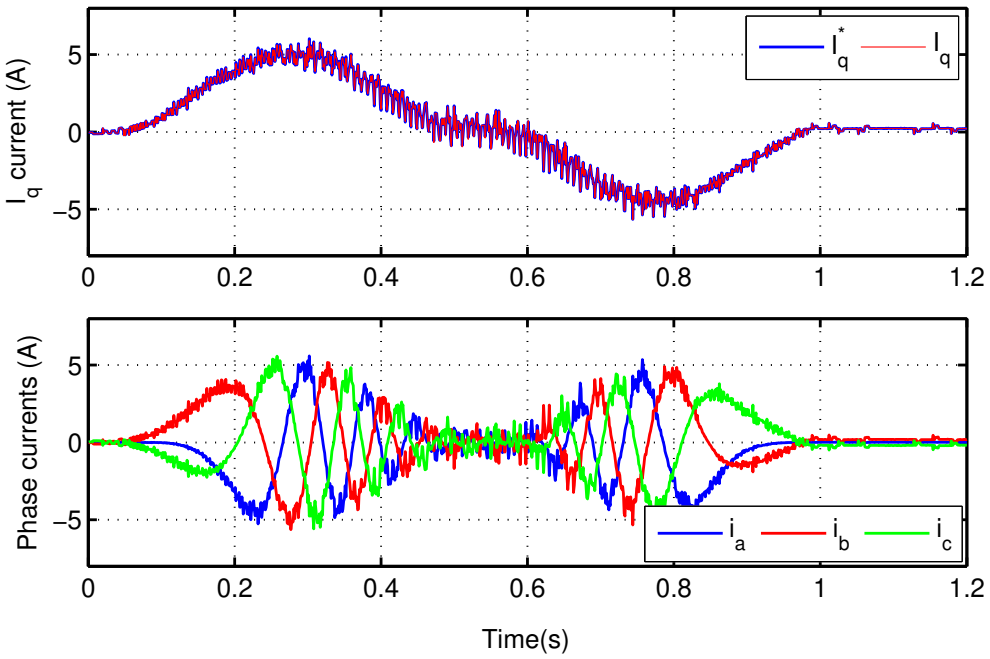

Figure 5.32: Change of currents with limited-jerk sinusoidal motion

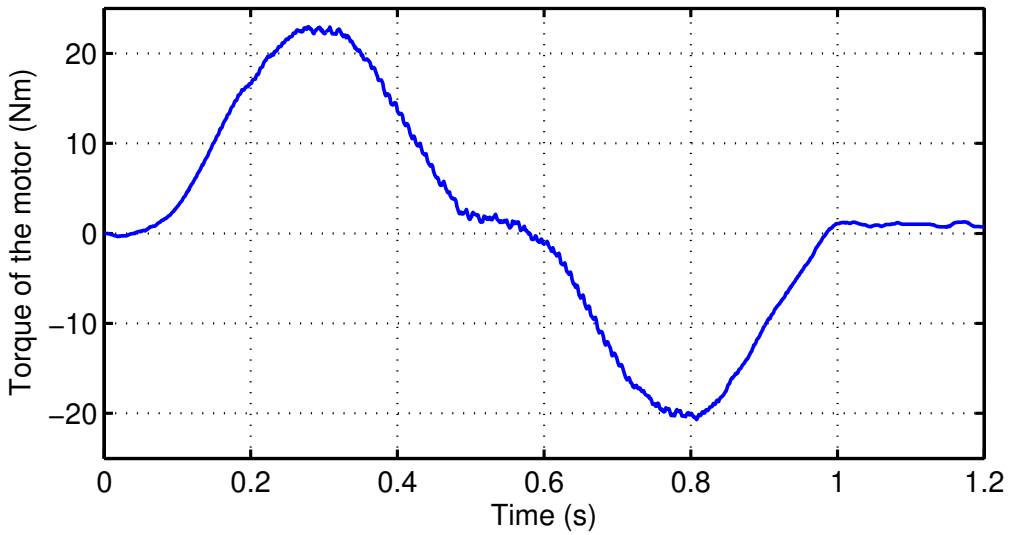

Figure 5.33: Torque change with limited-jerk sinusoidal motion

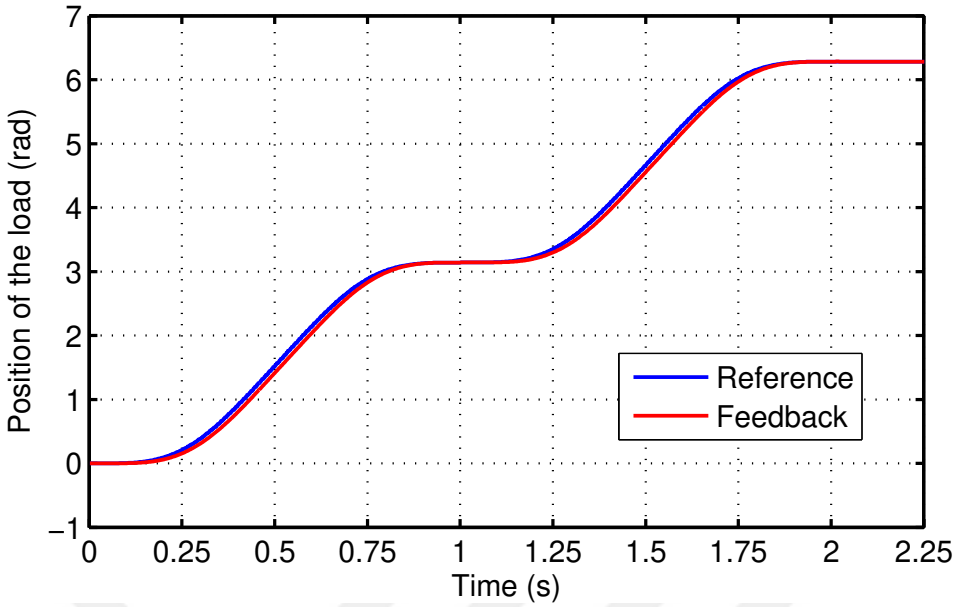

Figure 5.34: Position change with limited-jerk sinusoidal motion for two cycles

As it is expected, the position change of the load is completely stopped within the targeted time and the velocity reference keeps its smooth waveform as they are given in the Fig. 5.35.

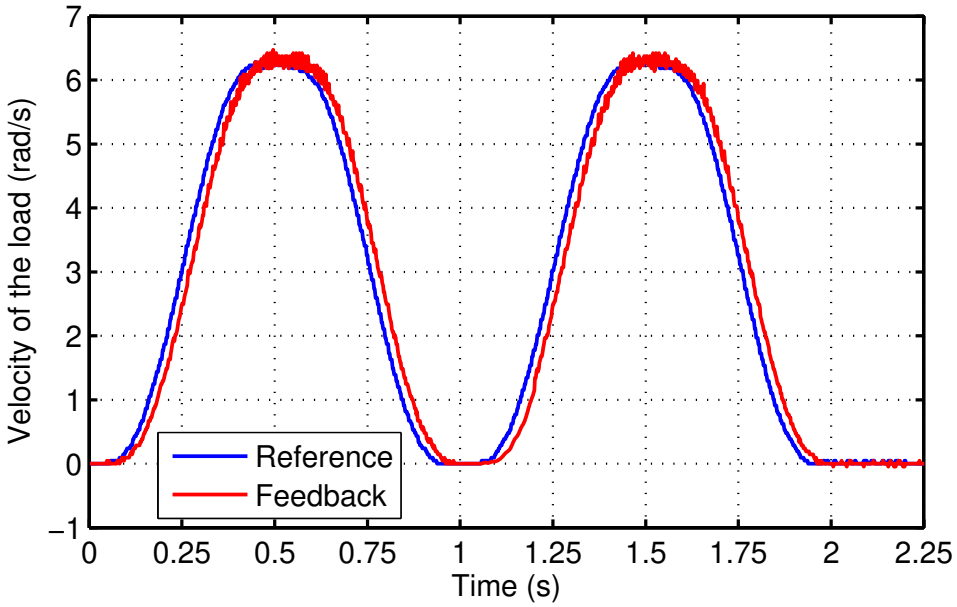

Figure 5.35: Velocity change with limited-jerk sinusoidal motion for two cycles

Smoothness for the velocity of the load is achieved with a smooth quadrature current that does not create instantaneous electrical torque change on the motor. The current that creates the motion with minimized vibration is given in the Fig. 5.36.

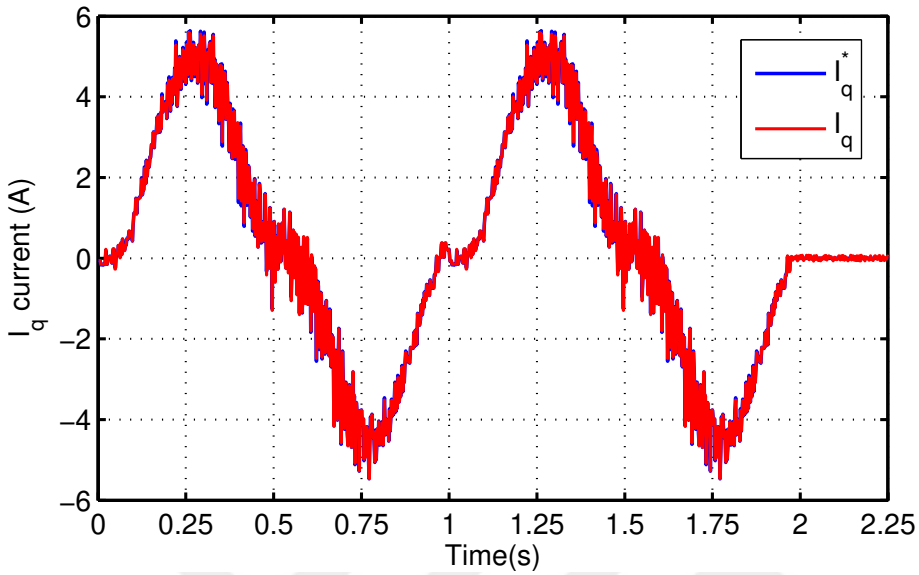

Figure 5.36: Change of currents with limited-jerk sinusoidal motion for two cycles

For the currents which have similar shapes as a sine wave, the torque, which is given in the Fig. 5.37, is created at the output of the motor.

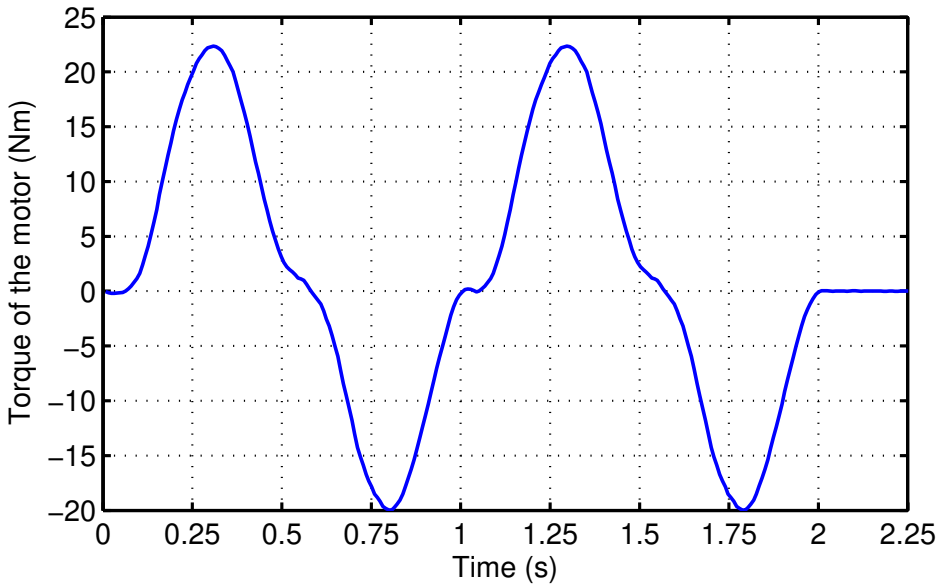

Figure 5.37: Torque change with limited-jerk sinusoidal motion for two cycles

Different from the motion with constant acceleration, the peak values of the torques for this trajectory are same for the both parts of the motion. It also does not have any transient torque demand at the beginning of the second part of the motion since the first motion is completely finished within its targeted time.

5.3 Comparison of the Results of the Experiments

As the trajectory is updated and the position reference is getting smoother, the waveform of the velocity and the currents also get smoother as seen from the outcomes of the experiments. By this way the load follows the reference with less overshoot and chance of completing the motion within the defined time target increases. For the motion with the sinusoidally limited-jerk, the load reaches to the destination in desired time without any overshoot and time delay.

Another advantage of the smoothness of the position reference is noticeable by checking the derivative of the torque as given in the Fig. 5.38 and Fig. 5.39.

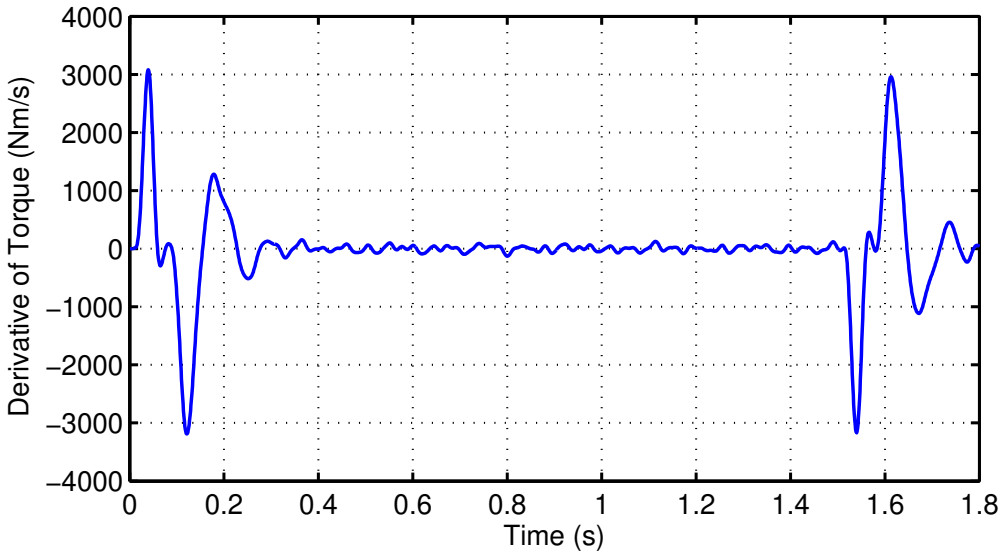

Figure 5.38: Derivative of torque for constant velocity motion

Transients in the change of torque for the constant velocity motion profile creates very high derivatives as given in the Fig. 5.38. The load can fully stop after around 200 ms than the targeted time and waveform shows the cause reason for the undesired

vibrations in the system. These transients are also bad when another motion is needed to be performed just after the first one is completed. Experiments show that when the first motion with motion with constant velocity is completed and the system is in recovery period, if it is needed to perform a second motion then the current limitation of the power electronics circuitry does not let the motion to be completed.

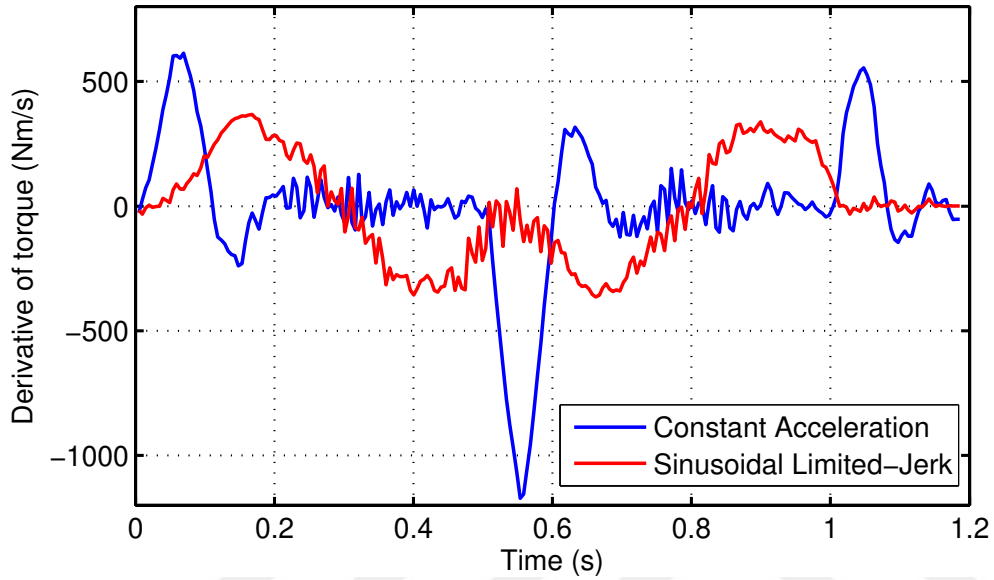

Figure 5.39: Derivative of torques for different trajectories

The results for the constant acceleration and the limited-jerk sinusoidal waveforms are given together in the Fig. 5.39 for a better comparison. The result with the sinusoidal limited-jerk completes the motion within the expected time and with around 3 times smaller torque derivative compared with the constant acceleration case which requires around 100 ms extra time to settle.

Experimental results for different trajectories with sequential motions show that when a second motion is being performed, the motion with constant acceleration is effected from the first part of the motion. This situation can also be observed from the Fig. 5.40 which is the derivative of the torque values for the motions with constant acceleration and the sinusoidal limited-jerk. Proposed motion is composed of sinusoidal waveforms during all parts of the motion whereas the motion with constant acceleration creates impulsive peaks for the jerk. All results for all different trajectories are shared together in the Table (5.2).

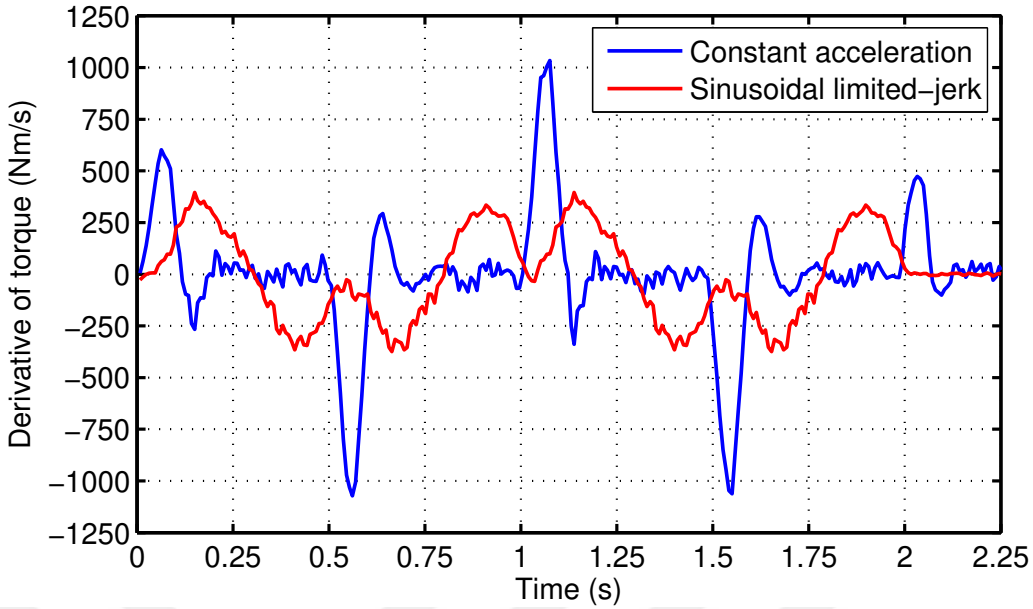

Figure 5.40: Derivative of torques for different trajectories for two cycles

Table 5.2: Comparison of the experimental results

Trajectory type	**Settling time**	**Peak torque**	**Copper losses**	**Peak of torque derivative**
Constant velocity	200 ms	34 Nm	71.8 Wh	3157 Nm/s
Constant acceleration	100 ms	17 Nm	35.6 Wh	1172 Nm/s
Sinusoidal limited-jerk	0	23 Nm	53.9 Wh	367 Nm/s
Double constant acceleration	100 ms	18 Nm	71 Wh	1073 Nm/s
Double sinusoidal limited-jerk	0	23 Nm	107.9 Wh	395 Nm/s

Completed steps and experimental results show that an electromechanical system that controls a permanent magnet synchronous motor with field oriented control technique is established and controllers for the velocity and the position loops are designed after their open-loop system identifications are completed. Simulation results for different trajectories showed that proposed motion type brings certain advantages which are beneficial to the system performance and the lifetime. In this chapter, simulated sce-

narios are tested on a real system with an enlarged scope. In the final chapter of the study, both simulation and experimental results are going to be used to indicate the proven advantages of the proposed approach to the motion control.

CHAPTER 6

CONCLUSION AND FUTURE WORK

In this study, H_∞ controllers for the velocity and the position loops with a desired bandwidth are designed and used for the control of the electromechanical system. Controller design method requires the priori knowledge of the system and that is obtained by open-loop system identification using N4SID algorithm. For both simulation and experimental test setups, FOC technique is used to create the reference points of the a-b-c phase currents and different trajectories are applied as the position references to the system. In this chapter, these results are evaluated and possible contributions to the field are shared together with the future work of the study.

6.1 Conclusion

Before starting with the evaluation of the simulation and the experimental results, it is important to emphasize the importance of the selected supportive methods. For this study, they are field oriented control, N4SID system identification and the H_∞ controller which have their own advantages that can be used in harmony in the same system. These advantages are brought to the study and independent of the selected motion profile, performance of the system is improved.

FOC technique and current decoupling method are used to separate and control the currents into the terms of the excitation and the torque generation. Independent from the current controller, FOC has already improved the efficiency of the drive [14]. System identification has removed the necessity of priori knowledge of the motor and load parameters under the effective environmental condition and helped to controller design phase to have a better closed-loop bandwidth by adding all the parasitic

effects into the transfer function. After SI, H_∞ controller is designed to have an optimal solution within the targeted bandwidth and performance of the electromechanical system is improved for all the trajectories before they are applied. Therefore, all of the following advantages, which are measured directly or evaluated on results given in Table (6.1), are only related with the differences of the motion profiles.

Table 6.1: Comparison of the experimental results

Trajectory type	**Settling time**	**Peak torque**	**Copper losses**	**Peak of torque derivative**
Constant velocity	200 ms	34 Nm	71.8 Wh	3157 Nm/s
Constant acceleration	100 ms	17 Nm	35.6 Wh	1172 Nm/s
Sinusoidal limited-jerk	0	23 Nm	53.9 Wh	367 Nm/s
Double constant acceleration	100 ms	18 Nm	71 Wh	1073 Nm/s
Double sinusoidal limited-jerk	0	23 Nm	107.9 Wh	395 Nm/s

• The most important advantage of the jerk limitation is the *elimination of the undesired vibration* in the system. For the motion with the trajectory of constant velocity, large torque ripples cause considerable vibrations and discontinuity for the jerk. Simulation results for this motion type is given in the Fig. 4.34 show that impulsive jerk changes are created. Experimental results given in the Fig. 5.38 also proves this statement. In the trajectory with trapezoidal velocity, results given in the Table (6.1) show that peak torque value is 2 times lower compared to the motion with constant velocity. However, even with the trapezoidal velocity trajectory which corresponds to constant acceleration, instantaneous torque variation causes vibration, which in turn reduces the service life of the mechanical parts and at the corners of acceleration intervals impulse jerks are created as given in the Fig. 4.35 and the Fig. 5.39. For the motion with sinusoidal limited-jerk, undesired torque ripples that cause mechanical fatigue are completely eliminated as it is given in the Fig. 4.33 and the Fig. 5.33. Without ripples in the torque, jerk discontinuity is not created as given in both Fig. 4.35 and the Fig. 5.39. Similarity between these figures an the Fig. 2.5 show that the proposed method is implemented as desired and initial target is achieved.

• The second advantage of this method is its *punctuality*. As it is also required in the systems that Aselsan has been developing, for all radar electronic warfare and electronic support projects some of the features are fast system response and high precision position controlling [36]. This property is not only useful for defense industry but also for other applications which requires precision and fast response such as robotics and lithography machines. The trajectory with the constant velocity can not finish the motion within the desired duration and compensation of the overshoot takes around 200 ms as given in the Table (6.1). Due to the limitations of the power electronics circuitry, even the same motion time can not be achieved with this profile and it takes longer time to reach the destination. These results clearly show the importance of the limitation of the acceleration. Once the next profile is considered, it is seen that constant acceleration can reach to the destination within the same time of sinusoidal limited-jerk. But actually the motion with the constant acceleration does not fully stop and requires an additional 100 ms to complete the movement as given in the Fig. 5.24 and the Fig. 5.25. While other trajectories require torque and current changes even after the reference reaches its final value, the proposed method does not demand any additional torque or current as given in the Fig. 5.32 and the Fig. 5.33.

• The last advantage of the proposed solution is the *readiness to next commands*. For the applications that time is important such as pick and place robots used in serial production or for radar electronic support systems that multiple targets are needed to be tracked, the time interval between two adjacent motion commands are desired to be as short as possible. Once a new movement in the same direction is needed to be performed just after the first one is completed, torque demand for the motion with constant velocity creates very high current demand as given in the Fig. 5.21 and since the motor drive can not handle it, the motion is interrupted and the mechanical load can not reach to the desired destination. The situation is better with the motion with constant acceleration and the system can perform a second command just after the first one. However, torque demand of the system is increased compared to the normal operation as given in the Fig. 5.28 and it also creates impulsive jerks in the system as in the Fig. 5.40. However in the sinusoidal limited-jerk case, the system can perform the next command without creating any delay and abrupt torque changes resulting in the time optimality of motion, vibration reduction and increment of the service life.

Both the simulation and the experimental results show that the performance of the system by means of punctuality, torque ripple reduction which can be also considered as vibration reduction, that triggers lifetime, is improved as a higher derivative of the position is limited. The only disadvantage of the proposed method is the increase in the copper losses

6.2 Contribution to the Field

For electromechanical systems in motion, the jerk limitation comes with the advantages of punctuality, vibration reduction and improved lifetime. Therefore it is possible and actually better to adapt this approach to all systems in motion. Effect of the method is more dominant for the systems that operate mostly with transient operations such as pick and place machines or robotics. For the motors that operate with constant velocity, advantages are valid only for the first acceleration phase but for other systems that accelerate, slow down and repeat it again, advantages are convenient. Within the scope of this study, the proposed jerk-limitation approach is applied to a system, which is in the design phase in Aselsan, that controls the velocity and the position of a radar in two axes. Proposed and simulated benefits of the jerk-limitation are also observed during the experimental tests and sinusoidal jerk-limitation is adapted to more projects within the company to decrease the mechanical fatigue and vibrations in the electromechanical systems.

By adapting the idea of jerk limitation, lifetime of the systems in motion can be extended [8] and mean time between failures (MTBF) can be improved as well. With a long-term observations on the produced systems with the jerk-limitation idea in Aselsan, it is expected to see the improvements on the lifetimes of the electromechanical components such as slip rings, rotary joints, ring gears and bearings. Vibration reduction might also affect the accuracy of the systems. Especially for the environments with very low friction, such as vacuum or magnetically levitating planar platforms, settling time of the position control loop can be eliminated. For the systems which are sensitive to the vibration, such as lithography machines used in the semiconductor industry, elimination of the vibration can decrease the volume of active vibration isolators.

Ergonomics is not evaluated within this study, since the developed electromechanical system does not have any human-machine interaction, but the jerk-limitation complies with the scope of ergonomics and therefore the study has an indirect contribution to this area, too. Researches show that humans can detect acceleration easily, but once it is not constant, non-zero jerk is created and actually it is possible to experience it as a discomfort feeling [20]. Reported human experiences show that acceleration can be noticed between 1.3 and 1.6 m/s^2, beyond 1.8 m/s^2 it is often considered as disturbing. For the jerk-limitation, experiences show that 2 m/s^3 is generally acceptable [37]. Elevators and electrical vehicles are the most commonly used interaction between people and the accelerating electromechanical systems. Especially for the elevators, high amount of studies are completed since its invention but still researchers are working on improving the performance of the elevators by force ripple and jerk minimization [38]. However, electrical vehicles are highly popular in the market and researchers also proposes new methods to improve the performance and comfort for the humans [39,40]. These studies are not limited with the main motion of the vehicle but also with their suspension systems [41].

As the industrialization continues and more machines are used in manufacturing and daily life; as the quantity and amount of the electrical vehicles are increased number of systems that this study can contribute is going to be increased proportionally.

6.3 Future Work

Current applications and literatures show that limiting the jerk with constant values are good for the quality of the motion. However, the snap which is the fourth derivative of the position with respect to time, and higher derivatives are not well understood for physics and for their impact on the human health [20]. In this study, the jerk is selected as a sinusoidal function and the trajectory is developed to be able to limit the jerk sinusoidally. However, higher derivatives of the jerk is not focused. If there might be an advantage to study on these values in the future, that topic can be an improvable area for this study. For this kind of a motion profile; field oriented control, system identification and H_∞ controllers can still contribute to the performance since they are helping to improve the performance for the rest of the reference trajectory.

Applying a system identification for the velocity and the position loops improved the quality of the controller design phase and helped to achieve the targeted closed-loop frequency bandwidth. SI process is completed for an environmental condition that system is going to be operate in the future and since the mechanical load is going to be inside a sealed radome, open-loop system would not be affected from external changes. However, not all the operating systems have this opportunity and performance of some of the systems are being affected by changing environment. Proposed method actually provide solution up to a point, if the environmental effect has a low natural frequency, such as a constant and slow wind, this additional disturbance can be ignored by the controller since its closed-loop bandwidth is higher and the performance of the system might not be affected. But if the external disturbance has larger impacts on the system and additional precautions are needed to avoid performance drop. Environmental changes for the systems without radome can change the characteristic of the open-loop system by changing the either electrical or mechanical parameters.Temperature change has certain impacts on both electrical and mechanical domains. It can change the static friction of the mechanical load, resistance and inductance values of the electrical motor and these changes can effect the performance. For this kind of situations, a few different methods can be used in the future to extend this study.

• Parameter observation can be done during the operation of the system and the controllers can be updated accordingly through the environmental changes. This solution removes the advantage of the independence to the system parameters. If the temperature in the motor is always known then its effect on the parameters can be predicted but even measuring the temperature is not directly possible in most of the cases. A low-order lumped-parameter thermal network (LPTN) temperature modeling technique can be used with fusion approach to increase the accuracy and the robustness of the estimation and temperature of the PMSM can be predicted [42]. Alternative of temperature estimation can be real-time parameter estimation and one way to achieve it can be using modified two-stage particle swarm optimization algorithm [43].

• Alternative of parameter estimation and implementing a parameter dependent controller can be using an adaptive control approach. For this purpose, an adaptive neural network based controller can be replaced with the H_∞ controller and torque ripples

can be minimized further by also adding the extended capability of handling external torque changes of the system [44]. Adaptive fuzzy controller [45] or the interconnection and damping assignment passivity-based control framework [46].

For both parameter estimation and adaptive control techniques, there are certain numbers of completed studies to extend this study to a solution with higher performance for all kind of environmental conditions.

REFERENCES

[1] C. Jing, Z. Jigua, and H. Yupping, "Optimization of speed loop control technology for permanent magnet synchronous motor servo system," *IEEE Conf. and Exp, (ITEC - Asia-Pacific)*, 2017.

[2] A. Alexandrou, N. Adamopulos, and A. Kladas, "Development of a constant switching frequency deadbeat predictive control technique for field-oriented synchronous permanent-magnet motor drive," *IEEE Transactions on Industrial Electronics, Vol.63, No.8*, August 2016.

[3] L. Dang, N. Bernard, N. Bracikowski, and G. Berthiau, "Design optimization with flux weakening of high-speed PMSM for electrical vehicle considering the driving cycle," *IEEE Transactions on Industial Electronics, Vol.64, No.12*, December 2017.

[4] J. Ziegler and N. Nichols, "Optimum settings for automatic controllers," *Trans. ASME, 65, pp.433-444*, 1942.

[5] A. Sayda, "Model identification and robust H-infinity controller design of a motor-synchronous generator group," *IEEE International Conf. on Control Applications*, October 2006.

[6] Y. L. K.H. Ang, G. Chong, "PID control system analysis, design and technology," *IEEE Transactions on Control Systems Technology, Vol.13, Issue.4*, July 2015.

[7] C. Foias, B. Francis, J. Helton, H. Kwakernaal, and J. Pearson, "H_∞ -control theory," *Springer-Verlag Berlin Heidelberg*, 1991.

[8] W. Pawlus, M. Hansen, M. Choux, and G. Hovland, "Mitigation of fatigue damage and vibration severity of electric drivetrains by systematic selection of motion profiles," *IEEE/ASME Transactions on Mechatronics, V.21, No.6*, December 2016.

[9] S. Shin, C. Choi, J. Youm, T. Lee, and C. Won, "Position control of PMSM using jerk-limited trajectory for torque ripple reduction in robot applications," *38th Annual Conf. on IEEE Industrial Electronics Society, pp.2400-2405*, October 2012.

[10] R. Haschke, E. Weitnauer, and H. Ritter, "On-line planning of time-optimal, jerk-limited trajectories," *IEEE/RSJ Int.l Conf. on Intelligent Robots and Systems, pp. 3248-3253*, September 2008.

[11] S. Macfarlane and E. Croft, "Jerk-bounded manipulator trajectory planning: design for real-time applications," *IEEE Transactions on Robotics and Automation, Vol.19, No.1*, February 2003.

[12] D. Novotny and T. Lipo, "Vector control and dynamics of AC drives," *Clarendon Press, Oxford*, 1996.

[13] Mathworks, "Picture for illustration of direct and quadrature axes." `https://nl.mathworks.com/help/physmod/sps/ref/pmsm.html/`, 2019. [Online; accessed 10-August-2019].

[14] M. Zhao, H. Zhao, and H. Chen, "A dynamic-decoupling controller of current for permanent magnet synchronous motor," *Control and Decision Conference (CCDC)*, May 2017.

[15] S. Amornwongpeeti, O. Kiselychnyk, J. Wang, C. Antaloae, M. Soumelidis, and N. Shah, "A combined MTPA and maximum efficiency control strategy for IPMSM motor drive systems," *International Conference on Electrical Systems for Aircraft, Railway, Ship Propulsion and Road Vehicles*, 2016.

[16] D. Mon-Nzongo, T. Jin, G. Ekemb, and L. Bitjoka, "Docupling network of field-oriented control in variable-frequency drivers," *IEEE Transactions on Industrial Electronics, V.64, Issue.7*, 2017.

[17] M. Popescu and P. Popescu, "Fast movements and jerk mechanics," *International Conference on Applied and Theoretical Electricity (ICATE)*, 2018.

[18] E. Nshama and N. Uchiyama, "Time and energy optimal trajectory generation in feed drive systems using kinematic corner smoothing with interrupted accel-

eration," *26th Mediterranean Conference on Control and Automation (MED)*, 2018.

[19] T. Singh, "Jerk limited input shapers," *Proceedings of the 2004 American Control Conference*, 2004.

[20] D. Eager, A. Pendrill, and N. Reistad, "Beyond velocity and acceleration; jerk, snap and higher derivatives," *European Journal of Physics, v.37 n.6*, 2016.

[21] A. Sadaka-Stephen, E. Pirondini, M. Coscia, and S. Micera, "Influence of trajectory and speed profile on muscle organization during robot-aided training," *IEEE International Conference on Rehabilitation Robotics (ICORR)*, 2015.

[22] H. Seki and S. Tadakuma, "Minimum jerk control of power assisting robot on human arm behavior characteristic," *IEEE International Conference on Systems, Man and Cybernetics*, 2014.

[23] S. Xuguang, X. Bugong, X. Wei, and L. Boren, "Design and implementation for jerk limited trajectory plan with real-time look-ahead interpolator," *27th Chinese Control Conference*, 2008.

[24] S. Lai, M. Lan, and X. Chen, "Efficient safe corridor navigation with jerk limited trajectory for quadrotors," *37th Chinese Control Conference*, 2018.

[25] M. Verhaegen and V. Verduşt, "Filtering and system identification," *Cambridge University Press*, 2007.

[26] A. Tangirala, "Principles of system identification, theory and practice," *RC Press*, 2015.

[27] K. Liu and Z. Zhu, "Quantum genetic algorithm-based parameter estimation of PMSM under variable speed control accounting for system identifiability and VSI nonlinearity," *IEEE Transactions on Industrial Electronics, Vol.62, No.4*, April 2015.

[28] L. Ljung, "System identification, theory for the user," *Prentice Hall PTR*, 1999.

[29] P. Overschee and B. Moor, "Subspace identification for linear systems: Theory, implementation, applications," *Kluwer Academic Publishers*, 1996.

[30] S. Borjas, C. Garcia, and L. Gualberto, "Subspace identification for industrial processes," *TEMA Tend. Mat. Apl. Comput.*, 2011.

[31] K. Glover and D. McFarlane, "Robust stabilization of normalized coprime factor plant descriptions with H_∞-bounded uncertainty," *IEEE Trans. Autom. Control, AC-34(8):821-830*, August 1992.

[32] B. Ulutas, "Distributed H_∞ control segmented telescope mirrors," *Doctor of Philosophy Thesis, University of Victoria*, 2014.

[33] V. Le and M. Safonov, "Rational matrix GCD's and the design of squaring-down compensators-a state space theory," *IEEE Trans. Autom. Control, AC-36(3):384-392*, March 1992.

[34] R. Chiang and M. Safonov, "H_∞ synthesis using a bilinear pole-shifting transform," *A/AA J. Guidance, Control and Dynamics*, 1992.

[35] M. Mutlu, O. Keysan, and B. Ulutas, "Limited-jerk sinusoidal trajectory design for FOC of PMSM with H-infinity optimal controller," *IEEE 18th International Power Electronics and Motion Control Conference (PEMC)*, 2018.

[36] Aselsan, "Datasheet of REDET system." `https://www.aselsan.com.tr/REDET_Mobile_Radar_Electronic_SupportElectronic_Attack_System_3246.pdf/`, 2017. [Online; accessed 19-August-2019].

[37] R. Howkins, "Elevator ride quality - the human ride experience," *VFZ - Verlog fir Zielgruppeinformationen GmbH*, 2015.

[38] S. Masoudi, M. Feyzi, and M. Sharifian, "Force ripple and jerk minimisation in double sided linear switched reluctance motor used in elevator application," *IET Electric Power Applications, V.10, Issue.6*, 2016.

[39] T. Shamir, "How should an autonomous vehicle overtake a slower moving vehicle: design and analysis of an optimal trajectory," *IEEE Transactions on Automatic Control, V.49, Issue.4*, 2004.

[40] Y. Wang, J. Chardonnet, and F. Merienne, "Speed profile optimization for enchanced passenger comfort: an optimal control approach," *International Conference on Intelligent Transporation Systems (ITSC)*, 2018.

[41] B. Şekerci, M. Canevi, and M. Söylemez, "A comparison of controller performances on the ride comfort of the active suspension system," *International Conference on Control Engineering and Information Technology (CEIT)*, 2019.

[42] O. Wallscheid and J. Böcker, "Fusion of direct and indirect temperature estimation techniques for permanent magnet synchronous motors," *IEEE International Electric Machines and Drives Conference (IEMDC)*, 2017.

[43] E. Tofighi, A. Mahdizadeh, and M. Feyzi, "Real-time estimation and tracking of parameters in permanet magnet synchronous motor using a modified two-stage particle swarm optimization algorithm," *IEEE International Symposium on Sensorless Control for Electrical Drives and Predictive Control of Electrical Drives and Power Electronics*, 2013.

[44] K. Gulez and A. Adam, "Adaptive neural network based controller for direct torque control of PMSM with minimum torque ripples," *SICE Annual Conference*, 2007.

[45] L. Long, "Adaptive fuzzy back-stepping control system of permanent magnet synchronous motor," *Chinese Control and Decision Conference (CCDC)*, 2017.

[46] L. Jin, S. Yu, and J. Du, "Adaptive and integral control of PMSM with uncertainties and disturbances in the port-controlled hamiltonian framework," *Proceedings of the 32nd Chinese Control Conference*, 2013.